Quaternary Science Reviews 129 (2015) 1–36

Contents lists available at ScienceDirect

Quaternary Science Reviews

journal homepage: www.elsevier.com/locate/quascirev

Invited review

Sequence of events from the onset to the demise of the Last Interglacial: Evaluating strengths and limitations of chronologies used in climatic archives

A. Govin [a, *, 1, 4], E. Capron [b, **, 4], P.C. Tzedakis [c], S. Verheyden [d, 2], B. Ghaleb [e], C. Hillaire-Marcel [e], G. St-Onge [f, g], J.S. Stoner [h], F. Bassinot [i], L. Bazin [i], T. Blunier [j], N. Combourieu-Nebout [k], A. El Ouahabi [l], D. Genty [i], R. Gersonde [m], P. Jimenez-Amat [n], A. Landais [i], B. Martrat [l], V. Masson-Delmotte [i], F. Parrenin [o], M.-S. Seidenkrantz [p], D. Veres [o, 3], C. Waelbroeck [i], R. Zahn [q]

[a] MARUM – Center for Marine Environmental Sciences, University of Bremen, Leobener Strasse, 28359 Bremen, Germany
[b] British Antarctic Survey, High Cross, Madingley Road, CB3 0ET Cambridge, UK
[c] Environmental Change Research Centre, Department of Geography, University College London, London WC1E 6BT, UK
[d] Royal Belgian Institute of Natural Sciences, Jennerstraat 13, B-1000 Brussels, Belgium
[e] GEOTOP, Université du Québec à Montréal, Montréal, H3C 3P8, Canada
[f] Institut des sciences de la mer de Rimouski (ISMER), Canada Research Chair in Marine Geology, Université du Québec à Rimouski, Rimouski, Canada
[g] GEOTOP Research Center, Canada
[h] College of Earth, Ocean, and Atmospheric Sciences, Oregon State University, 104 CEOAS Admin Bldg., Corvallis, Oregon 97331-5503, USA
[i] Institut Pierre-Simon Laplace/Laboratoire des Sciences du Climat et de l'Environnement, UMR 8212, CEA-CNRS-UVSQ, 91190 Gif-sur-Yvette, France
[j] Centre for Ice and Climate, Niels Bohr Institute, University of Copenhagen, Denmark
[k] UMR 7194 CNRS "Histoire Naturelle de l'Homme Préhistorique", Département de Préhistoire, Muséum national d'histoire naturelle, Institut de Paléontologie Humaine, 75013 Paris, France
[l] Department of Environmental Chemistry, Institute of Environmental Assessment and Water Research (IDÆA), Spanish Council for Scientific Research (CSIC), 08034 Barcelona, Spain
[m] Alfred Wegener Institute Helmholtz Centre for Polar and Marine Research, Am Handelshafen 12, D-27570 Bremerhaven, Germany
[n] Institute of Environmental Science and Technology and Department of Geography, Universitat Autònoma de Barcelona, 08193 Bellaterra, Spain
[o] Laboratoire de Glaciologie et Géophysique de l'Environnement, UJF, CNRS, 54 rue Molière, 38402 St Martin d'Hères, France
[p] Centre for Past Climate Studies, Department of Geoscience, Aarhus University, Høegh-Guldsbergs Gade 2, Aarhus C DK-8000, Denmark
[q] Institució Catalana de Recerca i Estudis Avançats (ICREA) and Institut de Ciència i Tecnologia Ambientals (ICTA), Departament de Física, Universitat Autònoma de Barcelona, 08193 Bellaterra, Spain

ARTICLE INFO

Article history:
Received 5 May 2015
Received in revised form
18 September 2015
Accepted 22 September 2015
Available online 24 October 2015

Keywords:
Last Interglacial
Penultimate deglaciation
Last glacial inception
Chronology

ABSTRACT

The Last Interglacial (LIG) represents an invaluable case study to investigate the response of components of the Earth system to global warming. However, the scarcity of absolute age constraints in most archives leads to extensive use of various stratigraphic alignments to different reference chronologies. This feature sets limitations to the accuracy of the stratigraphic assignment of the climatic sequence of events across the globe during the LIG. Here, we review the strengths and limitations of the methods that are commonly used to date or develop chronologies in various climatic archives for the time span (~140 –100 ka) encompassing the penultimate deglaciation, the LIG and the glacial inception. Climatic hypotheses underlying record alignment strategies and the interpretation of tracers are explicitly described. Quantitative estimates of the associated absolute and relative age uncertainties are provided.

Recommendations are subsequently formulated on how best to define absolute and relative chronologies. Future climato-stratigraphic alignments should provide (1) a clear statement of climate

* Corresponding author. Institut Pierre-Simon Laplace/Laboratoire des Sciences du Climat et de l'Environnement, Bâtiment 12, Domaine du CNRS, Avenue de la Terrasse, 91190 Gif-sur-Yvette, France.
** Corresponding author. British Antarctic Survey, High Cross, Madingley Road, CB3 0ET Cambridge, UK.
E-mail addresses: aline.govin@lsce.ipsl.fr (A. Govin), ecap@bas.ac.uk (E. Capron).
[1] Present address: Institut Pierre-Simon Laplace/Laboratoire des Sciences du Climat et de l'Environnement, UMR 8212, CEA-CNRS-UVSQ, 91190 Gif-sur-Yvette, France.
[2] Also at Vrije Universiteit Brussel, Belgium.
[3] Present address: Institute of Speleology – Romanian Academy, Clinicilor 5, PO Box 58, 400006 Cluj-Napoca, Romania.
[4] Both authors contributed equally to this work.

http://dx.doi.org/10.1016/j.quascirev.2015.09.018

Corals
Speleothems
Ice cores
Marine sediments
Peat and lake sediments
Climate dynamics

hypotheses involved, (2) a detailed understanding of environmental parameters controlling selected tracers and (3) a careful evaluation of the synchronicity of aligned paleoclimatic records. We underscore the need to (1) systematically report quantitative estimates of relative and absolute age uncertainties, (2) assess the coherence of chronologies when comparing different records, and (3) integrate these uncertainties in paleoclimatic interpretations and comparisons with climate simulations.

Finally, we provide a sequence of major climatic events with associated age uncertainties for the period 140–105 ka, which should serve as a new benchmark to disentangle mechanisms of the Earth system's response to orbital forcing and evaluate transient climate simulations.

1. Introduction

Based on eustatic sea level variations, the Last Interglacial (hereafter LIG) covers approximately the time interval between 129 and 116 thousand of years (hereafter ka) (Dutton and Lambeck, 2012; Masson-Delmotte et al., 2013). The LIG appears exceptionally warm in the Antarctic EPICA Dome C (EDC) ice core in the context of the past 800 ka (e.g. Masson-Delmotte et al., 2010b) and in many marine sediment records (e.g. Lang and Wolff, 2011). It is characterised by atmospheric concentrations of greenhouse gases close to pre-industrial levels (Loulergue et al., 2008; Lüthi et al., 2008), particularly high boreal summer insolation values (Laskar et al., 2004), and a global mean sea level up to 5–10 m above present-day (e.g. Kopp et al., 2009; Dutton and Lambeck, 2012; Masson-Delmotte et al., 2013; Dutton et al., 2015). The LIG represents therefore an excellent case study to investigate climate feedbacks shaping the response to orbital forcing as well as the response of ice sheets and ocean circulation to polar warming.

This context has motivated an increased focus on the LIG through new paleoclimate records, recent data compilations (e.g. Turney and Jones, 2010; McKay et al., 2011; Capron et al., 2014) and climate simulations performed with state-of-the-art General Circulation Models (e.g. Bakker et al., 2013; Lunt et al., 2013; Otto-Bliesner et al., 2013). However, climatic feedback mechanisms and the sequence of events over this time period remain only partly unveiled (e.g. Cheng et al., 2009; Masson-Delmotte et al., 2010b; Landais et al., 2013). This lack of understanding represents a major source of uncertainty for estimating global mean temperature change during this period, so far estimated to be less than 2 °C above pre-industrial (Masson-Delmotte et al., 2013; Otto-Bliesner et al., 2013; Bakker and Renssen, 2014).

Key limitations arise from the scarcity of suitable radiometric dating techniques and the lack of precise absolute age constraints such as dated tephra layers and magnetic excursions, which prevents the definition of accurate and independent age models for most records during the LIG. As a result, indirect approaches are used and LIG chronologies are often based on record alignment strategies, i.e. one record on a depth-scale is aligned onto a "dated reference" record (whose chronology is derived from radiometric dating techniques – e.g. alignment to speleothem records – or from another climato-stratigraphic alignment – e.g. alignment of a paleoclimatic record of a sediment core to one of another sediment core), assuming simultaneous regional changes for a given climate variable (e.g. temperature). Alignment hypotheses on LIG climate synchronicity can be tested using more recent and well-dated (radiocarbon-dated or layer-counted) material. In the following, we differentiate the terms "synchronisation" and "alignment" when defining relative chronologies. The term "synchronisation" is applied when records are linked through the use of markers with a global (e.g. atmospheric gas composition, ^{10}Be, magnetic events) or regional (e.g. tephra) distribution. We choose to use the term "alignment" when the linking of records relies only on the hypothesis of simultaneous regional changes in a given climatic variable. While coral and speleothem records benefit from radiometric absolute age, the lack of an unequivocal climatic interpretation of tracers such as oxygen (δ^{18}O) and carbon (δ^{13}C) isotopic composition of speleothem calcite complicates the use of these archives as targets in record alignments.

As a consequence, several reference chronologies are currently used with substantial absolute age uncertainties. For instance, an absolute age uncertainty of 4 ka is estimated for the LR04 benthic foraminifera δ^{18}O stack over the LIG (Lisiecki and Raymo, 2005). In addition, age discrepancies have been identified between existing reference chronologies. For example, age differences of several hundreds of years exist between the successive ss09sea (North Greenland Ice Core Project members, 2004), GICC05modelext (Wolff et al., 2010), EDC3 (Parrenin et al., 2007) and the most recent AICC2012 (Bazin et al., 2013; Veres et al., 2013) ice core chronologies over the last glacial inception. Age differences of thousands of years also exist between the Dome F and EDC3 Antarctic chronologies (Kawamura et al., 2007; Parrenin et al., 2007; Fujita et al., 2015). Moreover, different alignment strategies can lead to inconsistencies. For instance, the benthic foraminifera δ^{18}O record of the penultimate glacial-interglacial transition from North Atlantic sediment core MD95-2042 is ~6 ka younger when aligned onto the LR04 benthic δ^{18}O stack than when its sea surface temperature (SST) is aligned onto the Italian Corchia cave calcite δ^{18}O (Drysdale et al., 2009). Finally, alignment strategies such as transferring marine sediment cores onto ice core and speleothem chronologies rely on specific climatic assumptions that are not always clearly stated or robust.

Altogether, the variety of existing time scales and record alignment techniques lead to some confusion and a general lack of awareness of how chronologies are defined across the penultimate deglaciation and the LIG. As a result, age uncertainties and discrepancies between the reference records have often been overlooked or even completely ignored in data compilations and subsequent model-data comparison exercises. Bakker and Renssen (2014) suggest that the temperature bias introduced by the assumption that data-based LIG maximum temperature are all peaking at the same time could explain, at least partly, the observed current mismatch between the climatic data compiled into one single time slice by Turney and Jones (2010) and recent climate model snapshot simulations from Otto-Bliesner et al. (2013). In addition, a recent LIG data synthesis of ice and marine high-latitude temperature records (Capron et al., 2014) shows that the use of several LIG time slices and of a common temporal framework reduces model-data mismatches. Thus, despite abundance of paleoclimatic sequences around the globe, the inherent difficulties of comparing paleorecords from different depositional realms and the lack of sufficiently precise absolute age may lead to misinterpretations of paleoclimatic signals and still limit robust comparisons with climate model simulations. It is critical to overcome these limitations in order to decipher the nature and pattern of the

full penultimate deglaciation, the course of the LIG and the subsequent return into a glaciated Earth and their link with internal and external forcing.

Apparent age differences are also generated by a lack of rigour in the way these time periods are referred to. The term "Eemian" has been frequently used interchangeably with "Last Interglacial" (e.g. Jessen and Milthers, 1928; Cape Last Interglacial Project members, 2006; NEEM community members, 2013). However, the Eemian is originally defined as the period of forest cover at Amerfoort, the Netherlands (Harting, 1875) and has been extended to other sites using biostratigraphic or climatostratigraphic units, whose boundaries are diachronous across the world (e.g. Hedberg, 1958; Kukla et al., 2002; Shackleton et al., 2003). Other terms often incorrectly used interchangeably are Marine Isotope Stage (MIS) 5e and the isotopic event 5.5 (see the recent review by Railsback et al., 2015). Defined in marine sediments from the $\delta^{18}O$ of foraminifera (Emiliani, 1955; Shackleton, 1969), MIS 5e runs between the midpoints of transitions, and therefore includes not only the LIG climatic optimum but also part of the previous deglacial transition and following glacial inception (Fig. 1). The $\delta^{18}O$ of foraminifera is also a local signal depending on both the local temperature and water $\delta^{18}O$, and departs from a global sea level signal (e.g. Waelbroeck et al., 2008). In contrast, the isotopic event 5.5 was defined in benthic foraminifera $\delta^{18}O$ stack records (Pisias et al., 1984; Martinson et al., 1987) and refers to the very short time interval composed of the two 5.51 and 5.53 isotopic events (Fig. 1), which may occur at different times or be absent in individual foraminifera isotopic records. Definitions of the term "Last Interglacial" vary across studies (see discussion in section 9.2). We do not aim here to provide additional definitions to this time period, but rather to clarify how we use the following terms in our study. For practicality, we employ here the term "acme" to highlight the interval of peak values in a given climate or environmental record that is contained within the LIG. In certain cases, the acme lasts for the entire length of the LIG (e.g. as observed in the global sea level curve and Sanbao speleothem $\delta^{18}O$ record, Fig. 1A and 1D), but in others it only represents a portion of the LIG (e.g. as seen in the benthic $\delta^{18}O$ and EDC ice δD records, Fig. 1B and 1C). In addition, the term "Termination II" has been originally defined as the deglacial period covered by the decrease in foraminifera $\delta^{18}O$ (Broecker and van Donk, 1970). We favour here the use of the term "penultimate deglaciation" against "Termination II" to refer to the climatic transition occurring between full glacial and interglacial conditions (Fig. 1). Thus, in this study, the "penultimate deglaciation" does not strictly refer to the period of ice loss, but to the whole range of changes that leads to, surrounds and includes ice volume changes. Finally, we use the term "last glacial inception" as the time interval occurring from the demise of the LIG acme to the onset of Greenland Stadial 25 (hereafter GS-25, following the recent numbering by Rasmussen et al., 2014) or to MIS 5d extremum in records where glacial millennial-scale variability is not clear (Fig. 1). With this approach, the timing and the duration of the penultimate deglaciation, of the LIG acme and the last glacial inception vary from one record to another (Fig. 1).

This work is an initiative of the Past4Future European project, which has investigated climatic and environmental variations during the last two interglacials (http://www.past4future.eu/). Similarly to the INTIMATE (INTegration of Ice-core, MArine and TErrestrial records) project which proposed protocols to harmonize chronologies of paleoclimatic records over the last 60 ka (e.g. Lowe et al., 2008; Blockley et al., 2012; Brauer et al., 2014), we aim here to increase the awareness of the paleoclimatic community, both on the data and the modelling sides, on the approaches that are commonly used to define chronologies in climatic archives during the penultimate deglaciation, the LIG and the glacial inception. More specifically, we review strengths and limitations of existing absolute constraints, and synchronisation or alignment strategies

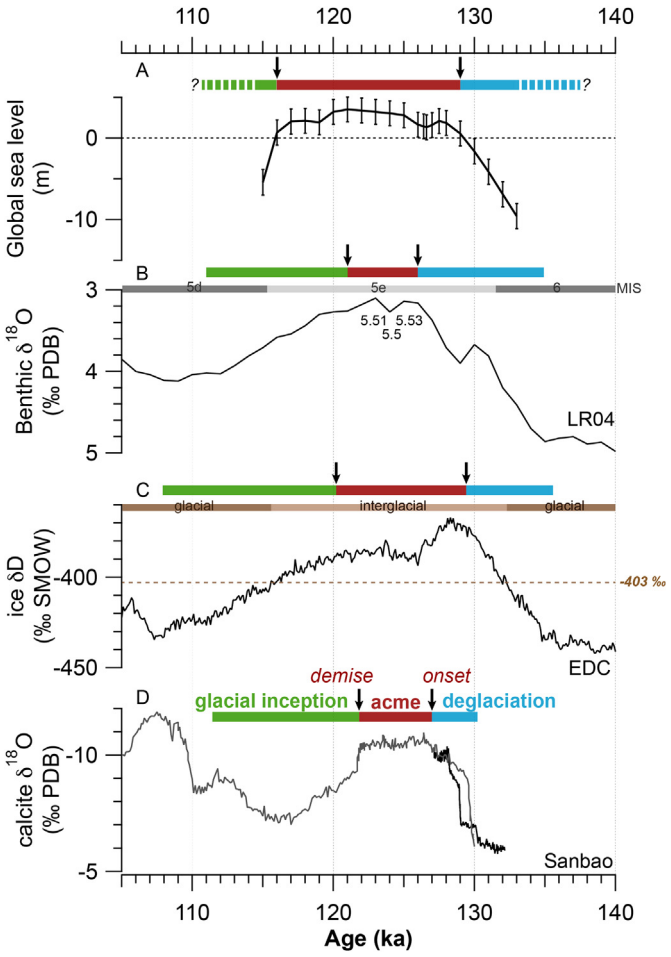

Fig. 1. Illustration of how terms are used in this study based on four records. (A) Global mean sea level (Dutton and Lambeck, 2012; Masson-Delmotte et al., 2013), (B) LR04 benthic foraminifera $\delta^{18}O$ stack (Lisiecki and Raymo, 2005), a tracer integrating global ice volume, and deep-water temperature and seawater $\delta^{18}O$ changes, (C) EPICA Dome C (EDC) ice δD record (Jouzel et al., 2007) presented on the AICC2012 time scale (Bazin et al., 2013; Veres et al., 2013), which is used as a tracer for Antarctic surface temperature and (D) calcite $\delta^{18}O$ record from the Chinese Sanbao (SB23, SB25) speleothems (Wang et al., 2008; Cheng et al., 2009), a tracer for hydrological changes in Asian monsoonal regions. We use here the terms "acme" to highlight the interval of peak values observed in a given paleoclimatic record (red bar), "onset" as the time when the LIG acme starts and "demise" as the time when the LIG acme ends (black arrows). We also use the term "penultimate deglaciation" to refer to the climatic transition occurring between full glacial and interglacial conditions (blue bars), and the term "last glacial inception" (green bars) to refer to the time interval occurring from the demise of the LIG acme to the onset of Greenland Stadial GS-25 (or to MIS 5d extremum in records where glacial millennial-scale variability is not clear, e.g. in B). Concretely, the LIG acme has been delimited here using break points, which were defined through "ramp" regressions with the RAMPFIT software (Mudelsee, 2000) in B, C and D, and by using the 0 m sea level value in A (following Masson-Delmotte et al., 2013) (see Fig. 13 and Table S8). Note that these criteria constitute pragmatic choices that allow us to illustrate the terminology used in the text, and are not necessarily recommendations. With this approach, the LIG acme may, depending on records, last for the entire length of the LIG (e.g. A, D) or represent a portion of the LIG (e.g. B, C). For instance, in marine sediments, this delimitation of the LIG acme is different from the definition of (1) Marine Isotope Stage MIS 5e (defined by midpoints of foraminifera $\delta^{18}O$ transitions in marine sediments, see grey bars in B) (following Shackleton, 1969) and of (2) the isotopic event 5.5 (composed of the two 5.51 and 5.53 isotopic events defined in benthic foraminifera $\delta^{18}O$ stacks, see B) (Pisias et al., 1984; Martinson et al., 1987). In ice cores, our approach differs from the one based on the −403‰ δD threshold value (brown bars and horizontal dotted line in C) (EPICA Community members, 2004). These four examples (A–D) highlight the fact that, with this approach, the timing and duration of the penultimate deglaciation, of the LIG acme and of the last glacial inception vary from one record to another.

used in marine (corals, sediments) and terrestrial (speleothems, ice cores, lake and peat sediments) archives (see Fig. 2 and Table S1 for site locations), and provide recommendations on how to best derive LIG chronologies in climatic archives. Hence, we describe per type of archive (sections 2–6) the hypotheses underlying the classical alignment methods, the common interpretation of parameters used to determine age models and the quantitative estimate of absolute and relative age uncertainties. We discuss the strengths and limitations of climato-stratigraphic alignments using examples (section 7) and present how magnetic stratigraphy could strengthen the available LIG stratigraphic inventory (section 8). Finally, we propose a sequence of major climatic events with related age uncertainties across the penultimate deglaciation, the LIG period and the last glacial inception (section 9).

2. Absolute dating of aragonitic corals

Dating fossil shallow coral reefs is critical for assessing the timing and magnitude of sea level changes during the penultimate deglaciation, LIG and last glacial inception (e.g. Stirling et al., 1998; Thompson and Goldstein, 2005). Of course, major uncertainties concerning the elevation/bathymetry of paleosea-levels arise from isostatic and tectonic effects, as well as from the precise bathymetric distribution of dated corals (e.g. Kopp et al., 2009; Dutton and Lambeck, 2012; Masson-Delmotte et al., 2013). In the present study, we will strictly refer to dating uncertainties. We therefore summarize here the most recent understanding of potential and limitations with respect to the use of U-series ages in scleractinian (i.e. aragonitic) corals for documenting LIG boundaries, relative sea-level changes and climate instabilities. We refer the reader to the reviews by e.g. Bourdon et al. (2003) and Hillaire-Marcel (2009) for full information on all aspects of U-series dating (also see Figure S1). High amounts (about 2–4 ppm) of uranium (U) from seawater (henceforth the "authigenic" uranium) are incorporated into such scleractinian coral skeleton (e.g. Swart and Hubbard, 1982; Cheng et al., 2000). This results in easily measurable amounts of daughter isotopes (^{230}Th in particular) for the calculation of radiometric ages. It also makes such fossil carbonates less sensitive to minor diagenetic effects on the ^{238}U-^{234}U-^{230}Th and ^{235}U-^{231}Pa decay series. Comparatively, most of the uranium found in calcitic corals and other biogenic carbonates, including aragonitic mollusk shells, originates from diagenetic processes, and cannot provide sufficiently precise time series for the LIG (e.g. Zazo et al., 2002). Thus, we focus below on the U-series dating of scleractinian corals and its intrinsic limitations.

2.1. Age calculation and its intrinsic uncertainties

In recent years, most ages have been obtained through high precision TIMS or MC-ICP-MS measurements and are generally given with a ±2σ uncertainty. Earlier, they were mostly obtained through alpha particle counting and generally cited with a ±1σ uncertainty. Some vagueness persists with respect to the way quoted uncertainties include or not all potential sources of analytical errors (internal vs. external precision), which makes direct comparison of databases somewhat hazardous. Efforts are on their way for the selection of standard material to be calibrated and distributed between laboratories as a mean to define effective overall analytical uncertainties in each laboratory. Meanwhile, some caution is recommended with respect to the interpretation of error bars cited with published ages.

Moreover, radiometric age equations include decay constants of all concerned isotopes, which are known with some uncertainty (Table S2). The comparison of such U-series ages to any other time scale, such as glaciological ages, astronomically-tuned ages and other radiometric ages (e.g. ^{39}Ar–^{40}Ar, ^{14}C), requires the U-series decay constant uncertainties to be carried into the final age error calculation. Within the age range of LIG marine corals, these uncertainties correspond to potential age differences up to about ± 0.8 or ± 1.3 ka (within a 95 % confidence interval) for the U-series time scale vs. absolute time, depending on the statistical approach used to assess them.

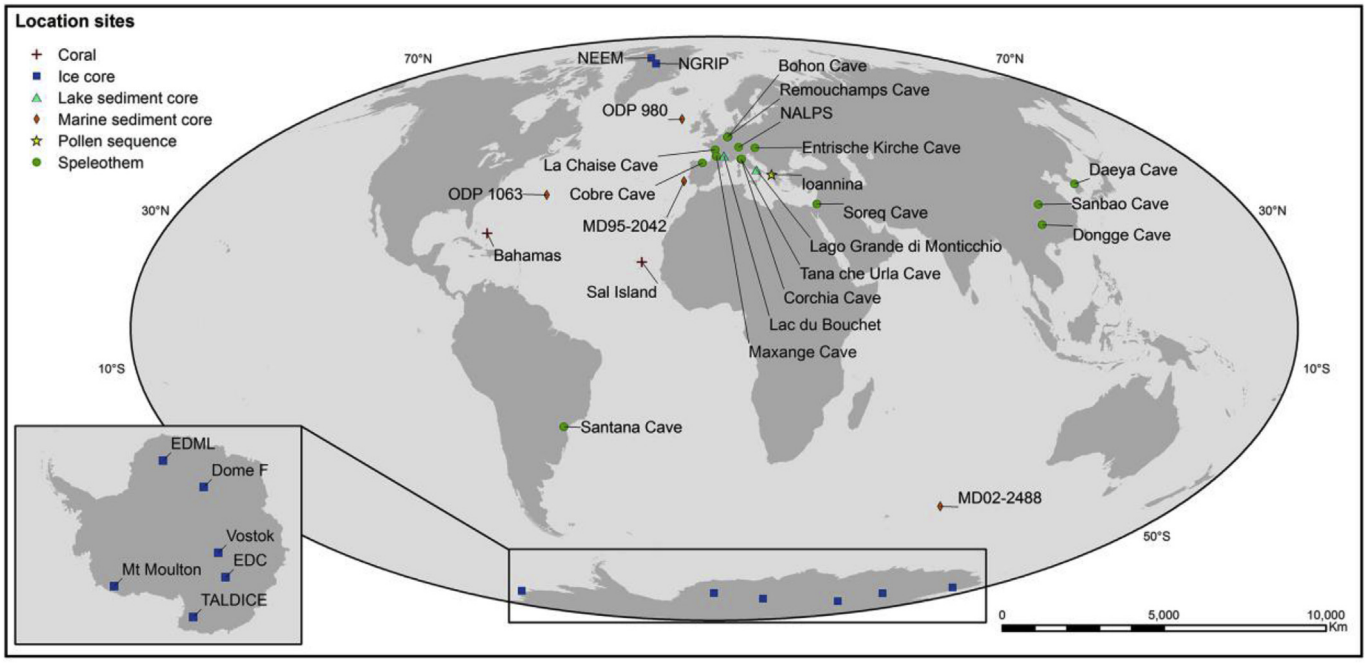

Fig. 2. Location of sites included in this study (see Table S1 for coordinates and references): coral (brown cross), ice core (blue square), lake sediment (turquoise triangle), marine sediment (red diamond), pollen sequence (yellow star), and speleothem (green dot).

2.2. Chemical and "physical" closure of the system

Although scleractinian corals are rich in authigenic U, bias in U-series age calculations can arise from diagenetic processes. Two categories of processes might be considered here. The first one is essentially linked to the behaviour of U under reduced vs. oxidizing conditions resulting respectively in potential gains of diagenetic U or losses of authigenic U through time (a process often associated with the transformation of aragonite into calcite, e.g. Chiu et al., 2005). The second process, is less clearly understood, but often documented in the literature as U-decay series isotope behaviours in biogenic carbonate. It shows time-dependent enrichments in ^{234}Th-^{234}U and ^{230}Th, eventually leading to excesses in ^{234}Th-^{234}U and ^{230}Th, respectively above ^{238}U and ^{234}U, through time (e.g. Hillaire-Marcel et al., 1986). Both processes result in age offsets in corals (Mey, 2008; Hillaire-Marcel, 2009). To illustrate such processes, Thompson et al. (2011) used two superimposed bodies of reef coral, I and II, from the Bahamas (Fig. 3). By plotting the calculated U-series age vs. the initial ^{234}U/^{238}U for all samples from both reefs, they proposed to use linear trends trough reef I and reef II clusters, to correct for the diagenetic process leading to the addition of daughter isotopes to fossil coral skeletons (Fig. 3). The authors argue that 70 %–80 % of the observed age variability for a given reef body can be explained by these trends, i.e. by diagenetic processes (Thompson et al., 2011). The remaining 20–30 % of the observed variability, which is shown by the dispersion of multiple analyses of the same individual coral, is attributed to some chemical uranium mobility (Fig. 3). Algorithms have been proposed to derive open-system ages based on variable assumptions (e.g. Thompson and Goldstein, 2005; Goy et al., 2006). Generally, such model ages lead to uncertainties of several thousand years when estimating a "corrected age" within the LIG time frame (see examples and discussion in Goy et al., 2006 or Carboni et al., 2014).

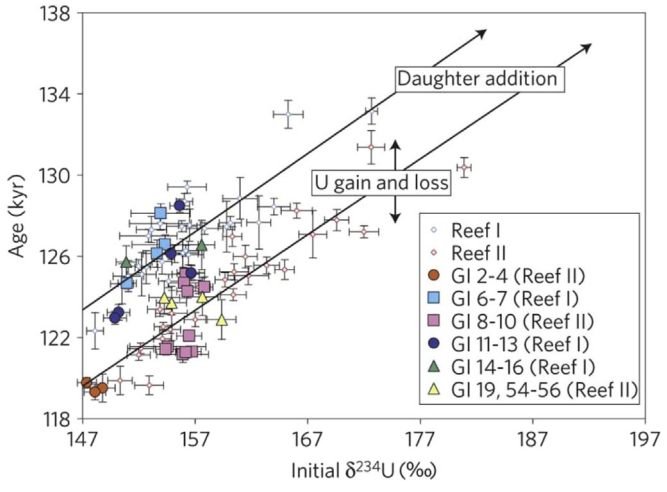

Fig. 3. Example of U–Th age clusters from LIG corals of the Bahamas assigned to two distinct reef units (Figure reprinted by permission from Macmillan Publishers Ltd: Nature Geoscience (Thompson et al., 2011), copyright 2011). Calculated U-series ages are plotted against the initial ^{234}U/^{238}U ratio (in delta notation, relative to the secular equilibrium value of 1) of authigenic U for different individual corals from reef I (small blue symbol) and reef II (small red symbol). The variability within the reefs (linear regressions) marks the presence of diagenetic processes that led to the addition of daughter isotopes in fossil coral skeletons. In contrast, large symbols represent discrete pieces of the same individual coral, which must be the same age for each individual, and the dispersion of such discrete measurements indicates U mobility in individual corals. Whereas a detailed statistical analysis might support some bimodal distribution, any attempt at deriving more precise ages would be speculative. Thompson et al. (2011) use the linear regression plotted to "correct the ages for diagenetic disturbance of the U–Th isotope ratios". However, aside the statistical large uncertainty of the y-intercepts of these linear trends, it is clear that one could not put forth any single diagenetic mechanism, with continuous rate through time, which would explain a linear redistribution of data.

Thus, the most suitable situation is when dating corals with a U-series isotope evolution is exclusively controlled by in-situ radioactive decay processes, i.e. the so-called "closed system" situation. Note that this expression generally refers to a chemically closed system (i.e. without any diagenetic U-fluxes). It does not fully cover the issue of discrete processes that are related to U-decay series isotope behaviours and lead to long-term enrichments in ^{234}Th-^{234}U and ^{230}Th, as evoked above. Furthermore mineralogical stability might not be proof of a chemical closure (Pons-Branchu et al., 2005). Calcite may be produced when grinding samples (e.g. Labonne and Hillaire-Marcel, 2000). The most unquestionable way to document such "closed systems" consists in confronting two distinct chronometers in so-called "concordia" or "pseudo-concordia" approaches (Edwards et al., 1997; Cheng et al., 1998). Here, concordias may be set from ^{231}Pa/^{235}U vs. ^{230}Th/^{234}U-^{238}U chronometers (Figure S1). As the ^{238}U/^{235}U ratio is practically constant at the U-series disequilibria time scale in most sedimentary settings (see Andersen et al., 2014 for examples of potential offsets), ^{231}Pa/^{235}U vs. ^{230}Th/^{234}U-^{238}U ages may be obtained directly from ^{231}Pa, ^{230}Th, ^{234}U, ^{238}U measurements. Whereas ^{231}Pa/^{235}U ages can be calculated straightforwardly, the calculation of the ^{230}Th-^{234}U-^{238}U age requires the assumption of a constant initial ^{234}U/^{238}U ratio for the authigenic uranium. As the seawater ^{234}U/^{238}U ratio has likely varied only within 1.5 % of its present activity value (~1.145) over the last 360 ka (Henderson, 2002), this condition might be seen as fulfilled in LIG scleractinian corals. ^{231}Pa- and ^{230}Th ages calculated accordingly should be concordant in a chemically closed radioactive system (see Fig. S1 for details). Unfortunately, the precision achieved for ^{231}Pa measurements is not comparable to that of ^{230}Th. Adding uncertainties about the initial ^{234}U/^{238}U composition of the coral uranium and the decay constants involved, ^{231}Pa/^{235}U vs. ^{230}Th/^{234}U-^{238}U concordia ages lack precision, especially within the LIG time range (i.e. when activity ratios of ^{231}Pa/^{235}U get closer to the secular equilibrium value) and therefore cannot be used in a straightforward manner to ascertain a closed system.

Most authors will follow a "pseudo-concordia" approach, which is based on the combination of information from several isotopes from the ^{238}U decay-series. For example, they will use ^{234}U/^{238}U vs. ^{230}Th/^{234}U ratios, hypothesize an initial ^{234}U/^{238}U ratio identical to that of the modern ocean, and assume, when data fall on the "pseudo-concordia" curve (e.g. Fig. 4), that the coral has secured a "closed system". Adding ^{226}Ra (the daughter of ^{230}Th, Fig. S1) measurements provides information on the last ~50 ka history of the samples, and as illustrated in Fig. 4, such measurements point to almost systematic offsets from perfect "pseudo-concordia" curves, either due to some Ra and likely U chemical mobility, or simply in relation with the slow ^{230}Th, ^{234}Th-^{234}U enrichment process evoked above. Of course, any earlier partially open system (prior to ~50 ka) could not be documented by this ratio. However, departures from closed conditions might still be shown by ^{234}U/^{238}U departure from ^{234}U/^{238}U vs ^{230}Th/^{234}U pseudo-concordia (e.g. Hillaire-Marcel, 2009). U/Ca variability along growth layers may also shed more light on the behaviour of U in fossil corals, especially the preservation of the seasonal signature or its blurring through U-mobility in the sample.

2.3. Detrital and taphomomical contaminations

Large coral colonies are generally easy to clean mechanically. Solitary corals might be more difficult to clean (e.g. Goy et al., 2006). Often, taphonomical evolution results in more or less

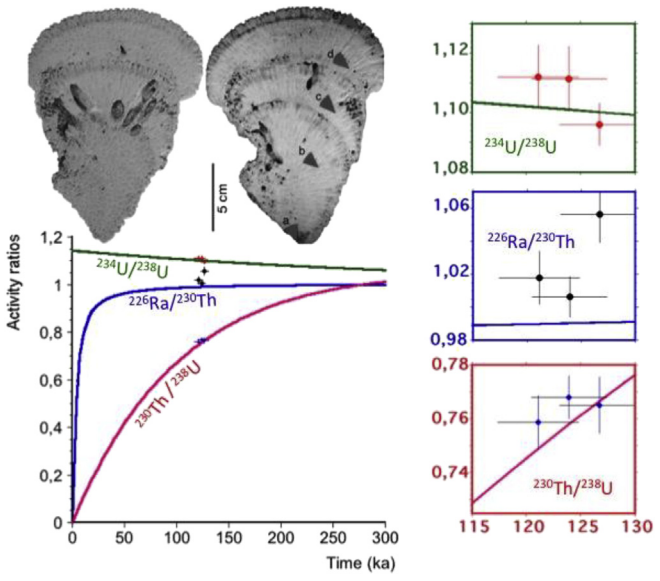

Fig. 4. Detailed measurements in a LIG specimen of *Siderastrea radians*, a scleractinian coral from Sal island (Cabo Verde) still of pristine aragonite (top left) (Zazo et al., 2010). Data are plotted with their ± 2σ error. Bottom left: evolution of $^{226}Ra/^{230}Th$, $^{230}Th/^{238}U$ and $^{234}U/^{238}U$ activity ratios through time in a closed system, assuming a constant initial $^{234}U/^{238}U$ ratio of ~1.14 for the authigenic U. On the right, blow up of measured values vs. theoretical decay curves. It evidences an unequivocal deviation of $^{226}Ra/^{230}Th$ from a totally closed system decay calculation (see section 2).

discrete contaminations of samples (due mostly to burrowing organisms, as illustrated by the second generation *Siderastrea radians* in Fig. 4).

Correction for this detrital contamination is usually based on the use of ^{232}Th as a tracer of the contaminating fraction (e.g. Lao et al., 1993; Henderson and Anderson, 2003). The knowledge of activity ratios between ^{238}U-series isotopes linked to this detrital fraction and its ^{232}Th is critical in order to subtract this fraction from the total ^{238}U and daughter isotope content analysed in order to calculate ages (e.g. Ludwig and Paces, 2002). When physical cleaning of coral samples fails to remove all contaminating fraction, the most suitable approach consists in making several measurements in any given sample as a means to calculate an isochron age (e.g. Ludwig, 2003). This supposes that if each sub-sample contains variable proportions of contaminant vs. authigenic ingrowth fractions, all should depict narrowly clustered isotopic composition of this contaminating fraction. Note that potential analytical artefacts may occur through chemical cleaning and leaching procedures (e.g. Hillaire-Marcel and Causse, 1989). There is yet another less precise but easier way to put constraints on the isotopic composition of the detrital fraction when several specimens from a given site, collected in a given stratigraphic order, yield clustered ages (e.g. LIG, Holocene). It consists in assuming that all samples contain a similar detrital fraction, isotopically speaking, and in calculating through iterations ages fitting with the stratigraphic order observed. This approach has been used for speleothem studies (e.g. Hellstrom, 2006) but might in favourable cases also apply for the dating of corals. Note that any contamination of fossil coral by an aragonitic micrite would not be captured by this approach based on ^{232}Th-labelled contaminating fractions. Nevertheless, whatever the approach used to correct for the detrital contamination of samples, a robust statistical assessment of an isochron age, as proposed by Ludwig and Titterington (1994), results usually in a very large uncertainty (several times the calculated error of any given sample within the LIG time range, e.g. Carboni et al., 2014).

2.4. Recommendations and perspectives

The limitations listed above are a substantial source of uncertainty in the comparison of existing records. Achieving a millennial or sub-millennial resolution for the dating of corals of LIG age is currently out of reach. The best resolution achievable is illustrated by clusters around two high LIG sea level stands observed in several studies (e.g. Kopp et al., 2009; Thompson et al., 2011). Reconciliation of this modal distribution with continuous times series (e.g. speleothems, marine cores) may be achievable with a more careful assessment of the relative closure and contamination of samples. Isochron ages on specimens with near-expectation $^{226}Ra/^{230}Th$ and $^{234}U/^{238}U$ activity ratios might reveal the most effective way to do it. From a methodological point of view, a much better understanding of the behaviour of actinides in biogenic carbonates would be gained either with more precise ^{231}Pa-^{235}U ages, or the possibility to run a series of measurements in a given sample through laser ablation and MC-ICP-MS measurements. Future generation of instruments should offer this possibility.

3. Dating of speleothems

Speleothems currently provide the best-dated material to investigate changes in terrestrial climate across the penultimate deglaciation and the LIG. Absolute dates obtained on speleothems might also offer a tool to improve the chronologies of ice cores and marine sediments, assuming that the measured tracers are well understood and represent similar and in-phase climatic events in the different archives (e.g. Drysdale et al., 2009; Barker et al., 2011). Here, we address the absolute and relative age constraints available for speleothems, as well as the related uncertainties. Then, we describe how speleothem records might be used as alignment targets for other archives and the difficulties that arise when performing such exercises, in particular related to the current limitations attached to the interpretation of measured climate and environmental tracers.

3.1. Absolute dating and stratigraphic markers

Speleothems have the advantage of being absolutely dated over the last 600 ka with the U–Th methodology (Hellstrom, 2006) (see section 2 for details and limitations of the U-series dating method). Stalagmites are preferred over other speleothems (e.g. stalactites) because the deposition of calcite at a single location (the stalagmite apex) leads to a well-structured and generally continuous sedimentological profile. Speleothems also offer up to intra-annual time resolution when seasonal layering is present (Baker et al., 1993; Shopov et al., 1994). Layer counting is used to refine the chronology of U–Th dated speleothems (Domínguez-Villar et al., 2012). Although layering has been observed in LIG speleothems (S. Verheyden, unpublished results), layer counting has only been used so far in speleothems covering the Holocene.

Currently, U–Th dating leads to dating uncertainties better than ~0.5 % (Dorale et al., 2004; Li et al., 2005; Cheng et al., 2009), which corresponds to a typical 2σ error of ~1.0 ka for LIG speleothems (e.g. Kelly et al., 2006; Drysdale et al., 2009; Jo et al., 2011). However, higher uncertainties of up to several thousands of years are not rare and mostly related to detrital Th incorporation (e.g. in post LIG speleothems from Entrische Kirche cave, Austrian Alps, Meyer et al., 2012) or to post depositional alteration (e.g. in a LIG speleothem from Corchia cave, Italy, Drysdale et al., 2004). Improved elemental separation techniques, better instrumentation, well-suited speleothems (i.e. with high U content, low detrital content, no alteration and high growth rates) can lead to particularly precise ages with 2σ errors lower than 0.1 ka, as obtained in the Chinese

speleothem from the Sanbao cave during the penultimate deglaciation (Cheng et al., 2009).

Increasing dating precision requires sampling with a minimal time-window that is laterally broad but as small as possible along the growth axis, in order to avoid that the sampling uncertainty (i.e. the entire deposition period covered by the sample) increases the analytical error associated with the age determination. For MC-ICP-MS dating, 100–400 mg of powder is generally needed depending on the U content of the calcite. The U content varies from one cave to the other due to variations in U-content of the host rock. Dated samples characterised by high (low) U content and high (low) growth rate can cover a few years (several hundreds of years). For example, a sample taken over ~2 mm along the growth axis of a speleothem with a growth rate of ~0.5 mm/century will cover 400 years, getting close to the analytical uncertainty in some cases. Therefore, besides a high U content and low detrital Th content, high speleothem growth rate is an essential prerequisite for obtaining precise ages.

Changes in the growth rate through time may also lead to an important "accordion effect" in the depth-age relationship along the speleothem. Indeed, the growth rate, which is mostly controlled by the calcium content of dripping water and the drip rate (Baker et al., 1998; Dreybrodt, 1999), can vary from 0 to a few μm/a during cold and dry periods and reaches more than 1 mm/a during warmer and more humid climate intervals (Genty and Quinif, 1996; Baker et al., 1998; Genty et al., 2001; Verheyden et al., 2006). Such an effect should be taken into account when discussing chronologies based on linear interpolation between absolute dates. In the future, acquiring many precise radiometric dating and petrographic observations is hence necessary to obtain detailed growth rate records, which, in addition to providing useful climatic information, help to enhance the confidence in interpolated chronologies. Algorithms to calculate growth rate curves, including the error on intermediate ages are currently in development (Scholz and Hoffmann, 2011; Breitenbach et al., 2012) but have still some difficulties to correctly handle hiatuses (Scholz et al., 2012).

Juvigné and Gewelt (1988) observed the presence of tephra minerals such as pyroxenes and amphiboles in a stalagmite from the Remouchamps cave (Belgium) and related them to the Rocourt Tephra (Gullentops, 1954), dated around 90–74 ka (Pouclet et al., 2008). Another "tephra of Remouchamps" dated at 106 ± 6 ka (Gewelt and Juvigné, 1986) was observed in speleothems from the Remouchamps and Bohon caves (Belgium) but never identified in surface deposits. Frisia et al. (2008) related sulphate concentration peaks in recent speleothems to historically known eruptions. Badertscher et al. (2014) also suggested that bromine is the ideal volcanic tracer in speleothems, regarding its rapid transfer from the atmosphere to the cave, which is not always the case for sulphate. Tephra layers in speleothems are so far largely understudied and using them in climatic alignments with other archives would require a precise identification of the tephra layer, which might be difficult to achieve unequivocally. However, the close link recently suggested between the presence of bromine, molybdenum and sulphur recorded in speleothems and volcanic ashes (Baldwin and Frappier, 2008; Badertscher et al., 2014) still opens interesting perspectives.

3.2. Aligning other archives to speleothem records

High-resolution records and precise dating of speleothems led recent studies to adjust the chronologies of marine sediments and ice cores by using climatic alignments to the most common tracer measured on speleothems, calcite $\delta^{18}O$ (e.g. Drysdale et al., 2009; Barker et al., 2011; Buizert et al., 2015; Jiménez-Amat and Zahn, 2015). This approach requires having a good understanding of the dominant drivers of calcite $\delta^{18}O$ (Table 1) to argument sufficiently the "climatic" link between calcite $\delta^{18}O$ and the tracers measured in other archives. Changes in temperature, rainfall amount and rain sources are the dominant drivers (Table 1). These changes are often interconnected and the dominant climatic parameter (e.g. temperature vs. rainfall amount) may differ from one speleothem to another, explaining the observed variability in speleothem records (see Lachniet (2009), Fig. 5, Table 1). Moreover, opposite influences of surface air temperature and the directly related cave air temperature on calcite $\delta^{18}O$ explain the important amplitude of the variability and sometimes nearly absent glacial-interglacial changes observed in speleothem $\delta^{18}O$ records. High variability is particularly visible in European speleothems where the relative importance of the temperature effect (compared to rainfall $\delta^{18}O$ effect) is larger than in speleothems from monsoon areas (Fig. 5, Table 1).

Based on the high similarity of marine and continental paleoclimate changes recorded in the Middle East region, and the fact that the Eastern Mediterranean Sea is today the main source of moisture for rainwater controlling cave water and thus calcite $\delta^{18}O$, Bar-Matthews et al. (2003) aligned Eastern Mediterranean planktonic foraminifera $\delta^{18}O$ records to Israel speleothem $\delta^{18}O$ records over the last 250 ka. Alignments between marine and speleothem records have also been produced in Asian monsoonal areas. For instance, Caballero-Gill et al. (2012) aligned the planktonic $\delta^{18}O$ record from a northern South China Sea core to the Chinese Hulu and Sanbao speleothem $\delta^{18}O$ records over the last 350 ka. Although a more detailed investigation on the climatic relation between the $\delta^{18}O$ of both archives is certainly useful, alignment between planktonic $\delta^{18}O$ and $\delta^{18}O$ of speleothems formed by rainwater originating from the region where foraminifera grew up seems relevant. Well-dated Asian speleothem records have also been used as targets, both on glacial-interglacial and millennial time scales, to refine ice core chronologies (e.g. Barker et al., 2011; Buizert et al., 2015). Similarities are observed between the variability expressed on millennial to precessional time scales in Asian speleothem $\delta^{18}O$ records and in global atmospheric composition (CH_4 and $\delta^{18}O_{atm}$ of trapped air in ice cores) (e.g. Wang et al., 2008; Landais et al., 2010). The underlying mechanisms may, however, be complex and involve the overall impact of associated climate variability on methane production and changes in precipitation isotopic composition used for biosphere oxygen production, and the net effect of possible contrasted changes in each hemisphere (e.g. Cruz et al., 2006; Jo et al., 2014).

Asian calcite $\delta^{18}O$ variations are interpreted as changes in monsoon intensity commonly explained by latitudinal shifts in the position of the inter-tropical convergence zone and of tropical rainfall belts (Wang et al., 2001, 2006). Asian records show relatively similar variations throughout the large climatic changes during the penultimate deglaciation and the last glacial inception (Fig. 5). They also exhibit millennial-scale climatic variability which led to the identification of East Asian Monsoon events that are likely related to Greenland Interstadial (GI) events (Cruz et al., 2006; Wang et al., 2008; Cheng et al., 2009; Jo et al., 2011) (Fig. 5). These similarities have been used to create a WAIS Divide ice core chronology (WD2014) based on GICC05 adjusted through alignment with the Hulu cave speleothems (Buizert et al., 2015), and to suggest a way of improving the EDC3 chronology (already including one speleothem alignment during the penultimate deglaciation, Parrenin et al., 2007) by using further absolute dates from the Hulu and Sanbao caves (Barker et al., 2011). Modelling work suggests that the atmospheric readjustments during monsoon intensity changes occur on decadal timescales in response to Northern Hemisphere high-latitude forcing (e.g. Chiang and Bitz, 2005; Cvijanovic and Chiang, 2013). But a precise

Table 1
Interpretation of main speleothem proxies and selected records offering continuous series, relatively high temporal resolution and chronologies, and covering the penultimate deglaciation and the LIG.

Tracer	Interpretation	Selected LIG cave records
Calcite $\delta^{18}O$	Monsoon areas: low calcite $\delta^{18}O$ values indicate more intense monsoons, higher summer monsoon rainfall contribution, or less extra-tropical contribution. Temperate areas: calcite $\delta^{18}O$ is sensitive to precipitation $\delta^{18}O$ (itself potentially related to temperature and precipitation effects, including precipitation seasonality), to cave temperature effects, and it can also be affected by climate-sensitive kinetic effects (section 3).	Dongge (Yuan et al., 2004; Kelly et al., 2006) SanBao (Wang et al., 2008; Cheng et al., 2009) Santana (Cruz et al., 2006) Corchia (Drysdale et al., 2005, 2007; 2009) Tana che Urla (Regattieri et al., 2014b) La Chaise BDinf (Couchoud et al., 2009) Soreq (Bar-Matthews et al., 2003)[a]
Calcite $\delta^{13}C$	Plant type changes (C3, C4) in some areas. When only one plant type is present, low calcite $\delta^{13}C$ values are generally associated to higher soil and vegetation activity, itself enhanced with warmer temperatures in the absence of water stress.	Santana (Cruz et al., 2006) Tana che Urla (Regattieri et al., 2014b)
Growth rate	High growth rates generally indicate warm and wet conditions.	La Chaise BDinf (Couchoud et al., 2009) Maxange (unpublished results from Genty and Wainer) Tana che Urla (Regattieri et al., 2014b) Corchia (Drysdale et al., 2005, 2007; 2009)
Mg/Ca and Sr/Ca	Multiple factors: e.g. water availability, temperature, organic matter, dust deposition at the surface.	A robust and well-understood high-resolution record is not yet available.

[a] Soreq cave $\delta^{18}O$ record is based on multiple speleothems (Bar-Matthews et al., 2003).

assessment of the synchronicity hypothesis based on high-resolution records from speleothem and ice cores is still missing.

In contrast, whereas calcite $\delta^{18}O$ records from European speleothems display clear changes during the penultimate

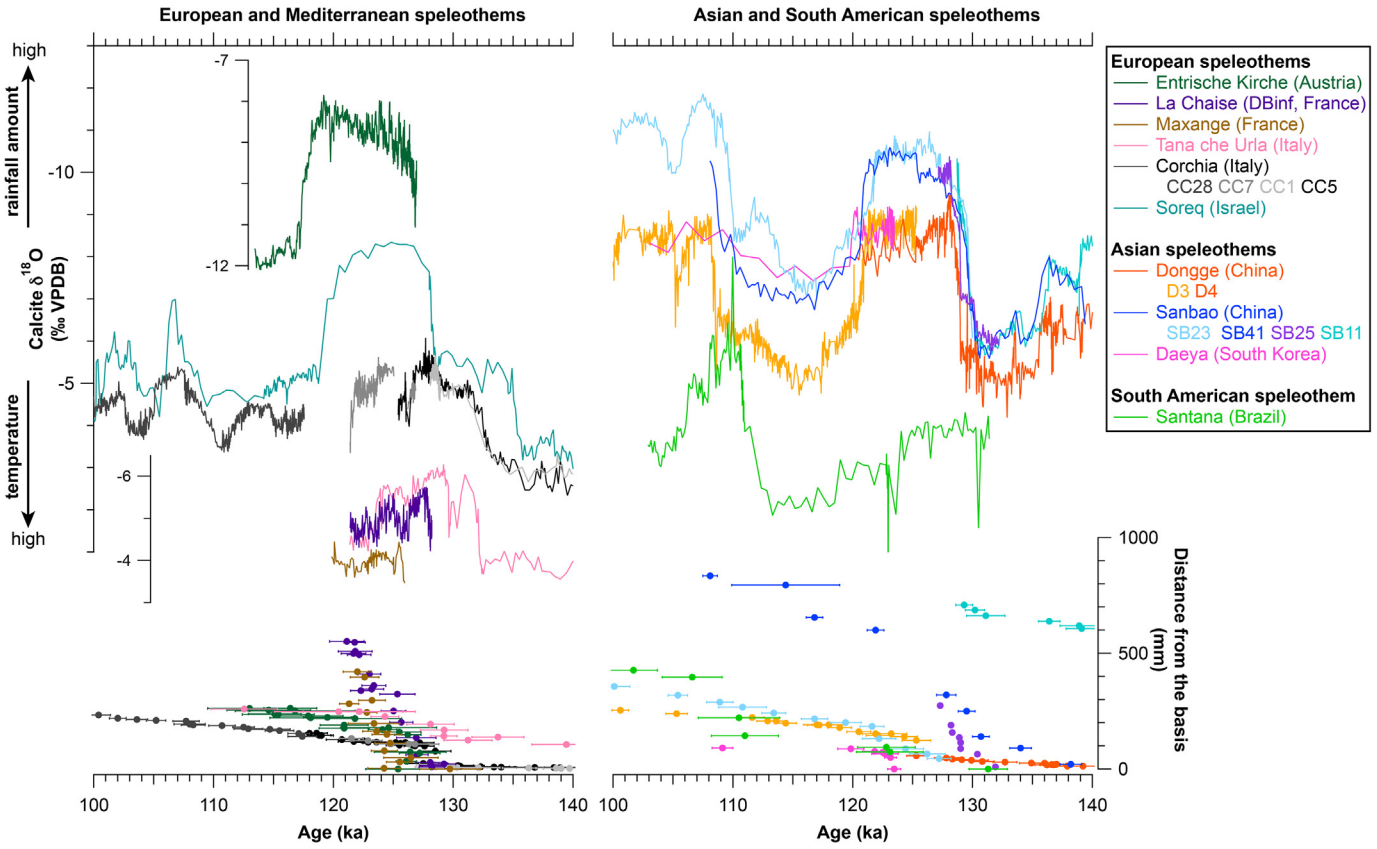

Fig. 5. Calcite $\delta^{18}O$ (top) and growth rate (bottom, with 2σ dating errors) records of selected speleothems for the period 140–100 ka. These speleothems were selected for (1) their high density of high-precision U–Th ages, (2) their relatively high growth rate so that dated samples cover a relatively short time-period and (3) their continuous growth rate over long time-intervals. Selected European and Mediterranean records (left) are from the Entrische Kirche cave (Austria) (Meyer et al., 2008), La Chaise cave (DBinf, France) (Couchoud et al., 2009), Maxange (France) (Genty and Wainer unpublished), Tana che Urla cave (Italy) (Regattieri et al., 2014b), Corchia cave (Italy) (Drysdale et al., 2005, 2009), and Soreq cave (Israel) (Bar-Matthews et al., 2003). For higher clarity, $\delta^{18}O$ records from Maxange, La Chaise and Tana che Urla are plotted on a different Y-axis. The $\delta^{18}O$ record from Entrische Kirche cave is also plotted on a specific (not reversed) Y-axis due to an inverse $\delta^{18}O$-climate relationship compared to other speleothems (Meyer et al., 2008). Selected Asian records (right) are from the Dongge cave (China) (Yuan et al., 2004; Kelly et al., 2006), Sanbao cave (China) (Wang et al., 2008; Cheng et al., 2009), Daeya cave (South Korea) (Jo et al., 2011). The sole South American record covering the entire LIG is from the Santana cave (Brazil) (Cruz et al., 2006). Arrows along the $\delta^{18}O$ vertical axis indicate the general influence of changes in temperature and rainfall amount on speleothem calcite $\delta^{18}O$ (e.g. Lachniet, 2009). See Fig. 2 for site locations.

deglaciation (Bar-Matthews et al., 1997; Drysdale et al., 2005, 2009; Regattieri et al., 2014a), as well as millennial-scale climate variability during the glacial inception (Drysdale et al., 2007; Boch et al., 2011), spatial differences in the timing of the deglaciation highlight the need for more precisely dated records (Fig. 5). Speleothem growth records evidence a relatively synchronous change towards higher growth rate at ~128–127 ka, although south European speleothems seem to start their growth earlier than those from the North. Consequently, European speleothems start to grow when a certain temperature threshold, which may vary regionally, is reached during the deglaciation.

Millennial-scale climate variability recorded in European speleothems at the onset of the last glacial period also exhibits the fingerprint of Greenland ice core events (e.g. Lauritzen, 1995; Plagnes et al., 2002; Muñoz García et al., 2007; Hodge et al., 2008; Boch et al., 2011) (see also section 4.2). Events similar to GS-25 and GS-24.1 are recorded through increases in calcite $\delta^{18}O$ from the CC28 speleothem from Corchia cave between 112.0 ± 0.8 ka and 108.8 ± 1.0 ka and between 105.1 ± 0.9 ka and 102.6 ± 0.8 ka, respectively (Drysdale et al., 2007). While this result could suggest the possibility to align polar and continental climate records on millennial time-scales at the end of the LIG (similarly to MIS 3, Spötl and Mangini, 2002; Genty et al., 2003), only few records are available and additional well-dated and high-resolution speleothem records, in particular from northern Europe, are needed.

The regional discrepancies in the initiation of interglacial conditions, in particular in Europe, illustrate a spatially variable timing of the penultimate deglaciation and the onset of the LIG acme, i.e. a duration of the LIG acme that potentially varies across the world (Fig. 5). Such spatial variability has to be kept in mind when aligning records from other archives to speleothem records. To perform with more confidence such alignments, progress on the interpretation of tracers is necessary as well as further assessments on the phase relationship between climatic events identified in different archives to test the hypothesis of synchronicity. More recent (e.g. < 40 ka) and well-dated (radiocarbon-dated or layer-counted) material could be particularly useful to test whether similar synchronicity is observed between records from speleothems and from other archives during earlier climatic changes.

3.3. Recommendations and perspectives

Only few well-dated and continuous speleothem records cover the LIG at high resolution (Table 1). While speleothems can provide accurate chronologies, their tracers still need to be better understood, based on systematic monitoring of environmental parameters (temperatures, drip rates, pCO_2) and drip water isotopic composition in caves.

Additional high-resolution speleothem time-series are needed in undocumented areas but also in Europe, where records exhibit spatial heterogeneity. Ideally, new records should present growth rates as high as possible and numerous U–Th dating points in order to (1) reduce dating uncertainty, (2) enhance the robustness of radiometric chronologies on centennial to millennial time scales, (3) maximise constraints on the "accordion effect" induced by growth rate changes and (4) optimize the assessment of the synchronicity between records. Analytical developments such as laser sampling for U–Th dating (Hellstrom, 2006; Hoffmann et al., 2009) and improved detrital corrections (Zhao et al., 2009) will help to reduce chronological uncertainties (Hellstrom, 2006).

In the future, calcite $\delta^{13}C$, which depends on the changes in vegetation and soil microbial activity and is hence strongly influenced by temperature (Genty et al., 2003) (Table 1), could complement calcite $\delta^{18}O$ records in alignments with ice core, pollen or SST records. For example, millennial-scale climate variability has been identified in calcite $\delta^{13}C$ records, in particular during MIS 3 and the last deglaciation (Genty et al., 2003; Fleitmann et al., 2009). However, speleothem $\delta^{13}C$ records covering the penultimate deglaciation and the LIG remain scarce and further investigations on their stronger dependence to temperature compared to calcite $\delta^{18}O$ are needed during this time period. Overall, alignment exercises to speleothems should be handled critically with respect to the selection of aligned records and the assumption of synchronously recorded climate events. The development of multi-proxy approaches, including underused tracers such as growth rate, calcite $\delta^{13}C$ or elemental composition (Table 1), is also needed to strengthen the understanding of embedded climate signals and widen alignment possibilities.

Finally, the development of magnetic measurements in speleothems coupled with U–Th radiometry opens new perspectives to transfer the speleothem radiometric chronology to marine sediments and ice cores using magnetic or cosmogenic markers identified in both archives (see section 8).

4. Chronologies in ice cores

Tracers of polar climate, water cycle, aerosol deposition and global atmospheric composition measured in Antarctic ice cores have permitted to explore the sequence of events occurring over the penultimate deglaciation, the LIG and the glacial inception (e.g. Masson-Delmotte et al., 2010a; Landais et al., 2013; Pol et al., 2014). The recent NEEM ice core provides the first Greenland record over the LIG (NEEM community members, 2013). A full climatic exploitation of these records requires a coherent chronological framework. While absolute dating of the LIG is not yet possible from ice core layer counting (Svensson et al., 2011), efforts to quantify and reduce ice core chronological uncertainties are ongoing within the community.

A specificity of ice core age scales is the requirement to date both the ice and the gas, and therefore to produce two consistent chronologies. This is due to the fact that air is completely enclosed into the ice only at about 50–120 m under the ice sheet surface, where the firn has progressively reached the density of ice at the Lock In-Depth (LID). As a result, for a given depth, the air is always younger than the surrounding ice by centuries to thousands of years. This age difference between ice and gas of same depth (called Δage) is not constant along an ice core due to varying surface temperature and accumulation rate through time. This ice-gas offset can also be considered as a depth difference between ice and gas of same age, noted Δdepth. Knowing the temporal evolution of the Δage is essential for establishing reliable links between ice and gas chronologies.

This section focuses on established dating constraints and strategies that can be applied to date the LIG and the penultimate deglaciation. For this purpose, we discuss the new Antarctic ice core reference chronology, AICC2012 (Bazin et al., 2013; Veres et al., 2013) that has been built using the Bayesian tool named "Datice" (Lemieux-Dudon et al., 2010), which combines ice core dating techniques developed over the last decades. We provide an overview and discuss the different stratigraphic constraints and associated dating uncertainties implemented in AICC2012 for the time interval 140–100 ka. Finally, we provide an outlook on potential additional chronological constraints and techniques that could further help to improve polar ice core age scales during the LIG.

4.1. The AICC2012 chronology

4.1.1. Dating strategy

New methodologies based on the idea of an optimal use of the different sources of chronological information and of the various

glaciological constraints were first developed by Parrenin et al. (2001) for the Vostok ice core. Using an inverse approach combining a glaciological ice flow model and chronological tie-points, this methodology has been applied to the EDC ice core to produce the EDC3 chronology (Parrenin et al., 2007) (Table 2), which is currently widely used in paleoclimatic studies. Beyond 70 ka, the EDC3 timescale mostly relies on orbital tuning age markers (atmospheric $\delta^{18}O$ of O_2 ($\delta^{18}O_{atm}$) and air content). Additional absolute age markers were included in particular to constrain the timing of the penultimate deglaciation and the duration of the LIG. For instance, the abrupt increase in CH_4 recorded at the end of the deglaciation was assumed to be synchronous within 2 ka with the abrupt shift in speleothem calcite $\delta^{18}O$ recorded in East Asia and the Eastern Mediterranean regions at 130.1 ± 2 ka (Bar-Matthews et al., 2003; Yuan et al., 2004).

The most coherent ice and gas timescale, AICC2012, has been recently produced over the last 800 ka without speleothem-derived tie points (Bazin et al., 2013; Veres et al., 2013) (Table 2) and is an improvement with respect to EDC3. While EDC3 results from a glaciological model taking into account stratigraphic and age constraints from the EDC ice core only, the Datice tool integrates chronological and glaciological constraints from Vostok, EDC, EDML, TALDICE and NGRIP ice cores to produce AICC2012. Therefore, the AICC2012 chronology represents the best compromise between absolute and relative tie-points, and glaciological constraints (snow accumulation rates and thinning function) for the five ice cores, with the additional goal to be consistent with the Greenland GICC05 reference chronology (Svensson et al., 2008) (Table 2). While earlier ice core gas timescales were based on outputs from firnification models (e.g. Blunier et al., 2007; Loulergue et al., 2007), the Antarctic Δage estimate for AICC2012 was estimated from measurements of $\delta^{15}N$ of N_2 in air bubbles, giving access to a more realistic LID than when estimated by firnification models (Parrenin et al., 2012).

4.1.2. Absolute age markers and stratigraphic links over the LIG

Fig. 6 shows the different types of age markers and associated 1σ uncertainties used to constraint AICC2012 between 140 and 110 ka (lists provided in Tables S3–4, see Bazin et al. (2013) and Veres et al. (2013) for a full description).

The closest absolute age marker constraining the AICC2012 chronology over the LIG is the Mont Moulton tephra layer using a revisited age of 93.2 ± 4.4 ka (Dunbar et al., 2008; Kuiper et al., 2008). All other constraints on absolute ages rely on three different orbital dating approaches that are all independent of Antarctic climate (Table S3, Fig. 6). First, four age markers are inferred from $\delta^{18}O_{atm}$ in the Vostok ice core for the 140–100 ka interval based on the strong relationship between $\delta^{18}O_{atm}$ (which reflects both changes in global ice volume and the hydrological cycle) and mid-June 65°N insolation (Bender et al., 1999; Petit et al., 1999). To account for possible time delays between changes in precession and changes in $\delta^{18}O_{atm}$ (Leuenberger, 1997; Jouzel et al., 2002), a 1σ uncertainty of 6 ka is attached to those orbital gas markers. Second, the elemental ratio $\delta O_2/N_2$ measured in the trapped air displays variations similar to those of the local 21 December insolation in the Vostok, EDC and Dome F ice cores and can thus be used for dating purpose with a 1σ uncertainty of 2–4 ka (Kawamura et al., 2007; Suwa and Bender, 2008; Landais et al., 2012). Three ice age markers deduced from $\delta O_2/N_2$ have been introduced in the AICC2012 chronology associated with a 1σ uncertainty of 4 ka. Third, it has been shown that part of the variance in total air content in the EDC ice core over the last 440 ka can be explained by the variations of an integrated summer insolation parameter that has an obliquity component (Raynaud et al., 2007). A tie point based on the EDC air content record at 101.0 ka (± 4 ka) has been defined. Note that, although measured in the trapped air, both $\delta O_2/N_2$ and air content markers are used to constrain the ice age scale rather than the gas age scale since they are understood to be controlled by the local insolation changing snow grain properties during the bubble close off (Bender, 2002; Raynaud et al., 2007). From sensitivity tests with Datice, Bazin et al. (2013) have shown that the chronological information obtained from these different orbital constraints is coherent, confirming their complementarity in the construction of ice core timescales.

In addition to these absolute age constraints, multiple stratigraphic links are also included. First, 48 gas stratigraphic links based on CH_4 and $\delta^{18}O$ of O_2 record synchronisations are included and the associated 1σ uncertainties, which originate from the combined uncertainties linked to the resolution of each gas record and the matching bias, vary from 0.8 ka to 3 ka. Second, 46 volcanic stratigraphic markers, which can be identified by continuous electrical conductivity, di-electrical profiling and sulphate measurements (Clausen et al., 1997; Wolff et al., 1999), are also used to constrain AICC2012. They are associated with a 1σ uncertainty varying between 20 and 350 years. Finally, three additional constraints on the depth difference between a concomitant event in the ice and in the gas phases (Δdepth) are also available for the NGRIP ice core during glacial millennial-scale events with the use of $\delta^{15}N$ in the trapped air (e.g. Severinghaus et al., 1998; Kindler et al., 2014).

Fig. 6 displays the CH_4 concentration and water isotopic profiles of the five cores onto their respective AICC2012 timescale. Overall, we observe a relatively good alignment of the different CH_4 profiles except for the NGRIP CH_4 record before ~118 ka. The latter is due to the fact that beyond ~118 ka, there is no more age constraint available for this ice core.

4.1.3. Transfer of the NEEM ice core onto AICC2012

Back to 108 ka, the NEEM ice core has been directly matched onto the NGRIP ice core on the GICC05 chronology (NEEM community members, 2013). Despite the fact that some NEEM ice core sections are disturbed and folded after the LIG, a chronological climatic sequence back to 128.5 ka has been obtained based on the match to NGRIP and EDML $\delta^{18}O_{atm}$ and CH_4 on the EDML1 timescale, which is by construction coherent with the EDC3 timescale (Capron et al., 2010; NEEM community members, 2013). Including the NEEM ice core in Datice would not bring any robust dating constraints because of the complex ice flow and the stratigraphic disturbances. Here, we therefore transfer the NEEM record onto AICC2012 (Fig. 7) using the ice age correspondence between EDML1 and AICC2012 given by the NEEM community members (2013).

We estimate a combined absolute dating uncertainty of at least 2 ka, which corresponds to the association of three sources of uncertainty: (1) the synchronisation error of the NEEM gas records onto the EDML/NGRIP gas records (~1 ka), (2) the uncertainty on the NEEM Δage determination (~0.5 ka) and (3) the AICC2012 absolute error for the EDML ice core (about 2 ka, Bazin et al., 2013).

4.2. AICC2012 dating uncertainties and comparison with other age scales

Based on the −403‰ threshold value used in EDC ice δD to define an interglacial (EPICA Community members, 2004), the timing and duration of the LIG remains largely unchanged in AICC2012 (116.3–132.5 ka) compared to EDC3 (115.6–132.4 ka). However, thanks to the numerous time markers provided through the integration of multiple ice cores (Bazin et al., 2013), the absolute LIG age uncertainty is reduced to ~1.8 ka (1σ) compared to the 3 ka error attached to EDC3 (Parrenin et al., 2007).

Table 2
Summary of methods used to construct ice core chronologies across the time interval 100–140 ka (section 4).

Timescale	Method	Strengths	Limitations/difficulties	Timescale's reference
EDC3 (EDC)	**Inverse method** (Parrenin et al., 2001). Based on: • a snow accumulation and mechanical flow model. • a set of independent age markers along the EDC core.	Combination of glaciological and stratigraphical constraints.	• Speleothem age used to date the mid-point transition of Termination II. • Large uncertainties on the Δage calculation due to strong limitation in the firn densification models. • Large absolute age uncertainty associated with orbital markers (up to 6 ka). • Modelling uncertainties not taken into account.	Parrenin et al. (2007)
DF-2006 (Dome F)	**Orbital tuning** (Bender, 2002). Based on the alignment of air $\delta O_2/N_2$ data onto a local insolation curve.	Orbital tuning method not relying on climatic assumption: it provides the possibility to explore the phasing between climate and external forcing.	• Physical process linking local insolation and $\delta O_2/N_2$ variations not fully understood. • Possible underestimation of absolute age uncertainties due to the need to the correction of $\delta O_2/N_2$ data for the storage effect at −20 °C. • Limitation in the identification of precise tie-point due to the signal noise.	Kawamura et al. (2007)
AICC2012 (NGRIP, EDC, EDML, TALDICE, Vostok)	**Bayesian Datice tool** (Lemieux-Dudon et al., 2010). Combination of glaciological modelling and age markers from multiple ice cores.	• Uncertainties of sedimentation models taken into account. • Age confidence interval estimated for both ice and gas phases. • Independent from speleothem dates. • Common for four Antarctic ice cores and one Greenland ice core: so far, it is the most appropriate ice core timescale to compare multiple Antarctic climate records and to discuss interhemispheric climate issues. • Lower absolute uncertainty so far over the LIG (e.g. < 1.8 ka for the EDC core). • Δage optimized with respect to $\delta^{15}N$ data and gas and ice stratigraphic markers.	• Orbital markers associated with large absolute age uncertainty (4 or 6 ka). • Large age uncertainties for periods older than 130 ka. • Overestimation of the uncertainties of the ice time scale (Landais et al., 2015). • A 5 ka incoherence with speleothem timescales during the glacial inception possibly due to limitations in the orbital alignment. • Lack of constraints and background thinning uncertainties between 118 and 123 ka for the NGRIP ice core.	Bazin et al. (2013) Veres et al. (2013)
ss09sea (NGRIP)	**Ice flow modelling** (Johnsen et al., 2001). Forced by the accumulation rate deduced from the empirical relationship with water isotopic content of the ice.	• First age scale produced for the Greenland NGRIP ice core.	• Solely based on a glaciological flow model. • Strongly dependent on the empirical relationship between isotopes and accumulation. • The NGRIP record stops at ~123 ka. • Timescale adjusted during the glacial inception to be coherent with MD95-2042 timescale from Shackleton et al. (2002).	North Greenland Ice Core Project members (2004)
GICC05modelext (NGRIP)	**Layer-counting and ice flow modelling** (Wolff et al., 2010) based on the GICC05 time scale (Svensson et al., 2008) for the last 60 ka and extended using the ss09sea time scale beyond (with a shift of 705 yr to ensure continuity).	• Age scale coherent with the annual layer counted GICC05 chronology, which covers the last 60 ka.	• Only glaciological model and thus strongly dependent on the empirical relationship between isotopes and accumulation (see ss09sea). • The NGRIP record stops at ~123 ka. • Timescale adjusted during the glacial inception to be coherent with the MD95-2042 timescale from Shackleton et al. (2002) (see ss09sea).	Wolff et al. (2010)

We confront here the AICC2012 chronology to the absolute DFO-2006 ice core chronology, which was established for the Antarctic Dome F ice core (Kawamura et al., 2007) (Table 2). The DFO-2006 timescale was defined solely based on the orbital tuning of Dome F trapped air $\delta O_2/N_2$ record. The AICC2012 and DFO-2006 chronologies can be compared, assuming synchronous climate and water stable isotope changes in the central East Antarctic Plateau during the penultimate deglaciation and the glacial inception. This comparison highlights that AICC2012 ages are 3 ka younger than DFO-2006 ages for the Antarctic LIG early δD

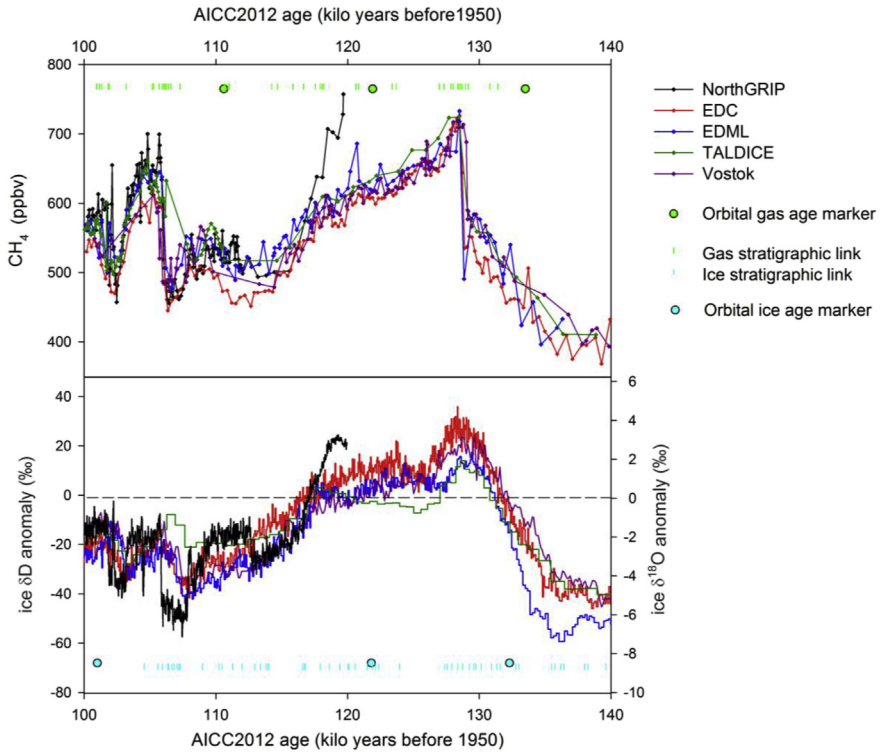

Fig. 6. Ice $\delta^{18}O$ and CH_4 concentration records from NGRIP (North Greenland Ice Core Project members, 2004; Capron et al., 2010), EDC (Jouzel et al., 2007; Loulergue et al., 2008), Vostok (Petit et al., 1999; Delmotte et al., 2004), EDML (Loulergue et al., 2007; Masson-Delmotte et al., 2011) and TALDICE (Buiron et al., 2011; Masson-Delmotte et al., 2011) ice cores during the 140–100 ka period displayed on the AICC2012 timescale (Bazin et al., 2013; Veres et al., 2013). Positions of stratigraphic links (vertical bars) and age markers (dots) deduced from the four ice cores are displayed (details given in Tables S3-4). Water isotope anomalies are calculated using the average isotopic value of the last 1000 years as a reference at each ice core site. See Fig. 2 for site locations.

optimum, and up to 6 ka younger during the glacial inception (Bazin et al., 2013). There are, therefore, significant differences in the absolute timing and duration of the LIG with these two approaches, beyond estimated uncertainties. These large differences are also highlighted in the recent comparison of the two chronologies based on a new synchronisation of volcanic markers between EDC and Dome F (Fujita et al., 2015).

In addition, we compare the AICC2012 chronology to independent absolute age constraints obtained on speleothem records. Assuming that the $\delta^{18}O$ of speleothem calcite is a tracer for large scale regional climate changes (section 3), European speleothem $\delta^{18}O$ (e.g. Spötl and Mangini, 2002) could be directly compared with Greenland NGRIP ice $\delta^{18}O$, while Chinese speleothem $\delta^{18}O$ (Cheng et al., 2009) should correlate to the sharp CH_4 changes measured in ice cores, as observed during the GS and GI events of the last glacial period and deglaciation. At the onset of the penultimate deglaciation, the timing of the abrupt decrease in Sanbao cave calcite $\delta^{18}O$ agrees with the timing of the similarly fast increase in CH_4 on AICC2012 (Fig. 7). For Corchia cave, the penultimate deglaciation is characterised by two decreases between 133 and 131 ka and between 129 and 128 ka, respectively (Drysdale et al., 2009). Note that dating tests performed by Bazin et al. (2013) prove that AICC2012 is not sensitive to the use of the speleothem tie point that was employed in EDC3 over the penultimate deglaciation.

The situation is different over the last glacial inception where larger discrepancies are observed between existing timescales, in particular over GI-25. A fingerprint of this first rapid event has been identified in speleothem records from Corchia cave (Drysdale et al., 2009), NALPS (Boch et al., 2011) and Sanbao cave (Wang et al., 2008). The onset of GI-25 event in the NGRIP ice core on AICC2012 is recorded 2.7 ka earlier than the abrupt calcite $\delta^{18}O$ decrease measured in NALPS (SCH7 speleothem). However, mainly constrained by a few orbital markers, such as $\delta^{18}O_{atm}$ and air content associated with large uncertainties of 6 ka and 4 ka, respectively (Veres et al., 2013), the AICC2012 chronology remains imprecise during the glacial inception. Also, GI-25 has an equivocal Antarctic counterpart and an equivocal signature in the NGRIP CH_4 record, questioning its bipolar structure and its spatial extent (Capron et al., 2012). As a result, no precise bipolar ice core synchronisation is available for this interval. Differences of several millennia are also observed in the timing of the NGRIP glacial inception between the AICC2012 and the GICC05modelext chronologies (see discussion in Veres et al., 2013) (Fig. 7; Table 2).

Recently Barker et al. (2011) have produced a chronology that results from the adjustment of the EDC3 chronology to the absolutely-dated Sanbao speleothems based on the assumption of simultaneous climatic changes in China and over Greenland for the last 400 ka (section 3). Based on a simple mathematical model assuming a thermal bipolar seesaw pattern between Antarctic and Greenland climates, and using the EDC ice $\delta^{18}O$ on EDC3, these authors have produced a synthetic Greenland climate curve (GL_T_syn, Fig. 7), which shows strong similarities with the Sanbao calcite $\delta^{18}O$ over the last 400 ka. The age difference between the EDC3 chronology and the new Sanbao dates over the penultimate deglaciation is of about 0.7 ka but reaches up to 2 ka during the glacial inception. Also, the comparison between the NEEM ice $\delta^{18}O$ and the GL_T_syn curve reveals major differences in LIG climatic variability: the NEEM record suggests a relatively stable climate during the LIG, while the GL_T_syn curve exhibits an early climatic overshoot. Although the age model of Barker et al. (2011), which provides an alternative chronology to EDC3 and AICC2012, has been

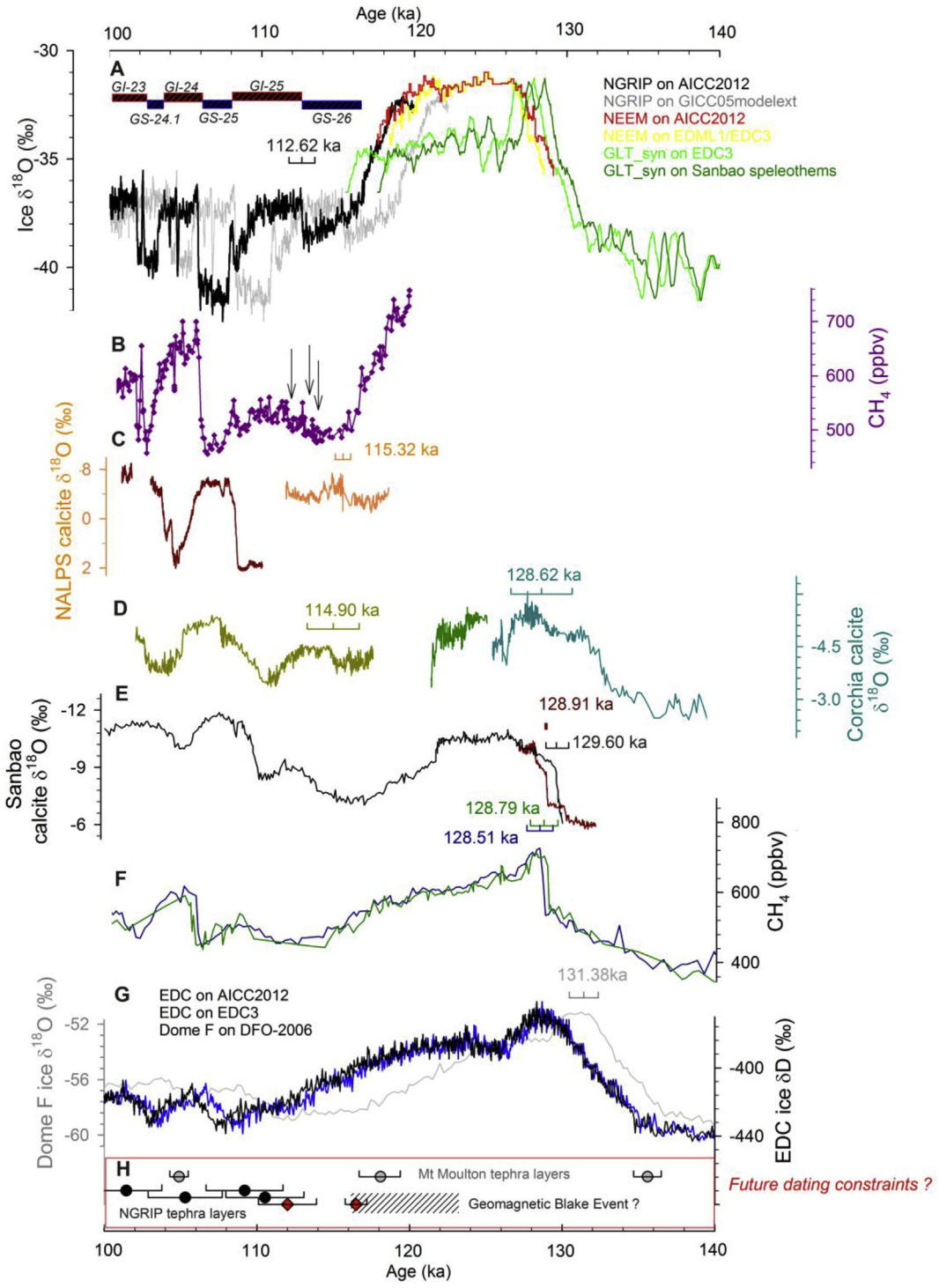

Fig. 7. From top to bottom: A. NGRIP ice $\delta^{18}O$ (black, North Greenland Ice Core Project members, 2004) displayed on the GICC05modelext (grey) and AICC2012 (black) ice timescales, NEEM ice $\delta^{18}O$ on the AICC2012 ice timescale (red) and on the EDML1 timescale (Ruth et al., 2007) which is by construction coherent with the EDC3 timescale (yellow) (NEEM community members, 2013), the Greenland synthetic curve (GL_T_syn) (Barker et al., 2011) presented on the EDC3 timescale (light green) and on a timescale constrained by Sanbao speleothem ages (Barker et al., 2011). The Greenland Interstadial/Stadial (GI/GS) succession numbering follows Rasmussen et al. (2014). For higher clarity, we do not detail here the numbering of the sub-millennial scale climatic events (see Rasmussen et al., 2014 for details). B. NGRIP CH_4 concentration (purple, Capron et al., 2010; 2012) on the AICC2012 gas timescale. Arrows indicate the millennial-scale CH_4 variations occurring during GS-26 and GI-25 making difficult to define a precise CH_4 tie point with Antarctic CH_4 records. C. Calcite $\delta^{18}O$ from NALPS speleothems (orange, Boch et al., 2011). D. Calcite $\delta^{18}O$ from Corchia cave (light green, Drysdale et al., 2009), (dark green, Drysdale et al., 2007). E. Sanbao cave $\delta^{18}O$ record (black, Wang et al., 2008), (brown, Cheng et al., 2009). F. Vostok (green) and EDC (blue) CH_4 records on the AICC2012 gas timescale. G. EDC δD (Jouzel et al., 2007) on the AICC2012 ice timescale (black, Bazin et al., 2013; Veres et al., 2013) and the EDC3 ice timescale (blue, Parrenin et al., 2007) and Dome F ice $\delta^{18}O$ on the DFO-2006 ice timescale (grey, Kawamura et al., 2007). Dates together with associated published error bars are indicated for the penultimate deglaciation and at the onset of GI-25 (when unambiguously identified). Potential future dating constraints are indicated in H: tephra layers radiometrically dated in the Mount Moulton (grey dot, Dunbar et al., 2008) and NGRIP (black dot, Davies et al., 2014) ice cores. The location of the Blake event is indicated as deduced from orbital dating in paleosols and loess record (shaded area, Zhu et al., 1994; Fang et al., 1997; Guyodo and Valet, 1999) and as $^{40}Ar/^{39}Ar$ dated in speleothems from Spain (diamonds, Osete et al., 2012). See Fig. 2 for site locations.

used as a reference chronology for aligning other archives (e.g. Margari et al., 2014), the GL_T_syn curve is no direct tracer for Greenland temperature and this caveat should limit the use of this signal and related time scale to very specific cases only.

4.3. Perspectives and recommendations

This overview of the tools available to define LIG chronologies in ice cores shows that ice and gas markers provide constraints on the LIG onset and demise, but not within the interglacial period. This feature remains a strong limitation to investigate climate variability within the LIG, which can be now explored at bi-decadal resolution from emerging high-resolution Antarctic records (e.g. Pol et al., 2014).

Progress on the duration of the LIG is expected from the new perspective of layer counting over sections of deep ice through high resolution continuous flow analysis and impurity measurements (Svensson et al., 2011). Including event duration in probabilistic models used to develop coherent ice and gas timescales for multiple ice cores will also help to quantify the uncertainty attached to the LIG duration (Parrenin et al. 2015; Lemieux-Dudon et al., 2015). Differences between the Dome F orbital chronology and AICC2012 should be further investigated, especially through the integration of gas and ice age markers from Dome F into the Datice tool or into the recently developed and similar IceChrono framework (Parrenin et al. 2015).

The use of a few orbital markers only leads to an imprecise timing of the LIG demise and of the onset of the glacial millennial-scale climatic variability in ice cores, which could, in the future, benefit from the tephra layers from Mount Moulton (Antarctica) absolutely dated at 118.1 ± 1.3 ka and 104.9 ± 0.6 ka (Fig. 7) (Dunbar et al., 2008). Until recently, no well-dated tephra layers were available in Greenland ice cores over this time period. Four tephra layers have been recently identified in the NGRIP ice core between 100 and 110 ka (S. Davies, personal communication). Radiometric dating of these tephra layers is currently limited and they would need to be geochemically and unequivocally aligned to surface deposits to provide improved dating constraints. To this end, identification and determination of glass shards may provide additional robust results.

Future high resolution ^{10}Be records should be helpful to better constraint accumulation rate changes over the LIG and enable the identification of the Blake and Post-Blake geomagnetic events occurring between 95 and 123 ka (e.g. Zhu et al., 1994; Fang et al., 1997; Guyodo and Valet, 1999) (see section 8 for details). Similarly to the identification of the Laschamp event (Raisbeck et al., 2007), the identification of the Blake and the Post-Blake events would strongly improve North-South ice core synchronisations and reduce age scale uncertainties.

Finally, the broadly used EDC3 and the new AICC2012 chronologies agree within their age uncertainties during the studied time period. However, because the integration of new glaciological constraints, age markers and stratigraphic links from five different ice cores in AICC2012 lowers down the LIG absolute age uncertainty (1σ) to about 1.8 ka (compared to more than 2 ka in EDC3) and uncertainties attached to the duration of events, we presently recommend using AICC2012 as the reference chronology for the Vostok, EDC, EDML and TALDICE ice core records over the 140–100 ka period. We also recommend using the AICC2012 chronology when investigating phasing issues between Greenland ice core records and Antarctic records included in AICC2012 to avoid introducing false offsets. However, there is not yet a strong basis to recommend the use of the AICC2012 chronology instead of the GICC05modelext time scale (Wolff et al., 2010) in studies based on Greenland ice core records only.

5. Chronologies in marine sediment cores

Marine sediments covering the LIG exhibit only few absolute age markers such as magnetic events and dated tephra layers. Hence, their chronologies are mainly derived from the synchronisation and climato-stratigraphic alignment of paleoclimate records. In this section, we evaluate the underlying hypotheses, limitations and age uncertainties of methods frequently used to develop chronologies for marine sediments over the penultimate deglaciation and the LIG (note that examples are given in section 7).

5.1. Tephrochronology

When present in archives, tephra horizons provide ideal stratigraphic markers to synchronise paleoclimate records and dating control points if the eruption is well dated (e.g. Lowe, 2011 for a recent review). However, the use of tephras as chronological markers still faces several drawbacks. Taphonomic issues such as the reworking, dissemination and dispersion of glass shards or crystals may lead to the formation of diachronous tephra surfaces, which jeopardize the use of tephrochronology (Lowe, 2011). Careful characterisation of tephras using multiple criteria is hence required to unequivocally identify their provenance (source volcano), match them to single eruptive events and synchronise them between remote sedimentary records (Lowe, 2011).

The compilation of 14 tephra horizons so far identified in the North Atlantic and Nordic Seas between 140 and 100 ka highlights their potential and limitations as stratigraphic markers in this region (Table S5). In particular, the 5e-Midt/RHY tephra horizon found at many sites from the Norwegian and Greenland Seas offers high potential for regional LIG alignments in the Nordic Seas (where oxygen isotopic alignment methods present severe limitations, section 5.2). Recently identified in one North Atlantic core (Davies et al., 2014), this horizon also constitutes a promising tie-point to help develop a common time frame between records from the North Atlantic and the Nordic Seas. Similarly, the 5e-Low/BAS-IV horizon is of specific interest to synchronise the beginning of the LIG in sites located north and south of the Icelandic ridge (e.g. Rasmussen et al., 2003b) and hence to check the spatial synchronicity of LIG climatic events in these regions. However, the diversity of tephra layers identified in single northern high-latitude sites (Table S5) (e.g. Brendryen et al., 2010; Abbott et al., 2013) highlights the local distribution of most LIG horizons and the difficulty of obtaining diagnostic geochemical fingerprinting of tephras (e.g. Lowe, 2011). Also, the present variety of climato-stratigraphic alignments and reference time scales used to define the relative ages that characterise most of these tephra horizons (Table S5), strongly limits their use as robust absolute age markers. Further work is hence required to widen the use of tephra-based correlations within the marine realm during the LIG (Davies et al., 2014).

5.2. Alignment to foraminifera oxygen isotope reference records

Alignments of δ^{18}O records measured in monospecific benthic foraminifera tests to reference δ^{18}O stacks (e.g. Lisiecki and Raymo, 2005) have been widely used to derive age models for marine sediments. This alignment method assumes that benthic δ^{18}O variations are synchronous around the world and at a first order reflect global ice volume changes (Shackleton, 1967) (or that the seawater temperature and δ^{18}O components of benthic δ^{18}O vary synchronously around the world, which is unlikely, see discussion below). Decreasing benthic δ^{18}O values during the penultimate deglaciation and minimum δ^{18}O values during the LIG are hence assumed to mainly reflect the sea level rise associated with ice-sheet melting during the penultimate deglaciation and the sea

level highstand characteristic of the LIG, respectively (e.g. Shackleton et al., 2003). Two reference records, which show consistent LIG variations within age uncertainties, are generally used: the LR04 benthic $\delta^{18}O$ stack of Lisiecki and Raymo (2005), which is of relatively low resolution (1 ka) for this time interval, and the high-resolution (~0.3 ka) benthic $\delta^{18}O$ record from the North Atlantic core MD95-2042 (Shackleton et al., 2003). The age model of the LR04 reference record is based on the alignment of the benthic $\delta^{18}O$ stack to a simple model that applies a non-linear temporal response between orbital forcing of summer temperature at 65°N and global ice volume (Imbrie and Imbrie, 1980), which simulates the response of ice sheets (growth or decay) to boreal summer insolation variations (Lisiecki and Raymo, 2005). Uncertainties related to the assumption of non-linearity between ice sheet dynamics and insolation changes, as well as to the response time of ice sheets to orbital forcing, which may have changed in the past due to e.g. varying ice sheet geometry, contribute to the high dating uncertainties of 4 ka (1σ) reported during the penultimate deglaciation and the LIG (Lisiecki and Raymo, 2005).

The age uncertainty associated with the benthic $\delta^{18}O$ alignment to reference records consists of (1) the uncertainty of alignment that depends on the resolution of the reference and aligned records, (2) the age uncertainty related to transient heterogeneous deep-water changes leading to asynchronous benthic $\delta^{18}O$ variations (see below) and (3) the absolute dating uncertainty of the reference record (examples are given in section 7.1). In the case of benthic $\delta^{18}O$ alignment to the LR04 stack, we estimate the matching age uncertainty to be around 1.4 ka (1σ) during the deglaciation and the LIG (calculation given in Tables S6-7). However, the large age error related to the asynchronicity of benthic $\delta^{18}O$ variations, which is estimated to be around 4 ka between the deep North Atlantic and North Pacific during the last deglaciation (Skinner and Shackleton, 2005), and the large dating uncertainty of LR04 (4 ka, Lisiecki and Raymo, 2005) can lead to very large combined age uncertainties up to 6 ka during the deglaciation and the LIG.

Although widely applied, the alignment of benthic $\delta^{18}O$ records presents two severe limitations. First, benthic $\delta^{18}O$ is not only influenced by ice volume and global sea level but is also affected by local deep-water temperature and seawater $\delta^{18}O$ changes. Consequently, benthic $\delta^{18}O$ variations do not occur at the same time and with the same amplitude around the globe. Diachronous benthic $\delta^{18}O$ changes, in particular between the deep Pacific and the deep Atlantic, are observed during deglaciations in response to diachronous deep-water temperatures and seawater $\delta^{18}O$ changes across ocean basins and water-masses (e.g. North Atlantic Deep Water vs. Circumpolar Deep Water) (e.g. Skinner and Shackleton, 2005; Lisiecki and Raymo, 2009; Waelbroeck et al., 2011). Therefore, while the alignment of benthic $\delta^{18}O$ records is a suitable method for sites that presently lie in the same water mass and have experienced synchronous past deep-water changes, it induces age errors of several thousand years across deglaciations for sites located in different water-masses (e.g. Waelbroeck et al., 2011) (see examples in Section 7.1). The alignment of planktonic foraminifera $\delta^{18}O$ records to reference $\delta^{18}O$ stacks is sometimes used in sediment cores where benthic foraminifera $\delta^{18}O$ records are discontinuous or not available (e.g. Bianchi and Gersonde, 2002; de Vernal and Hillaire-Marcel, 2008). Because planktonic $\delta^{18}O$ is even more sensitive than benthic $\delta^{18}O$ to local changes in SST and non-glacioeustatic seawater $\delta^{18}O$ (e.g. meltwater input, local changes in precipitation and evaporation), uncertainties related to heterogeneous hydrographical changes in the ocean are even higher when aligning planktonic $\delta^{18}O$ records to reference $\delta^{18}O$ stacks. Thus, such planktonic $\delta^{18}O$ alignments are not recommended.

The second limitation of foraminifera $\delta^{18}O$ alignment concerns sites from high northern latitudes (e.g. the Nordic Seas, the Labrador Sea), where both benthic and planktonic isotopic records are affected by highly depleted $\delta^{18}O$ values during the penultimate deglaciation (e.g. Seidenkrantz, 1993; Rasmussen et al., 2003a; Risebrobakken et al., 2006). The reason for such light foraminifera $\delta^{18}O$ anomalies during deglaciations is still not clear and may involve marine brine formation, meltwater bursts and other processes connected with seawater densification (e.g. Seidenkrantz, 1993; Dokken and Jansen, 1999; Bauch and Bauch, 2001). Regardless of the mechanisms involved, these negative $\delta^{18}O$ anomalies during the penultimate deglaciation make the beginning of the LIG very difficult to identify in sediment cores from the Nordic Seas and the Labrador Sea. Therefore, simple foraminifera $\delta^{18}O$ alignment, without other complementary information on SST and seawater $\delta^{18}O$ changes, is not an accurate method to derive LIG age models for high northern latitude marine sediment sites. Additional chronological constraints (e.g. tephra layers, section 5.1) are sometimes available (Rasmussen et al., 2003b).

5.3. Alignment of SST records to ice cores

The scarcity of absolute control points and limitations of foraminifera $\delta^{18}O$ alignments led to the development of alternative alignment methods in marine sediments. The recent improvements of ice core chronologies (section 4) stimulated the use of ice core records as targets to define LIG age models in high-latitude sediment cores (e.g. Govin et al., 2012; Capron et al., 2014). During the last deglaciation, synchronous surface-water and air temperature variations have been identified over wide areas surrounding the North Atlantic (Bond et al., 1993; Bjorck et al., 1996) and the Southern Ocean (e.g. Bianchi and Gersonde, 2002; Lamy et al., 2004; Siani et al., 2013). This alignment method, therefore, relies on the hypothesis that glacial-interglacial SST variations in the subpolar North Atlantic (Southern Ocean) occur in phase with air temperature changes over inland Greenland (Antarctica) (Govin et al., 2009, 2012).

A limitation of this alignment lies with the fact that Greenland ice core records do not reach beyond 129 ka (NEEM community members, 2013), i.e. do not cover the penultimate deglaciation, hence requiring assumptions of synchronicity between North Atlantic marine records and Antarctic ice cores. North Atlantic temperatures are then aligned to Antarctic CH_4 variations during the deglaciation and at the beginning of the LIG (see examples in section 7.1). The rationale behind this alignment to Antarctic CH_4 is that (1) with a lifetime of ~10 years, CH_4 is well-mixed in the atmosphere and exhibits synchronous variations in both hemispheres on paleoclimate time scales and (2) abrupt CH_4 increases are recorded in phase with abrupt Greenland warming during millennial-scale events of the last glacial period and the last deglaciation (Chappellaz et al., 1993; Rosen et al., 2014). The use of CH_4 as indicator of Greenland warming during the penultimate deglaciation has, however, some limitations. CH_4 variations mainly reflect changes in the strength of tropical CH_4 sources and sinks, with additional boreal input when the retreat of northern ice sheets enhances methane emissions from extending periglacial wetlands (Loulergue et al., 2008). The abrupt CH_4 increase recorded at ~129 ka in AICC2012 (Fig. 6) occurred in phase with speleothem records (section 4) (Bazin et al., 2013), suggesting a predominant tropical wetland source (Moller et al., 2013). However, regardless of the relative contributions of tropical vs. boreal methane emissions during the deglaciation, the abrupt CH_4 increase at ~129 ka is understood to reflect the rapid warming of northern high latitudes, as it is observed during the last deglaciation (Chappellaz et al., 1993; Rosen et al., 2014). In contrast, the gradual CH_4 increase observed between 140 and 130 ka (Fig. 6) may derive from changing tropical wetland emissions (Moller et al., 2013), and hence may not reflect a

gradual boreal warming. Therefore, as long as no direct Greenland temperature record is available, the alignment of SST records to ice cores will lead to uncertain chronologies at the beginning of the deglaciation before the abrupt CH_4 increase dated at 129 ka on AICC2012 (Tables S6-7).

Age uncertainties associated with the alignment of SST to ice core records include (1) the alignment uncertainty that depends on the resolution of SST and ice core records, (2) the age uncertainty related to the possibility of diachronous surface water and surface air temperature changes over wide geographical areas and (3) the dating uncertainty of the ice core chronology used as a reference. In the alignment of North Atlantic and Southern Ocean SST records to ice core records (see examples in section 7.1), we estimate age uncertainties during the penultimate deglaciation and the LIG ranging between 0.6 and 1.7 ka (1σ) relatively to the AICC2012 chronology and between 1.6 and 3.3 ka (1σ) when including the AICC2012 age uncertainty (see details of calculations in Tables S6-7). Defined tie-points are more robust during periods of rapid and large temperature changes, such as at the onset of the LIG (~129 ka) and demise of the LIG characterised by bipolar millennial-scale variability (112–105 ka) than during the deglaciation (140–130 ka). However, a caveat of this approach is that the geographical extension of high-latitude regions and the time scales over which SST and air temperature changes are synchronous remain so far uninvestigated. Our reported uncertainties may therefore be minimal estimates.

Temperature alignment of marine records to ice cores is a useful alignment method for high-latitude sites (above 40–45°, Capron et al., 2014), but underlying hypotheses and limitations must be kept in mind. Future transient simulations performed with coupled climate models including climate – ice sheet feedbacks may produce specific regional patterns of change and help to identify high-latitude regions of synchronous SST and air temperature variations. This alignment method is also totally dependent on the accuracy of ice core chronologies (section 4). Hence, it may be better suited for investigations of changes in the oceanic vs. atmospheric circulations than for discussions on global-scale climate changes, as it is probably the case for any alignment performed between archives with relative chronologies only.

5.4. Alignment of marine records to speleothems

Well-dated and high-resolution speleothem records covering the penultimate deglaciation and the LIG (section 3) stimulated attempts to derive age models of marine sediments from various regions by alignment to speleothems (e.g. Bar-Matthews et al., 2003; Drysdale et al., 2009). We detail here the strengths and limitations of such attempts by using the example of the alignment of SST records from the western Mediterranean Sea and Portuguese margin to the calcite $\delta^{18}O$ record of Corchia speleothems from NW Italy (Drysdale et al., 2009). This method relies on two assumptions: (1) variations in the strength of the North Atlantic meridional overturning circulation induce synchronous changes in regional SST, air temperature, evaporation and moisture advection to the Italian peninsula, and therefore Italian rainfall, and (2) the amount of rainfall reaching Corchia cave is the dominant driver of the calcite $\delta^{18}O$ signal (Drysdale et al., 2009). The millennial- and orbital-scale variability of Corchia $\delta^{18}O$ supports such connections between the North Atlantic climate and NW Italian rainfall, despite the complex climatic interpretation of speleothem $\delta^{18}O$ (section 3). Moreover, independent analyses (e.g. growth rate, trace elements) converge to relate Corchia $\delta^{18}O$ variability to rainfall amount changes (Drysdale et al., 2009).

Related age uncertainties include (1) the alignment uncertainty that depends on the resolution of SST and speleothem records, (2) the age uncertainty related to the interpretation of speleothem tracers and our understanding of factors controlling them and (3) the absolute dating uncertainty of speleothem chronologies. Radiometric U–Th dating of speleothems is characterised by relatively low dating errors (typically around 1 ka, 1σ, section 3) during the penultimate deglaciation and the LIG, leading to relatively reduced age uncertainties ranging between 0.7 and 1.8 ka (1σ) in aligned marine sediments (see details of calculation in Table S6). A caveat of this approach is that the synchronicity of marine and speleothem records cannot be tested using the same speleothem records for the last deglaciation and the current interglacial period, because available European speleothem records cover relatively short time intervals of few thousands to ten thousands of years. Our reported uncertainties (Table S6) may therefore be minimal estimates.

As a result, speleothems may provide alternative chronological methods to marine sediments from tropical and mi-latitude regions, in particular, although thorough investigations of climatic factors controlling aligned records (e.g. moisture availability) and of dynamical processes connecting them (e.g. atmospheric moisture transport) are required.

5.5. Recommendations and perspectives

Existing synchronisation and alignment methods used to define chronologies in marine sediments all present strengths and limitations summarized in Table 3. Relying on very specific assumptions that require careful examination, each method is often limited to specific regions (Table 3). The commonly used alignment of benthic $\delta^{18}O$ records is a suitable alignment method only for sites that lie within the same water-mass and have experienced synchronous past deep-water changes. The SST alignment to ice core records primarily provides reliable chronologies for high-latitude sites from the North Atlantic and the Southern Ocean. The high dating accuracy of speleothems makes them ideal alignment targets to derive age models in marine sediments in their vicinity (i.e. mostly in tropical and mid-latitude regions where speleothem records are available), provided that climate drivers of speleothem tracers are well understood and their phasing with their marine counterpart is known. More recent and well-dated (radiocarbon-dated or layer-counted) material could be particularly useful to test the hypotheses of climatic synchronicity between aligned archives.

Efforts in the diagnostic characterisation, extensive mapping and radiometric dating of tephra horizons, in particular in the North Atlantic and the Nordic Seas (Davies et al., 2014) could bring crucial age control points within the LIG (Table S5) and help improve equivocal LIG chronologies from the Nordic Seas (e.g. Capron et al., 2014). Paleointensity reference stacks with a good temporal resolution will be required to intensify the use of paleointensity records as synchronization tools in LIG marine sediments, whereas cosmogenic isotope production could provide a viable synchronisation technique between sediment and ice core records (section 8). Finally, absolute age markers provided by well-dated tephra horizons or improved understanding and dating of the Blake event (section 8) would constitute invaluable information to anchor the mostly floating LIG chronologies of marine sediments, as well as relate Greenland ice and North Atlantic sediment records to test hypotheses of climatic synchronicity.

6. Chronologies applied to pollen records

6.1. Marine pollen records

Linking land and sea records directly through joint pollen and marine-proxy analyses in the same deep-sea sequence allows an *in*

situ assessment of phase relationships between marine and terrestrial sequences. This has provided the first direct evidence for the correspondence between marine and terrestrial stages, including LIG records from the North American and European seaboards and beyond (e.g. Heusser and Shackleton, 1979; Turon, 1984).

More recently deep-sea coring sites have been specifically selected in order to undertake marine-terrestrial comparisons, with the Portuguese margin a prominent example of such an approach. Comparison of modern marine and terrestrial samples along western Iberia has shown that the marine pollen assemblages provide an integrated picture of the regional vegetation of the adjacent continent (Naughton et al., 2007). Work from core MD95-2042 has led to a re-evaluation of the timing and duration of LIG conditions in southern Europe and its relation to marine isotope stage boundaries and paleoceanographic changes (Shackleton et al., 2002, 2003). Marine-pollen records from NW Iberia and the Bay of Biscay (Sánchez Goñi et al., 2005, 2008) have permitted comparisons with the "classic" French terrestrial sequences of Grande Pile (Woillard, 1978) and Ribains (de Beaulieu and Reille, 1992). Marine-pollen studies from the western Mediterranean Sea have also highlighted the sensitivity of Mediterranean vegetation to North Atlantic climate variability (e.g. Combourieu Nebout et al., 1999, 2009).

Marine pollen records share the same chronology and associated uncertainties developed for paleoceanographic tracers from the same sediment sequence (section 5). While relative leads and lags between vegetation and ocean changes can be directly determined in the depth domain, estimates of their temporal offsets depend on the resolution of the record, the variations in sedimentation rate within the archive, pollen transport and reworking and the quality of the age control. Best practice would entail that pollen and marine tracer analyses are undertaken from the same sediment depths to ensure direct assessment of phase relationships and identical chronological uncertainties.

In the future, marine-pollen records could also be used to refine chronologies of marine sediments in specific regions. For example, on the premise that moisture availability in southern Europe exerts a dominant control over both the composition of vegetation and the isotopic signature of speleothems, one could consider aligning e.g. the percentage of temperate tree pollen recorded in sediments from the Portuguese margin to Corchia speleothem $\delta^{18}O$. Investigations with high-resolution records would, however, be required to check the underlying climatic hypotheses before routinely applying such alignment methods during the LIG.

6.2. Terrestrial pollen records

A significant body of palynological evidence has provided insights into the character of vegetation changes in Europe over the LIG. However, a persistent handicap has been the lack of precise absolute timescales. While paleomagnetic evidence and U-series dates on peat and lake sediments have been used to provide a broad chronostratigraphical context, i.e. assignment to the right chronostratigraphic stage (e.g. Heijnis, 1992; Frogley et al., 1999), they are not sufficiently precise to allow long-distance correlations, let alone a detailed assessment of phase relationships between different types of climatic archives. Sediment sequences with annual laminations have provided floating chronologies and estimates for the duration of pollen zones (e.g. Müller, 1974), but in the absence of independent chronological markers, long-distance alignments and absolute ages have remained problematic over the LIG. An exceptional situation occurs in the partly annually-laminated Lago Grande di Monticchio (LGdM) sequence from southern Italy, where a varve and extrapolated sediment accumulation chronology spanning the last 132 ka has been developed (Brauer et al., 2007; Allen and Huntley, 2009). The LIG interval (109.5–127.2 ka) is entirely laminated, providing a duration of 17.7 ka. While the absolute LGdM ages may be subject to errors compounded along the length of the sequence, a tephrochronological marker supported the estimated absolute LIG chronology and suggested a small overall uncertainty on the order of 1.3–1.6 ka (Brauer et al., 2007).

Unfortunately, annual laminations are not preserved in most sediment sequences, and therefore alternative approaches to developing terrestrial chronologies need to be explored. They include (1) direct pollen-orbital tuning, using recurrent patterns of vegetation change associated with climate conditions linked to specific orbital configurations (Magri and Tzedakis, 2000; Tzedakis et al., 2003); (2) alignment to speleothem records, on the basis that changes in moisture availability would affect synchronously vegetation composition and speleothem $\delta^{18}O$ signatures; (3) alignment to pollen records with independent chronologies (e.g. based on annual laminations); (4) alignment to pollen records from marine sediment cores. The underlying hypothesis in alignment approaches (2), (3) and (4) is that in records lying within the same climate province, isotopic and vegetation changes would be sufficiently time-parallel to permit the linking of records (similar to the idea that benthic $\delta^{18}O$ alignment should be restricted to sites that lie in the same water mass, section 5.2). These alignment methods are compared and discussed in section 7.3 using an example from southern Europe.

By comparison to southern Europe, a chronological framework for areas north of the Alps has been more difficult to develop. Within the classic Eemian region of NW Europe, pollen diagrams show strikingly similar vegetation successions, with some vegetation events considered sufficiently time-parallel to allow alignment (e.g. Zagwijn, 1996). Despite a large number of annually-laminated LIG records, the absence of independent chronological markers and of marine pollen records means that it has been difficult to anchor the floating chronologies. Estimates for the duration of the LIG in northern Germany (>50°N) suggest a duration of ~11 ka (e.g. Müller, 1974). This implies a shorter duration by 5–6 ka compared to southern Europe. However, it is unclear whether this is a result of an early LIG demise, or a delayed LIG onset, or a combination of the two (Tzedakis, 2003; Müller and Kukla, 2004), which complicates alignments with southern European records. For the geographical area in between (45–50°N), it has been assumed that the LIG onset and demise have been broadly synchronous with southern Europe (Tzedakis, 2003; Müller and Kukla, 2004), and this is supported by results from a marine pollen record from the Bay of Biscay (Sánchez Goñi et al., 2005, 2008). Over large distances (i.e. southern-to-central-to-northern Europe), however, interglacial zone boundaries, representing vegetation turnover events, are not expected to be synchronous, given time-transgressive spread of populations from glacial refugia and differences in local climatic character, and therefore cannot be used for more intensive alignment schemes.

6.3. Recommendations and perspectives

Beyond the radiocarbon range, lake and peat sequences are some of the most chronologically-challenged archives. In particular, the observation of different LIG durations between Northern and Southern European sequences calls for caution when performing alignments for terrestrial records and a careful check of underlying climatic assumptions. However, the sheer volume of LIG pollen data and ultimately the need to reconstruct terrestrial environments require the development of sufficiently precise chronologies so that

vegetation changes can be incorporated within the framework of atmospheric and ocean changes.

Emerging from this review are the advantages accruing from undertaking joint pollen and marine-proxy analyses in carefully selected deep-sea cores, thereby bypassing alignment uncertainties. A latitudinal transect of marine pollen records along continental margins would in principle help to address current uncertainties over the duration of forested phases at different latitudes (although not all continental margins are equally-suited to such an approach). Terrestrial pollen records could then be aligned with their marine counterparts to provide a chronostratigraphic matrix of marine-terrestrial events. Given their small absolute dating errors, speleothem records also represent prime alignment targets, provided that a case can be made that regional precipitation or temperature changes would affect synchronously vegetation composition and speleothem $\delta^{18}O$ signatures. Other approaches, such as the construction of a regional tephrochronological lattice (Lowe, 2011), are therefore needed to improve the link between these records and assess the relative phasing of intra-interglacial vegetation events over large distances. Also, synchronization could be tested between crypto tephras identified in non-varved terrestrial sequences from the Mediterranean region and those recently identified in the well-dated sequence from Lago Grande di Monticchio (Wulf et al., 2012).

7. Strengths and limitations of climato-stratigraphic alignments: illustrations

In this section, we illustrate the strengths and limitations of climato-stratigraphic alignments by comparing commonly used alignment methods that we applied in two marine sediment cores and one continental pollen sequence.

7.1. Benthic $\delta^{18}O$ vs. temperature proxy alignments in two high-latitude cores

We compare here the chronologies obtained (1) via benthic $\delta^{18}O$ alignment to the LR04 stack (Lisiecki and Raymo, 2005) (section 5.2) and (2) via SST alignment to ice cores (section 5.3) for two high-latitude sediment cores (Fig. 8): the North Atlantic core MD95-2042 (3142 m water-depth) from the Portuguese margin (Shackleton et al., 2002, 2003) and the Southern Ocean core MD02-2488 (3420 m water-depth) from the South Indian Ridge (Govin et al., 2009, 2012). These sites presently lie in different water-masses, North Atlantic Deep Water and Circumpolar Deep Water, respectively. For both cores, combined age uncertainties (i.e. including the dating uncertainty of reference time scales) are around 4.3 ka (1σ) for benthic $\delta^{18}O$ alignment, whereas they range between 1.6 and 3.3 ka (1σ) for SST alignment to ice cores (see calculations in Tables S6–7).

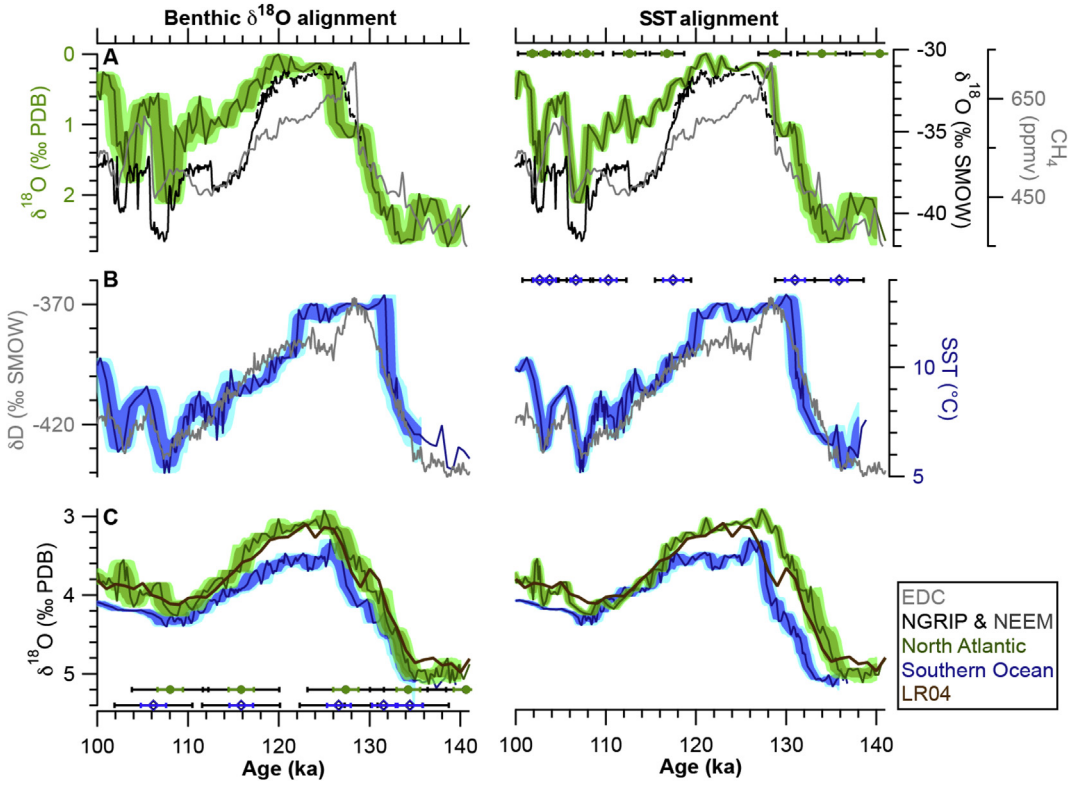

Fig. 8. Comparison of benthic foraminifera $\delta^{18}O$ alignment (*left*) and SST alignment (*right*) used to derive age models in two cores, one from the North Atlantic (MD95-2042, 3142 m) and one from the Southern Ocean (MD02-2488, 3420 m). A. MD95-2042 planktonic foraminifera (*G. bulloides*) $\delta^{18}O$ record (green line) (Shackleton et al., 2003) with relative non-parametric 1σ (dark green shading) and 2σ (light green shading) confidence intervals, in comparison to NGRIP ice $\delta^{18}O$ record (black line) (North Greenland Ice Core Project members, 2004), NEEM ice $\delta^{18}O$ record (dotted black line) (NEEM community members, 2013) and EDC CH_4 record (grey line) (Loulergue et al., 2008). B. MD02-2488 Sea Surface Temperature (SST) record (blue line) (Govin et al., 2012) with relative non-parametric 1σ (dark blue shading) and 2σ (light blue shading) confidence intervals, in comparison to EDC ice δD record (grey line) (Jouzel et al., 2007). All ice core records are presented on the AICC2012 time scale (Bazin et al., 2013; Veres et al., 2013). C. Benthic foraminifera $\delta^{18}O$ records from cores MD95-2042 (green line) (Shackleton et al., 2003) and MD02-2488 (Govin et al., 2012) (blue line) with corresponding relative non-parametric 1σ (dark shading) and 2σ (light shading) confidence intervals, in comparison to the LR04 reference stack (brown line) (Lisiecki and Raymo, 2005). Filled green circles and open blue diamonds in panels C (*left*) and A-B (*right*) mark tie-points used to define age models of cores MD95-2042 and MD02-2488, respectively. Associated 1σ age errors (Tables S6-7) are shown in blue/green for relative alignment age errors and in black for combined age uncertainties (i.e. including LR04 and AICC2012 dating errors). Confidence intervals (shading) were estimated from 1000 repetitions of age model constructions based on the defined tie-points and associated relative age uncertainties (same procedure as in Capron et al., 2014). See Fig. 2 for site locations.

Table 3
Summary of methods used to derive chronologies in marine sediments across the penultimate deglaciation and the LIG.

Method	Hypothesis	Age uncertainties	Strengths	Limitations/difficulties	Recommendations
Synchronisation of tephra horizons	Correct identification of the same tephra in different archives	• Absolute dating error (if available) • Synchronisation error	• Accurate synchronisation • Several tephra horizons identified during the LIG • Absolute dating control sometimes possible	• Taphonomic issues (reworking, dissemination, dispersion of shards) • Unequivocal identification of source volcano and eruptive event via diagnostic fingerprinting	High potential of synchronisation between the North Atlantic and the Nordic Seas: additional work required
Synchronisation of the Blake and Post-Blake geomagnetic excursions and of relative paleointensity records	Global signal		Potential to synchronise paleointensity to cosmogenic isotopic records from ice cores	• Large dating uncertainty of the Blake and Post-Blake geomagnetic excursions (Table 4) • Uncertainties associated with the magnetization acquisition process	Methods suitable for local to global synchronisation when sediments pass criteria of paleomagnetic reliability
Benthic foraminifera $\delta^{18}O$ alignment	In-phase benthic $\delta^{18}O$ variations	• Alignment error (e.g. resolution, matching) • Uncertainty related to the hypothesis (e.g. possibility of diachronous benthic $\delta^{18}O$ changes or diachronous high-latitude temperature changes) • Dating uncertainty of the reference	Common tracer: many available records	• Diachronous deep-water temperature and $\delta^{18}O$ changes across water-masses • Negative $\delta^{18}O$ anomalies in the Nordic Seas and Labrador Sea during Termination II	Method suitable between sites located within the same water-mass (e.g. NADW)
SST alignment to ice cores	In-phase high-latitude sea surface and air temperature changes		High-resolution ice core records for the last 800 ka	• Restricted to high latitudes • Precise geographical extension of synchronous temperature changes? • Sensitive to uncertainties in SST reconstruction methods (e.g. seasonality, living depth, transport)	Method suitable for North Atlantic and Southern Ocean sites (latitudes higher than 40 −45°)
Marine alignment to speleothems	In-phase regional changes in marine (e.g. SST, salinity, pollen) and continental (e.g. rainfall amount) tracers		• High dating accuracy • Very high-resolution speleothem records	• Mostly applicable in tropical and mid-latitude regions (where speleothem records are available) • Speleothem records sometimes discontinuous • Climatic drivers of speleothem tracers (moisture availability?)	Method suitable for sites (mostly from tropical and mid-latitude regions) located close to well-dated speleothems with well-understood tracers

When benthic $\delta^{18}O$ records of both cores are aligned to the LR04 stack, the rapid deglacial North Atlantic warming recorded by *G. bulloides* $\delta^{18}O$ (at ~125 ka) occurs ~3–4 ka after the NH high-latitude warming indicated by the CH_4 increase (at 129 ka, Fig. 8). This feature disagrees with synchronous North Atlantic and northern high-latitude warming observed over the last 90 ka, and in particular during the last deglaciation (e.g. Bond et al., 1993). This alignment also affects the north-south sequence of events. In this case, the establishment of warm interglacial North Atlantic conditions lags by ~6 ka the beginning of Southern Ocean peak warmth (Fig. 8), which greatly exceeds the lag of ~1.5 ka estimated from Greenland and Antarctic records (Masson-Delmotte et al., 2010a). Finally, in the case of benthic $\delta^{18}O$ alignment, North Atlantic and Southern Ocean temperature variations occur almost in phase between 113 and 100 ka (Fig. 8), in contrast with the typical bipolar seesaw pattern observed during glacial millennial-scale events (EPICA Community members, 2006). In contrast, when SST tracers are aligned to ice core records, temperature variations are by definition in phase between Greenland (Antarctic) and North Atlantic (Southern Ocean) records (Fig. 8). By construction, the establishment of peak interglacial North Atlantic conditions also lags by ~2 ka only the beginning of Southern Ocean peak warmth, in agreement with ice core records (Masson-Delmotte et al., 2010a). Finally, when using the chronology derived through SST alignment to the ice core records, the North Atlantic benthic $\delta^{18}O$ decrease during the penultimate deglaciation precedes by ~3 ± 1 ka the one recorded in the Southern Ocean core (Fig. 8) (Govin et al., 2012), in agreement with observations of other deglaciations (e.g. Skinner and Shackleton, 2005; Lisiecki and Raymo, 2009; Waelbroeck et al., 2011).

Altogether, chronologies obtained via SST alignment to ice cores exhibit lower combined age uncertainties and better reproduce known high-latitude climate features of the penultimate deglaciation and the LIG than benthic $\delta^{18}O$ alignments to LR04 stack. They are, therefore, more appropriate to compare the ocean evolution from northern and southern high latitudes at the onset and demise of the LIG, although they fully rely on the accuracy of ice core chronologies. Chronologies derived from benthic $\delta^{18}O$ alignments to LR04 are characterised by very high age uncertainties (up to 6 ka, section 5.2), which make them unsuitable to compare millennial-scale variability from northern and southern high latitudes during the penultimate deglaciation and the LIG.

7.2. Caution on the choice of tracers used in climato-stratigraphic alignments

Various types of proxies have so far been used in climato-stratigraphic alignments. For example, planktonic foraminifera $\delta^{18}O$ or SST records have been both used as tracers for surface-water conditions in alignments of marine sediments with speleothem $\delta^{18}O$ records (e.g. Bar-Matthews et al., 2003; Drysdale et al., 2009; Govin et al., 2012), although these proxies are not controlled by the same climatic parameters. While planktonic foraminifera $\delta^{18}O$ records are influenced by global and local seawater $\delta^{18}O$ in addition to local SST (e.g. Duplessy et al., 1991), SST reconstructions remain associated with relatively large uncertainties related to e.g. the seasonality and living depth of foraminifera (e.g. Jonkers et al., 2013; Sagawa et al., 2013) or the seasonality and transport of alkenones (e.g. Sicre et al., 2005; Rosell-Melé and Prahl, 2013). To illustrate the consequences of the use of one or another aligned proxy on chronologies defined in climato-stratigraphic alignments, we tested here two temperature alignments of the North Atlantic core MD95-2042 using either (1) the alkenone-derived temperature (Uk_{37}-SST) or (2) planktonic foraminifera $\delta^{18}O$ record as SST tracers. Note that the planktonic *G. bulloides* $\delta^{18}O$ record from core MD95-2042 is thought to largely reflect local SST changes at this site (Shackleton et al., 2000). The test was performed for alignments to both speleothem and ice core records (Fig. 9).

For this particular environmental setting on the Iberian margin, Uk_{37}-SST vs. planktonic $\delta^{18}O$ alignment methods reveal similar ages (within age errors) during the late LIG and the glacial inception, but large age differences (up to 5 ka) during the penultimate deglaciation and to a lesser extent (1–2 ka) during the early LIG (Fig. 9). Uk_{37}-SST alignments lead to very early deglacial changes in comparison to planktonic $\delta^{18}O$ alignments (Fig. 9). Despite small differences in the resolution of records, age differences between Uk_{37}-SST and planktonic $\delta^{18}O$ alignments mainly derive from the difficulty to identify the beginning of the deglaciation in the Uk_{37}-SST record, i.e. the time when surface waters start to warm up (e.g. dated at 136 or 131 ka in the planktonic $\delta^{18}O$ alignment to ice cores, Fig. 9). In particular, the speleothem Uk_{37}-SST alignment is very similar to the chronology published by Drysdale et al. (2009), with an early deglacial decrease in benthic $\delta^{18}O$ starting at ~141 ka and ending at ~132 ka (Fig. 9). Large benthic $\delta^{18}O$ offsets up to 7 ka at the beginning of the penultimate deglaciation are observed between Uk_{37}-SST alignments and the LR04 $\delta^{18}O$ stack (Fig. 9). Despite the large dating uncertainty of the LR04 stack (section 5.2), such large benthic $\delta^{18}O$ offsets seem to be difficult to reconcile with $\delta^{18}O$ offsets observed within the North Atlantic during the penultimate deglaciation (e.g. Lisiecki and Raymo, 2009) and our understanding of processes controlling benthic $\delta^{18}O$. Although it is not possible to assess which of these alignments produce the most robust chronologies due to the absence of well-dated markers, this example from the Iberian margin shows that the use of different SST tracers (e.g. alkenone-derived SST vs. planktonic foraminifera $\delta^{18}O$) can lead to very high age differences, especially at the onset of the penultimate deglaciation.

Recent studies show that different SST trends globally exist over the LIG depending on the method of SST reconstructions (e.g. Leduc et al., 2010; Jiménez-Amat and Zahn, 2015). They highlight that the chronologies of marine sediments from any region (especially when they are derived from different alignment methods and various tracers) should be considered with care throughout the LIG, in particular when investigating sequences of climatic events. Such considerations are not restricted to marine sediments and concern all types of climato-stratigraphic alignments, as for example further illustrated by uncertainties related to the interpretation of speleothem tracers (section 3.2, Table 1).

7.3. Comparison of different alignment targets

We estimate here to which extent the use of different alignment targets leads to different LIG chronologies, by using two examples, one from a marine sediment core and one from a continental pollen sequence.

In the first example, we compare four chronologies obtained in core MD95-2042 from the Portuguese margin by aligning the planktonic $\delta^{18}O$ record to four different targets. The MD95-2042 *G. bulloides* $\delta^{18}O$ record is aligned: (1) to ice core records on AICC2012 (Bazin et al., 2013; Veres et al., 2013), (2) to Corchia speleothem records (Drysdale et al., 2007, 2009) and to the GL_T_syn curve, itself used either on the (3) EDC3 or (4) Chinese speleothem time scales (Barker et al., 2011). Note that we included here the GL_T_syn curve for the sake of completeness of the exercise. However, this signal is not a direct tracer for Greenland temperature and relies on additional climatic hypotheses and calculations (see discussion in section 4.2). Hence, we do not recommend the use of the GL_T_syn curve as a target in climato-stratigraphic alignments. For comparison, we also include in this exercise the original MD95-2042 time

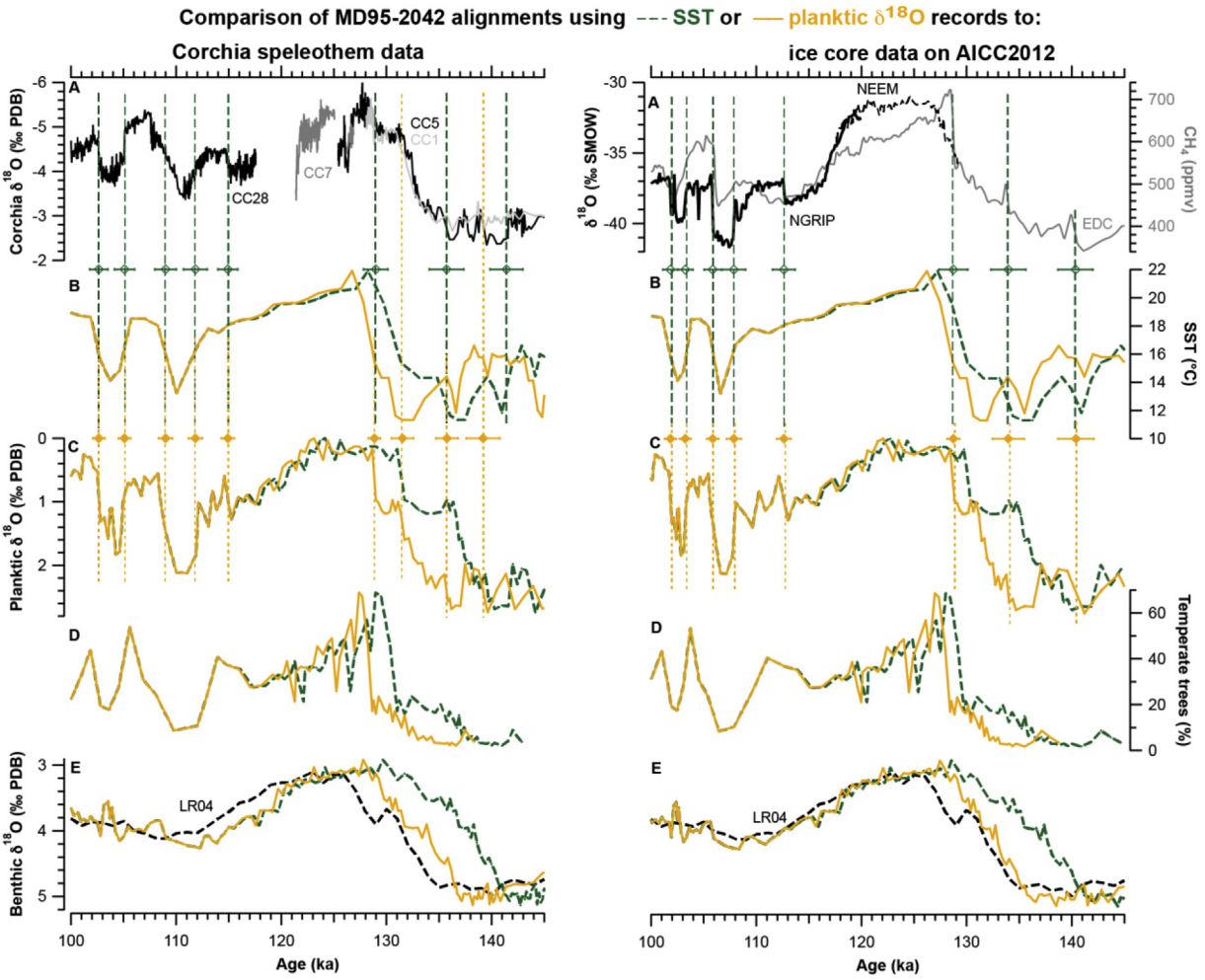

Fig. 9. Comparison of alignments applied to the North Atlantic core MD95-2042 to Corchia speleothem (*left panel*) and ice core data (*right panel*), using either the alkenone SST (dashed dark green line) or planktonic foraminifera *G. bulloides* $\delta^{18}O$ (orange line). (NB: *G. bulloides* $\delta^{18}O$ largely reflects local SST changes at that site (Shackleton et al., 2000)). A. (*left panel*) Calcite $\delta^{18}O$ records from Corchia speleothems: CC5 (black), CC1 (light grey) and CC7 (dark grey) data from Drysdale et al. (2009), and CC28 (black) data from Drysdale et al. (2007). (*right panel*) Ice core records: NGRIP ice $\delta^{18}O$ record (North Greenland Ice Core Project members, 2004) (thick line), NEEM ice $\delta^{18}O$ record (NEEM community members, 2013) (dotted line) and EDC CH_4 record (Loulergue et al., 2008) (grey line) presented on the AICC2012 time scale (Bazin et al., 2013; Veres et al., 2013). B-E. (*all panels*) MD95-2042 records (Shackleton et al., 2002): alkenone SST in B, planktonic *G. bulloides* $\delta^{18}O$ in C, the percentage of temperate trees (Eurosiberian and Mediterranean pollen species) in D, and benthic foraminifera $\delta^{18}O$ in E. These records (B–E) are plotted for the different alignment options using the same colour code (SST in dark green and planktonic $\delta^{18}O$ in orange). The LR04 $\delta^{18}O$ stack (Lisiecki and Raymo, 2005) is shown for reference (black dashed line in E). Symbols and vertical dashed/dotted lines, mark tie-points with 1σ age uncertainties relative to reference time scales. See Fig. 2 for site locations.

scale defined by aligning benthic $\delta^{18}O$ changes to radiometrically dated sea level changes (Shackleton et al., 2003) and the chronology derived from the benthic $\delta^{18}O$ alignment (section 7.1) to the LR04 stack (Lisiecki and Raymo, 2005). However, both latter alignments present severe limitations. The original MD95-2042 chronology is limited by the fact that (1) benthic $\delta^{18}O$ changes do not simply reflect sea level variations (e.g. Waelbroeck et al., 2008) and that (2) the local sea level data used by Shackleton et al. (2003) have not been corrected for glacio-isostasic processes (Dutton and Lambeck, 2012) and do not reflect global sea level changes. In contrast, the alignment to the LR04 stack ignores the possibility of diachronous benthic $\delta^{18}O$ changes across water-masses (see discussion in sections 5.2 and 7.1). Therefore, age uncertainties provided for these two alignments are likely underestimated.

Combined 1σ age uncertainties, which arise from resolution, alignment errors and absolute dating uncertainties of reference records, range between (1) 1.6 and 3.3 ka for alignment to AICC2012, (2) 0.7 and 1.8 ka for alignment to Corchia, (3) 1.6 and 3.4 ka for alignment to GL_T_syn on EDC3 time scale, (4) 1.4 and 2.2 ka for alignment to GL_T_syn on the Chinese speleothem time scale (Table S6). In contrast, age uncertainties reach ~4.2 ka for the benthic $\delta^{18}O$ alignment to LR04 (Table S6). Combined errors for all planktonic $\delta^{18}O$ alignments are higher during the penultimate deglaciation than during the glacial inception (Fig. 10), due to (1) uncertainties on the onset and evolution of North Atlantic deglacial warming that make graphical matching uncertain and (2) high dating errors of reference records prior to 130 ka, in particular for ice core chronologies (Table S6).

In the second example, we compare the LIG age models obtained in the continental sequence of Ioannina from NW Greece (Tzedakis et al., 2003) using five different alignment targets for the Ioannina 284 pollen record (Fig. 11): (1) direct pollen-orbital tuning based on the hypothesis that tree population minima occurred during cold and dry periods at times of March perihelion and that interglacial expansion of Mediterranean vegetation took place during periods of maximum summer temperature and evaporation regimes at times of June perihelion, in line with sapropel events (see details in Magri and Tzedakis, 2000 and Tzedakis et al., 2003),

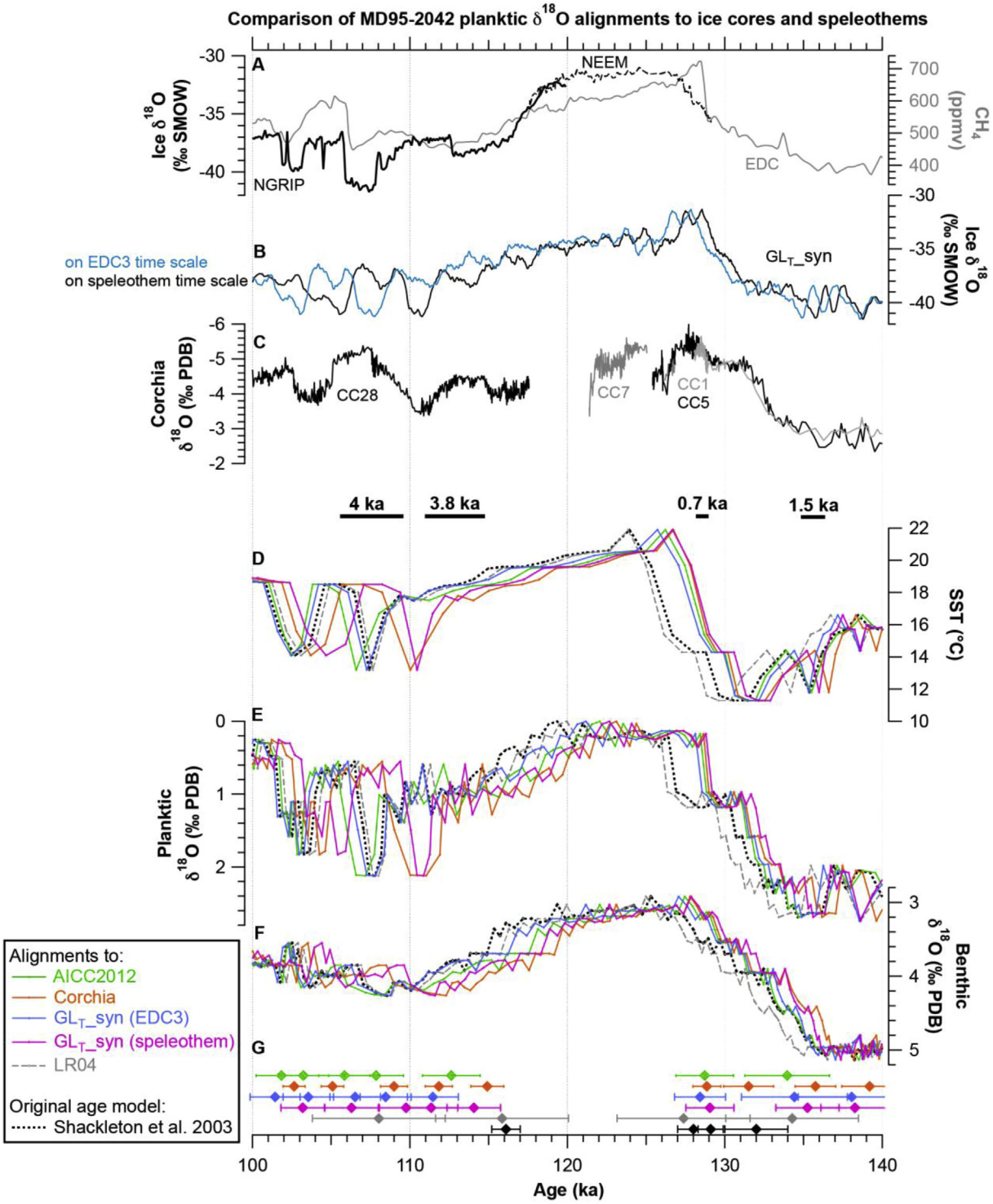

Fig. 10. Comparison of four alignments applied to the North Atlantic core MD95-2042 using its planktonic foraminifera $\delta^{18}O$ record: to ice core records on AICC2012 (Bazin et al., 2013; Veres et al., 2013) (green), to Corchia speleothem records (Drysdale et al., 2007, 2009) (orange, alignment similar to Drysdale et al., 2009) and to the Greenland synthetic curve (GL_T_syn) (Barker et al., 2011) presented on the EDC3 (blue) or speleothem (pink) time scale. The alignment of MD95-2042 benthic $\delta^{18}O$ to the LR04 stack (Lisiecki and Raymo, 2005) (grey dashed line) and the original chronology defined by Shackleton et al. (2003) (black dotted line) are also shown (see section 7.3 for their respective limitations). A. Ice core records: NGRIP ice $\delta^{18}O$ record (North Greenland Ice Core Project members, 2004) (thick line), NEEM ice $\delta^{18}O$ record (NEEM community members, 2013) (dashed line), and EDC CH_4 record (Loulergue et al., 2008) (grey line) presented on AICC2012 (Bazin et al., 2013; Veres et al., 2013). B. Greenland ice $\delta^{18}O$ synthetic record (GL_T_syn) shown on the EDC3 (blue) or speleothem (black) time scales (Barker et al., 2011). C. Calcite $\delta^{18}O$ records from Corchia speleothems: CC5 (black), CC1 (light grey) and CC7 (dark grey) data from Drysdale et al. (2009), and CC28 (black) data from Drysdale et al. (2007). D-F. MD95-2042 records (Shackleton et al., 2002): SST in D, planktonic foraminifera (*G. bulloides*) $\delta^{18}O$ in E and benthic foraminifera $\delta^{18}O$ in F. G. Tie-points defined for each alignment method (same colour code). For all alignment methods, error bars are 1σ age uncertainties, which include relative matching errors and the absolute dating uncertainty of reference records. For the original time scale defined by Shackleton et al. (2003) (black), error bars represent radiometric age errors of coral dating and do not include the uncertainty related to the fact that benthic $\delta^{18}O$ does not solely reflect sea level changes. Horizontal bars between panels C and D show the spread in ages of events between the different planktonic $\delta^{18}O$ alignment methods (the benthic $\delta^{18}O$ alignment to the LR04 stack and the original time scale defined by Shackleton et al. (2003) are excluded here). See Fig. 2 for site locations.

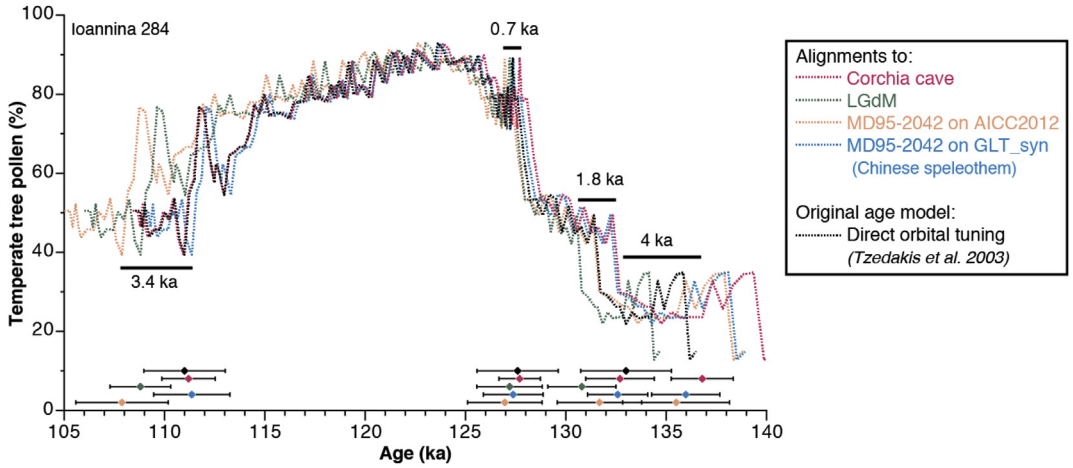

Fig. 11. Comparison of five different alignment targets to develop chronologies for the LIG section of the Ioannina 284 sequence, NW Greece (see section 7.3 for details). Also shown at the base of the diagram are the combined 1σ chronological uncertainties, arising from resolution, alignment errors and absolute dating errors, associated with each control point used in the different schemes. Horizontal bars denote spread in ages of events between different schemes. See Fig. 2 for site location.

(2) alignment to the speleothem $\delta^{18}O$ record from Corchia cave (Drysdale et al., 2007, 2009), (3) alignment to the pollen record from LGdM (Allen and Huntley, 2009) and alignment to the pollen record from core MD95-2042 (Shackleton et al., 2002, 2003) on (4) the GL_T_syn speleothem chronology (Barker et al., 2011) and (5) the AICC2012 chronology (Bazin et al., 2013; Veres et al., 2013). Combined uncertainties are around 2–2.3 ka for orbital tuning, 1.3–1.7 ka for alignment to Corchia, 1.5–1.7 ka to LGdM, 1.5–1.9 ka for alignment to MD95-2042 on the GL_T_syn speleothem time scale and 1.8–2.6 ka for alignment to MD95-2042 on the AICC2012 chronology, respectively.

Both alignment exercises reveal that most of age control points are concentrated during the penultimate deglaciation and the last glacial inception, with poor temporal control within the LIG interval, regardless of the alignment method (Figs. 10 and 11). This is due to the globally limited temporal resolution of records and the absence of marked climate variations during this interval.

For both exercises, there is also convergence on the timing of the onset of the LIG acme (~128–129 ka in the marine core and ~128 ka in the continental sequence) with most chronologies within 0.7 ka of each other (Figs. 10 and 11). This timing agrees with the onset of the LIG dated at 127.2 ± 1.6 ka in the annually laminated record from LGdM (Brauer et al., 2007). Spread of ages is larger during the penultimate deglaciation and reach up to 1.5 ka in the marine core and 4 ka in the continental sequence. These results reflect (1) the good agreement between the AICC2012, EDC3 ice core and Chinese and European speleothem chronologies during the deglaciation (Bazin et al., 2013) (section 4) and (2) increased alignment uncertainties during the penultimate glacial section of records (e.g. section 7.2). In contrast, there is wider spread of ages during the glacial inception. Age differences reach 3.8 ka at the onset of warm GI-25 and 4 ka at the onset of GI-24 in the marine core, and 3.4 ka at the onset of cold GS-25 in the pollen sequence. These offsets are higher than our estimated age uncertainties (below 1.8 ka, Table S6) and arise from the known divergence between ice core and speleothems chronologies at that time (section 4). In comparison, ages derived in the marine core from the benthic $\delta^{18}O$ alignment to LR04 and the original MD95-2042 chronology (Shackleton et al., 2003) mostly fall within the range of ages defined from planktonic alignments (Fig. 10). However, a systematic offset emerges during the deglaciation, where ages in the benthic alignments are up to 3 ka younger than in planktonic alignments (although such age differences remain within the large uncertainties of the LR04 chronology).

Therefore, this exercise illustrates the importance of reporting precisely the alignment method for a given studied site. Indeed, in this particular case, the different methodologies produce age differences up to 4 ka across the penultimate deglaciation and the LIG. This result calls for caution when comparing LIG marine (and/or continental) records using various alignment targets or different reference time scales. These uncertainties can indeed strongly affect the estimation of LIG temperature trends and the comparison between marine records and climate simulations (Bakker and Renssen, 2014).

7.4. Recommendations and perspectives

Detailed investigations based on archives with few or no absolute dating markers require careful selection of the climato-stratigraphic alignment method to be applied, depending on the paleoclimatic objectives. For example in marine sediments, benthic $\delta^{18}O$ alignment to reference records is unsuitable to investigate millennial-scale variability and sequences of events between the northern and southern high latitudes during the penultimate deglaciation and the LIG. In addition, our examples highlight decreased age uncertainties in the case of direct alignments to absolutely dated records (e.g. alignments to speleothems), if compared to alignments between archives with relative chronologies only (e.g. relative alignments to marine sediment or ice cores). Regardless of the alignment method, our examples also show a lack of reliable markers within the LIG interval, which limits investigations of submillennial-scale climate variability during peak interglacial times.

Finally, our exercise comparing alignment methods across the LIG for specific examples shows age differences up to 4 ka when different reference chronologies (e.g. ice cores vs. speleothems) or different types of aligned records (e.g. Uk_{37}-SST vs. planktonic foraminifera $\delta^{18}O$) are used. It is, therefore, fundamental, in comparisons of paleoclimatic records from different sites and model-data comparisons, to carefully examine the alignment method applied (is the underlying hypothesis verified? which tracers are aligned?) and assess the coherence of the different chronologies used, which both contribute to increase age uncertainties. It is also

essential in future studies to carefully estimate relative and absolute age uncertainties and integrate these uncertainties in paleoclimatic interpretations.

8. Future potential of magnetic stratigraphy

The Geomagnetic Polarity Time Scale (GPTS) (Cande and Kent, 1995; Ogg, 2012) represents the stratigraphic backbone on which the geologic timescale for the last ~150 Ma is based (see Opdyke and Channell, 1996 for a thorough review). Magnetic reversals are recorded in many types of geologic materials and their global synchronicity (on geologic time scales) and climatic independence make them a powerful stratigraphic tool for Quaternary sediment, ice core and speleothem records. However, the most recent polarity reversal, the Brunhes/Matuyama boundary, is dated at 0.781 Ma (Ogg, 2012), which renders the GPTS of no use for younger sequences such as those from the LIG. On the other hand, changes in geomagnetic field strength known as paleointensity, short duration changes in the position of the Geomagnetic Pole (>40° from axis of rotation, Barbetti and McElhinny (1972)) known as geomagnetic excursions, and local changes in field directions known as paleomagnetic secular variation (PSV), can all, in principle, provide much needed chronostratigraphic markers during the LIG (Stoner and St-Onge, 2007).

Possibly the most significant development in magnetic stratigraphy over the last few decades has been the recognition that when properly normalized and in optimal conditions, the intensity of the natural remanent magnetization obtained from marine sediments represents globally coherent variations in strength of Earth's magnetic field (e.g. Stoner et al., 2000; Valet et al., 2005; Channell et al., 2009). These relative paleointensity records, therefore, provide a unique opportunity for stratigraphic synchronisation even during times of constant polarity (Stoner et al., 1998; Channell et al., 2009, 2014). High-resolution studies suggest that relative paleointensity records could be globally coherent on timescales as short as a few thousand years (Stoner et al., 2000; Laj et al., 2004), though additional work is needed to define the ultimate resolution.

With 13–17 excursions now advocated in the Brunhes Chron (Lund et al., 2006; Singer, 2014), these short duration changes in the magnetic pole (<2 ka) (e.g. Laj et al., 2014) could provide "golden spikes" in the stratigraphic record. During the LIG, the Blake Event (~120 ka) (Thouveny et al., 1990; Laj and Channell, 2007; Singer, 2014) and the Post-Blake excursion (~100 ka) (Thouveny et al., 1990; Singer, 2014), as well as intensity lows associated with them, are recognized in several sediment records (though often with age discrepancies, Table 4), and not observed in many others. These inconsistencies highlight our incomplete understanding of the geomagnetic field in detail, a situation that at least partially results from the sediment magnetization acquisition and our incomplete understanding of the process (Roberts et al., 2013). The recent recovery of two excursional intervals from a precisely dated Spanish speleothem (B2 and B1 reversed intervals dated around 116 ka and 113 ka, respectively) purported to be associated with the Blake event between 116.5 ± 0.7 ka and 112.0 ± 1.9 ka (Osete et al., 2012; Rossi et al., 2014) offers enormous potential for constraining the age of this event and illustrates how magnetostratigraphic opportunities cut across ice, marine, lake and speleothem archives.

Directional changes referred to as paleomagnetic secular variations (PSV) can also provide precise correlation at centennial or better temporal level (e.g. Stoner and St-Onge, 2007; Ólafsdóttir et al., 2013), but our incomplete understanding of the geomagnetic field and magnetic recording process presently limits precise synchronization to records of similar resolution from proximal locations. When taken together, high-frequency variability in direction (PSV) and intensity (RPI) offers the exciting potential for new types of magnetic stratigraphy that could and should be employed for the LIG.

One unique aspect of paleointensity is its relationship to cosmogenic isotopes. Assuming a constant flux of galactic cosmic rays, the production rate of cosmogenic isotopes (e.g. ^{10}Be, ^{14}C, ^{36}Cl) primarily reflects variations in the strength of the Earth's and Sun's magnetic fields, with stronger (weaker) magnetic fields enhancing (weakening) the magnetic "shielding" effect and resulting in reduced (increased) cosmogenic isotope production (Lal, 1988; Masarik and Beer, 1999). Changes in cosmogenic isotope production rates and relative paleointensity (e.g. Mazaud et al., 1994; Stoner et al., 2000; Ménabréaz et al., 2014) show substantial agreement, especially during excursions (e.g. Carcaillet et al., 2004; Thouveny et al., 2004; Ménabréaz et al., 2014). Therefore, the relationship between geomagnetic paleointensity and cosmogenic isotope production provides a viable technique for synchronizing sediment and ice core records (e.g. Mazaud et al., 1994; Stoner et al., 2000; Carcaillet et al., 2004; Ménabréaz et al., 2014). A series of studies employing the combined use of relative paleointensity and direct measurements of cosmogenic isotopes from the same sediment intervals are moving us closer toward an understanding of the global-scale geomagnetic signal (e.g. Carcaillet et al., 2004; Thouveny et al., 2004; Ménabréaz et al., 2012). These records show substantial variability during the LIG that could pave the way for the development of highly detailed magnetic stratigraphies during this time interval (Fig. 12). Identifying the signature of the Blake event in ice core ^{10}Be records would further our understanding of the geomagnetic field during this time interval and moreover provide an important stratigraphic link between ice cores and other climatic archives (Christl et al., 2004). At present, these excursions can offer important LIG stratigraphic control in some locations, but the timing, spatial signature, and morphology of these features are still too poorly understood for routine application without additional stratigraphic calibration.

A concerted effort is mandatory to surpass the simple confirmation of excursions such as the Blake and post-Blake Events (Carcaillet et al., 2004; Thouveny et al., 2004) (Table 4), and develop a full understanding of geomagnetic field changes during the LIG, making it possible to use a variety of magneto-stratigraphic markers over a wide range of temporal and spatial scales and provide direct ties to the chronologies of ice cores from both hemispheres. Ultimately, the success of using geomagnetic paleointensity signals as a stratigraphic tool rests on our ability to achieve independent age control. This can be done by way of detecting them in U–Th dated speleothems (see Lascu and Feinberg (2011) for an overview of recent developments) or linking them through cosmogenic isotope abundance fluctuations with ice core chronologies, and by overcoming uncertainties associated with the magnetization acquisition process (see Roberts et al., 2013 for a review).

9. Sequence of events at the onset and demise of the LIG

We take advantage of this review of existing dating strategies to document the climatic sequence of events, with related age uncertainties, from the penultimate deglaciation to the glacial inception (period 140–105 ka). In selected high-resolution records from ice cores, speleothems, lake and marine sediments (Fig. 13), we identified using the RAMPFIT software (Mudelsee, 2000) (1) the onset of the deglacial period, (2) the onset of the LIG acme, (3) the demise of the LIG acme and (4) the establishment of glacial conditions (see Fig. 1 for how these terms are used in this specific study). Age uncertainties (1σ) reported in this section include (1) the "internal" error of the event (given by RAMPFIT), (2) the alignment error of the chosen alignment method for lake and

Table 4
Age estimates of the Blake and Post-Blake excursions in a few paleomagnetic records.

LIG excursions	Age (ka)							
	GITS Singer (2014)	ODP synthesis Lund et al. (2006)	PISO 1500 Channell et al. (2009)	ODP1063 Bermuda rise Channell et al. (2012)	^{10}Be Portuguese margin Carcaillet et al. (2004)	Speleothem Spain Osete et al. (2012)	Lac du Bouchet France Thouveny et al. (1990)	Lava flows Iceland Singer et al. (2014)
Blake	120 ka	123 ± 3 ka	120 ka	115.5 ka	~117 ka	116.5 to 112 ka	117 ka[b]	120 ± 12 ka (Amsterdam island)
Post-Blake	100 ka	~100 ka	100 ka	[a]	~95 ka	–	95 and 104 ka	104 ± 12 ka (New Mexico) 105 ± 1 ka (Lipari)

PISO 1500: Paleointensity and oxygen isotope stack for the last 1500 ka.
GITS: Geomagnetic Instability Time Scale.
[a] Not seen on detailed u-channel data, but observed on half-core shipboard data after demagnetization at a peak field of 20 mT.
[b] Reverse to normal transition interpreted as the end of the event.

marine sediments and (3) the absolute dating error of the used time scale (Table S8). Given age uncertainties do not include the age dispersion related to the use of different alignment targets (discussed in section 7.3 and illustrated by horizontal arrows in Fig. 13).

9.1. The penultimate deglaciation

We identify three successive phases of events during the penultimate deglaciation (Table 5).

(1) The first deglacial phase (138–135 ka) is characterised by early changes in atmospheric greenhouse gas concentrations, such as the increase in CO_2 (137.8 ± 2.7 ka) and CH_4 (137.1 ± 2.7 ka), in line with results from Landais et al. (2013). Sea level had already risen up to 85 m below the modern level at 137 ka (Thomas et al., 2009). Some European speleothem $\delta^{18}O$ records around the Mediterranean area (Corchia, Soreq, Fig. 5) also suggest early changes (~136 ka) during the penultimate deglaciation, coincident with the increase in obliquity (Drysdale et al., 2009) or related to early sea level changes.

(2) The second deglacial phase (~135–129 ka) corresponds to the interval of large iceberg discharges (possibly related to the cold Heinrich event H11), as highlighted by the North Atlantic peak in

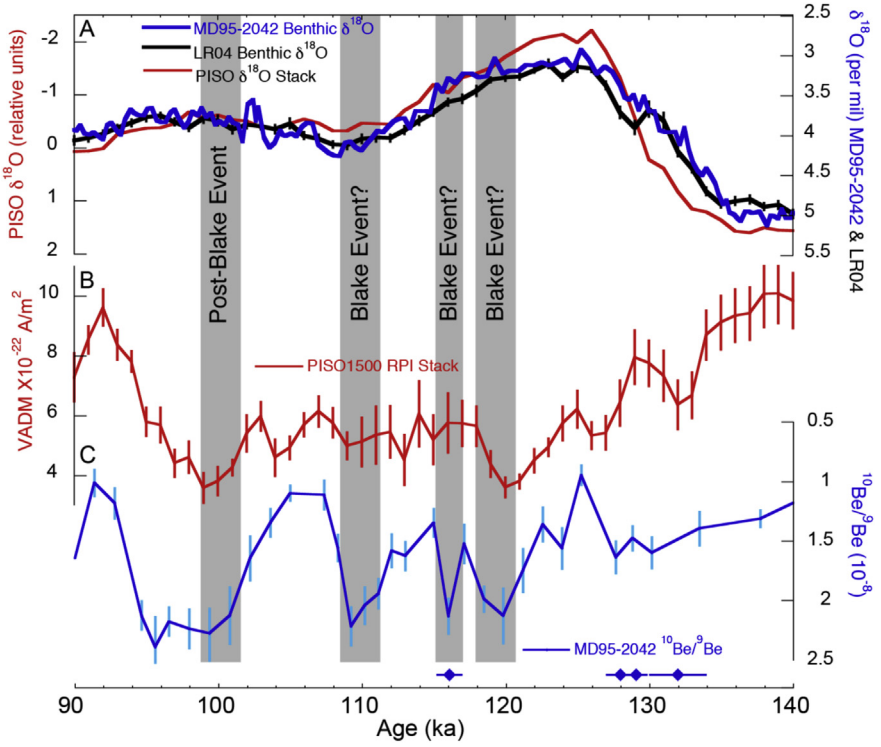

Fig. 12. Comparison between foraminifera $\delta^{18}O$, relative paleointensity, and $^{10}Be/^{9}Be$ ratios from 140 to 90 ka. (A) Foraminifera $\delta^{18}O$ record from the PISO-1500 stack (red, relative units) (Channell et al., 2009) (which combines benthic and planktonic $\delta^{18}O$ records of the 13 sites used to derive the 1.5-Ma long paleointensity stack), in comparison to LR04 (black) (Lisiecki and Raymo, 2005) and MD95-2042 (blue) (Shackleton et al., 2000, 2003) benthic ^{18}O records. Note that differences between PISO-1500, LR04 and MD95-2042 foraminifera $\delta^{18}O$ records are within age errors (e.g. ± 4 ka for LR04, Lisiecki and Raymo, 2005). (B) PISO-1500 paleointensity (RPI) stack (red) with its ± 1σ error (Channell et al., 2009). (C) $^{10}Be/^{9}Be$ ratio with the propagated ^{10}Be, ^{9}Be concentration uncertainties from core MD95-2042 (blue) (Carcaillet et al., 2004) on the Shackleton et al. (2003) chronology (blue diamonds mark tie-points with 1σ age errors). Note that this age model differs from the chronology originally published (Carcaillet et al., 2004). Grey bars mark the likely position of the Blake and Post-Blake events in the $^{10}Be/^{9}Be$ record from core MD95-2042. These events are less clearly visible in the PISO paleointensity stack. This result highlights the difficulty to identify the Blake and Post-Blake events in lower-resolution stacked records and the necessity to consider high-resolution relative geomagnetic paleointensity records in conjunction with cosmogenic isotope records to use these events to develop robust stratigraphies during the LIG. See Fig. 2 for site locations.

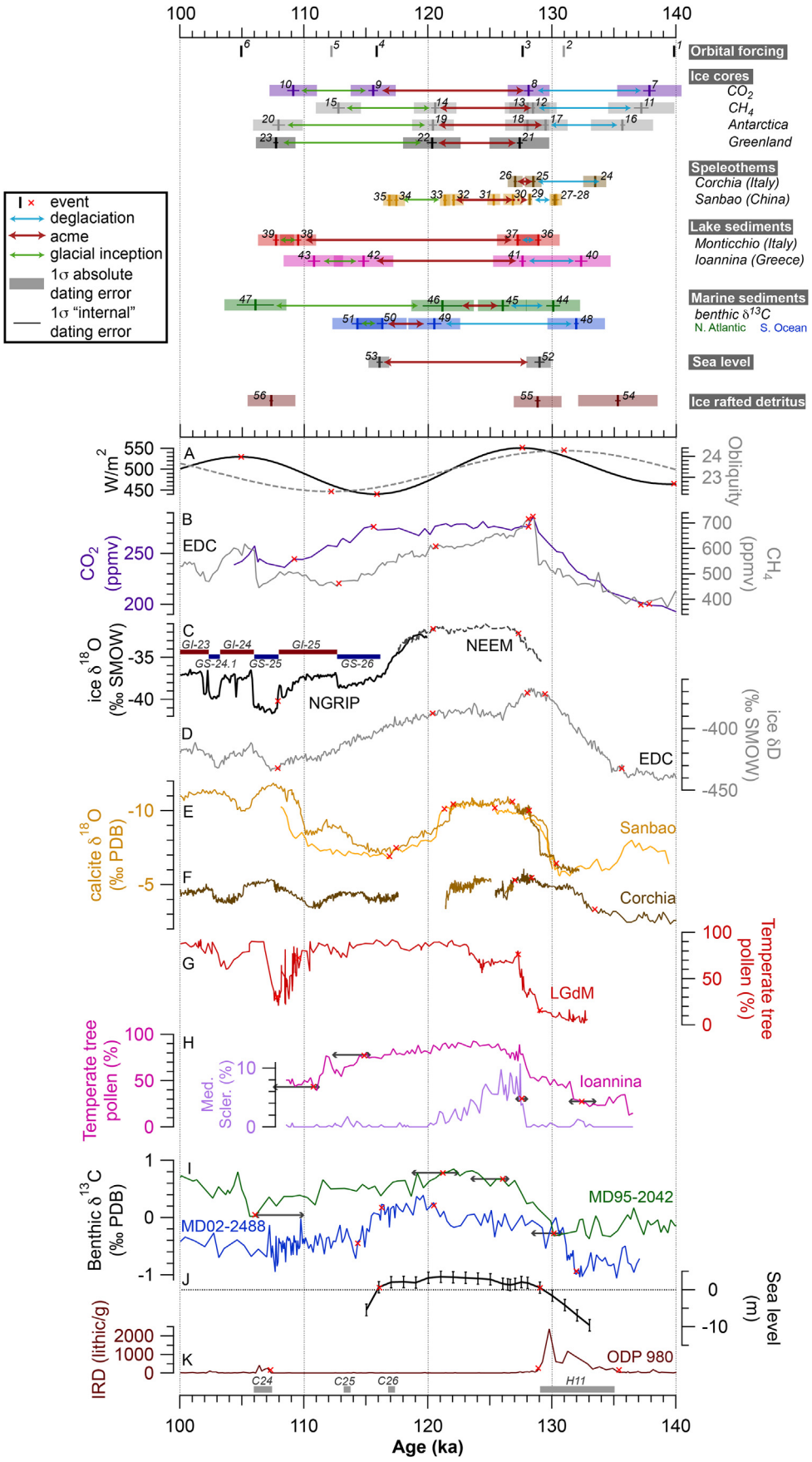

Fig. 13. Sequence of major climatic events across the period 140–100 ka. (*Lower panel*) Main paleoclimatic records. A. Obliquity (dashed grey) and 65°N summer (June 21) insolation (black) (Laskar et al., 2004). B. EDC CO_2 (purple) (Schneider et al., 2013) and CH_4 (grey) (Loulergue et al., 2008) concentrations. C. NGRIP (thick black) and NEEM (dashed black) ice

ODP980 ice rafted detritus (IRD) that starts around 135 ka (e.g. Oppo et al., 2006) (Table 5A). This event may be concurrent with a major North Atlantic freshwater event (Seidenkrantz, 1993), the slowdown of Atlantic meridional overturning circulation (Seidenkrantz et al., 1996) and a cooling event identified in the pollen record of La Grande Pile (France) (e.g. Woillard, 1978), which may be related to a Younger Dryas-type event of the deglacial phase at 131–130 ka (Seidenkrantz et al., 1996). New high-resolution records also reveal a ~2 ka pause in the NW Mediterranean Sea SST evolution (Martrat et al., 2014) and a climatic event lasting ~1.5–2 ka that affected the global carbon and oxygen cycles, as well as the global atmospheric composition during the deglacial warming (Landais et al., 2013). These features suggest millennial-scale and global-scale climatic processes at play during the penultimate deglaciation.

Antarctic reconstructed surface temperatures started increasing (at 135.6 ± 2.5 ka) at the beginning of the interval of North Atlantic iceberg melting, in line with the bipolar seesaw pattern observed during the last glacial and deglacial period (EPICA Community members, 2006). The increase in the percentage of temperate tree pollen recorded in Greece suggests the onset of warmer and wetter conditions at ~132.3 ± 2.3 ka (Fig. 13) in southern Europe. This is in phase with the onset of deglaciation dated at 130.6 ± 1.6 ka in southern Italy based on pollen species abundance and mean varve thickness from the LGdM laminated sequence (Brauer et al., 2007). Simultaneously, the ventilation of Southern Ocean and North Atlantic deep waters (at ~ 3100 and 3400 m, respectively) starts increasing at 131.9 ± 2.3 ka and 130.1 ± 2.2 ka (Fig. 13), respectively, which suggests the invigoration of the deep ocean circulation already during the deglacial IRD event indicated by the North Atlantic ODP980 record. Asian speleothem $\delta^{18}O$ records display a major calcite $\delta^{18}O$ shift around 130 ka (Fig. 5). The abrupt increase in Sanbao speleothem $\delta^{18}O$ between 129 and 130 ka (±0.5 ka), in good agreement with the well-dated Dongge D4 speleothem (Yuan et al., 2004; Kelly et al., 2006) indicates the rapid intensification of the Asian summer monsoon at the end of the North Atlantic ODP980 deglacial IRD event (e.g. Cheng et al., 2009). In parallel, the slow deglacial increase in CH_4 is interrupted at 128.9 ± 1.7 ka by an abrupt jump toward maximum values reached at 128.5 ± 1.7 ka. Finally, peak LIG Antarctic reconstructed temperatures are reached at 129.4 ± 1.8 ka, i.e. in phase, within age errors, with the end of the deglacial ODP980 IRD peak (128.8 ± 1.9 ka). This result agrees with the hypothesis that the early LIG Antarctic warming is a response to reduced deep ocean circulation induced by northern hemisphere freshwater input during the deglaciation (e.g. Masson-Delmotte et al., 2010a; Capron et al., 2014).

(3) The third phase (~129–120 ka) reflects the progressive establishment of the LIG acme. The sea level highstand is reached at 129.0 ± 1.0 ka (Dutton and Lambeck, 2012). After a progressive deglacial increase, maximum CO_2 values are reached at 128.0 ± 1.8 ka. Both CO_2 and CH_4 maxima follow directly the end of the major North Atlantic iceberg melting event. Simultaneously, speleothem $\delta^{18}O$ records indicate the development of warm and wet conditions in Europe (128.5–128 ± 0.9 ka) and in Asia (128.2 ± 0.5 ka), while Greenland warm conditions (indicated by NEEM ice $\delta^{18}O$) are recorded at 127.3 ± 2.4 ka, in phase with the onset of North Atlantic interglacial conditions (e.g. Capron et al., 2014; Martrat et al., 2014). The onset of well-ventilated North Atlantic deep waters (at ~3100 m) takes place around 125.9 ± 2.0 ka (Fig. 13). This feature may reflect the impact of persistent North Atlantic iceberg melting on the deep ocean circulation during the early LIG (Hodell et al., 2009; Govin et al., 2012). The onset of the LIG acme is simultaneously observed in southern Europe, as reflected by pollen sequences from Greece (127.5 ± 2.3 ka, Table 5A, Fig. 13) and Italy (127.2 ± 1.6 ka, Brauer et al., 2007). Finally, the maximum in the ventilation of Southern Ocean deep waters (at ~3400 m) at 120.4 ± 2.4 ka may derive from the lack of tie-points within the LIG (section 7.1) and would need to be checked with better-dated records.

The deglacial history proposed here agrees with previous hypotheses on the forcing and mechanisms driving the penultimate deglaciation (e.g. Cheng et al., 2009; Landais et al., 2013). Although the increase in boreal summer insolation (starting at 139.7 ka, Table 5A) is a necessary forcing of the deglaciation, the presence of large northern ice sheets, whose collapse is triggered by the rise in boreal summer insolation, is required to initiate the deglacial sequence of events (Cheng et al., 2009). Several mechanisms have been proposed to explain the initial deglacial rise in CO_2 and Antarctic reconstructed temperature (Table 5A), in response to the deglacial collapse of northern ice sheets: (1) bipolar seesaw mechanisms (involving an AMOC slowdown and reduced northward heat transport), (2) southward shift in the position of the southern hemisphere westerlies promoting the upwelling of poorly ventilated waters in the Southern Ocean, (3) decreased brine formation around Antarctica causing CO_2 outgassing and (4) decreased biological pump (see Cheng et al., 2009; Landais et al., 2013 for detailed discussions). The deglacial history that we propose here with related dating uncertainties may serve as a reference sequence of events to help disentangle climate mechanisms involved in this transition and assess transient climate model simulations.

9.2. The LIG acme

The duration of the LIG acme (see Fig. 1 for how this term is used in this study) varies widely depending on the climatic archives and tracers that are considered (Fig. 13). While the timing of the onset of the LIG acme is relatively simultaneous, mostly taking place between 129 and 126 ka, the timing of the demise of the LIG acme is more variable and ranges between 122 and 113 ka. This variability in the acme duration highlights the complexity of climate

$\delta^{18}O$ (North Greenland Ice Core Project members, 2004; NEEM community members, 2013). Dark red and blue bars mark the recent GI and GS nomenclature defined in Greenland ice cores (Rasmussen et al., 2014). D. EDC δD (grey) (Jouzel et al., 2007). All ice core records are presented on the AICC2012 time scale (Bazin et al., 2013; Veres et al., 2013). E. Calcite $\delta^{18}O$ records from the Chinese Sanbao SB41 (light brown), SB23 (intermediate brown) (Wang et al., 2008) and SB25 (dark brown) (Cheng et al., 2009) speleothems. F. Calcite $\delta^{18}O$ records from the Italian Corchia CC5 (140–125 ka, dark brown), CC7 (lighter brown) (Drysdale et al., 2009) and CC28 (117–100 ka, dark brown) (Drysdale et al., 2007) speleothems. G. Percentage of temperature tree pollen (dark pink) and Mediterranean Sclerophylls pollen (purple) from the Greek Ioannina sequence (Tzedakis et al., 2003) presented on the original orbital-tuning time scale (section 7.3). H. Percentage of temperature tree pollen (dark red) from the Italian Lago Grande di Monticchio (LGdM) sequence (Brauer et al., 2007) presented on the original independent (varve) chronology. I. Benthic foraminifera $\delta^{13}C$ records from the North Atlantic MD95-2042 core (dark green) (Shackleton et al., 2002) and the Southern Ocean MD02-2488 core (blue) (Govin et al., 2012), both presented on AICC2012 (sections 7.1 and 7.3). J. Global mean sea level variations (black) (Dutton and Lambeck, 2012). K. Ice rafted detritus (IRD) from the North Atlantic ODP980 core (Oppo et al., 2006) presented on the AICC2012 time scale (see Capron et al., 2014). Horizontal grey bars mark the North Atlantic cold events H11, C26, C25 and C24 defined in marine sediments (e.g. Oppo et al., 2006; Bauch and Kandiano, 2007). Horizontal grey arrows in panels H–I illustrate the age dispersions induced by the use of different alignment methods applied in marine core MD95-2042 and the Ioannina continental sequence (section 7.3). (*Upper panel*) Timing and dating uncertainties of major paleoclimatic events. Using the same colour code as for records presented in the lower panel, thick vertical lines mark the date of events. Thin horizontal lines mark the 1σ "internal" dating uncertainty within the archive (i.e. relevant when comparing the timing of events within the same archive). Shaded rectangles highlight the 1σ combined dating uncertainty, which includes the "internal" age uncertainty, the alignment error (for marine and some lake sediments) and the absolute dating uncertainty of the used time scale (Table S8). Arrows mark the period of deglaciation (blue), of the LIG acme (red) and of the last glacial inception (green). Events are characterised by a unique number (list given in Table S8) and highlighted by red crosses on dedicated records in the lower panel. See Fig. 2 for site locations.

Table 5
Sequence of characteristic paleoclimatic events during (A) the penultimate deglaciation and (B) the last glacial inception. If not specified otherwise, events are defined from selected records using the RAMPFIT software (Mudelsee, 2000; code from 2013). Numbers in brackets (in italic) are event numbers indicated in Fig. 13 and Table S8. The given age errors include the "internal" error on the timing of events (given by RAMPFIT), the error related to the transfer of records on a specific time scale (for lake and marine sediments) and the absolute dating uncertainty of used time scales (see Table S8 for details).

Phase	Date (ka)	Age error (ka, 1σ)	Climatic events
A. During the penultimate deglaciation			
Insolation	149.4[a]		*(not shown)* Obliquity starts increasing
(forcing)	139.7[a]		*(1)* Insolation (65°N, June 21) starts increasing
Phase 1 (~138–135 ka)	137.8	2.7	*(7)* CO_2 (EDC) starts increasing
early changes	137.1	2.7	*(11)* CH_4 (EDC) starts increasing
Phase 2 (~135–129 ka)	135.6	2.5	*(16)* Antarctic reconstructed surface air temperature (EDC δD) starts increasing
interval of large ice sheet melting	135.3[a]	3.2	*(54)* Beginning of deglacial IRD peak in the North Atlantic (ODP980)
	133.4–136	1.1	*(24)* European speleothem (Corchia, Soreq) $\delta^{18}O$ starts decreasing
	132.3[b]	2.3	*(40)* Temperate tree pollen starts increasing in Greece (Ioannina)
	131.9[c]	2.3	*(48)* Southern Ocean (MD02-2488) benthic foraminifera $\delta^{13}C$ starts increasing
	130.1[d]	2.2	*(44)* North Atlantic (MD95-2042) benthic foraminifera $\delta^{13}C$ starts increasing
	129–130	0.5	*(27–28)* Asian speleothem (Sanbao, Dongge) $\delta^{18}O$ starts decreasing
	129.4	1.8	*(17)* Antarctic reconstructed surface air temperature (EDC δD) reaches maximum LIG values
	128.8[a]	1.9	*(55)* End of deglacial IRD peak in the North Atlantic (ODP980)
Phase 3 (~129–120 ka)	129.0	1.0	*(52)* Global mean sea level reaches the LIG highstand
establishment of LIG conditions	128.5	1.9	*(12)* CH_4 (EDC) reaches maximum LIG values
	128–128.5	0.9	*(25)* European speleothem (Corchia, Soreq) $\delta^{18}O$ reaches minimum LIG values
	128.2	0.5	*(29)* Asian speleothem (Sanbao SB25, Dongge) $\delta^{18}O$ reaches minimum LIG values
	128.0	1.8	*(8)* CO_2 (EDC) reaches maximum LIG values
	127.5[b]	2.3	*(41)* Mediterranean Sclerophyll pollen reaches maximum LIG values in Greece (Ioannina)
	127.3	2.4	*(21)* Greenland (NEEM) ice $\delta^{18}O$ reaches maximum LIG values
	127.2	1.6	*(37)* Temperate tree pollen reach LIG max values in Italy (Monticchio)
	125.9[d]	2.0	*(45)* North Atlantic (MD95-2042) benthic foraminifera $\delta^{13}C$ reaches maximum LIG values
	120.4[b]	2.1	*(49)* Southern Ocean (MD02-2488) benthic foraminifera $\delta^{13}C$ reaches maximum LIG values
B. During the last glacial inception			
Insolation[e]	130.8[a]		*(2)* Obliquity starts decreasing
(forcing)	127.5[a]		*(3)* Insolation (65°N, June 21) starts decreasing
Phase 1 (~122–120 ka)	121.1[d]	2.5	*(46)* North Atlantic (MD95-2042) benthic foraminifera $\delta^{13}C$ starts decreasing
early changes	121–122	0.8	*(32–33)* Asian speleothem (Sanbao, Dongge) $\delta^{18}O$ starts increasing
	120.6	1.7	*(14)* CH_4 (EDC) starts decreasing
	120.3	1.7	*(19)* Antarctic reconstructed surface air temperature (EDC δD) starts decreasing
	120.3	2.3	*(22)* Greenland (NEEM) ice $\delta^{18}O$ starts decreasing
Phase 2 (~118–113 ka)	117.2	0.7	*(34)* Asian speleothem (Sanbao, Dongge) $\delta^{18}O$ reaches glacial values
intensification of glaciation	116.0	0.8	*(53)* Global mean sea level starts decreasing
	116.2[c]	2.0	*(50)* Southern Ocean (MD02-2488) benthic foraminifera $\delta^{13}C$ starts decreasing
	115.5	1.8	*(9)* CO_2 (EDC) starts decreasing
	114.7[a,b]	2.4	*(42)* Temperate tree pollen starts decreasing in Greece (Ioannina)
	114.3[b]	2.0	*(51)* Southern Ocean (MD02-2488) benthic foraminifera $\delta^{13}C$ reaches glacial values
Phase 3 (~113–106 ka)	112.7	1.8	*(15)* CH_4 (EDC) reaches glacial values
establishment of glacial conditions	110.7[a,b]	2.4	*(43)* Temperate tree pollen reaches glacial values in Greece (Ioannina)
	109.5	1.4	*(38)* Temperature tree pollen start decreasing in Italy (Monticchio)
	109.1	1.9	*(10)* CO_2 (EDC) reaches glacial values
	107.8	2.0	*(20)* Antarctic reconstructed surface air temperature (EDC δD) reaches glacial values
	107.7[a]	1.6	*(23)* Greenland NGRIP ice $\delta^{18}O$ reaches glacial values
	107.3[a]	1.9	*(56)* Beginning of GS-25 IRD peak in the North Atlantic (ODP980)
	106.0[d]	2.5	*(47)* North Atlantic (MD95-2042) benthic foraminifera $\delta^{13}C$ reaches glacial values

[a] Visually estimated.
[b] The pollen records from the Ioannina sequence are presented on the original orbital-tuning time scale (Tzedakis et al., 2003). See section 7.3 and Fig. 11 for age differences induced by the use of different alignment targets.
[c] Records from the Southern Ocean MD02-2488 are presented here on the AICC2012 time scale (via temperature alignment, see section 7.1).
[d] Records from the North Atlantic core MD95-2042 are presented here on the AICC2012 time scale (via temperature alignment). See section 7.3 and Fig. 10 for the age model differences induced by the use of different alignment targets.
[e] Insolation patterns during the early LIG are also responsible for spatially different climate evolutions during the LIG interval.

feedbacks at stake during transitions preceding and following the LIG acme.

Such variability also illustrates the difficulty to define the timing and duration of past interglacials. How should interglacial times be defined: as the period of relatively stable conditions, using mid-points of transitions or threshold values? Which record should be used? We provide two additional examples to illustrate this issue. The EPICA Community members (2004) used a mean Holocene threshold value of −403‰ to define interglacial times in the EDC δD record, which results in a LIG duration of 16.2 ± 1.6 ka on the AICC2012 chronology (Bazin et al., 2013) (section 4.2). The LIG duration hence includes part of the deglacial and glaciation intervals. In contrast, Tzedakis et al. (2012) defined the duration of past interglacials based on millennial-scale variability recorded in the Greenland synthetic record (Barker et al., 2011). Defined from the end of the deglacial North Atlantic iceberg melting event to 3 ka before the onset of bipolar-seesaw variability (indicated by the onset of the GS-25 event), the LIG interval then lasted ~15 ka (Tzedakis et al., 2012). In that case, the interglacial interval excludes most of the penultimate deglaciation but may include part of the

glacial inception. These examples highlight how definitions of past interglacials may vary and how carefully interglacial durations from various studies should be compared.

Thanks to improved temporal resolutions, millennial-scale events can be identified in marine sediment and ice cores during the LIG acme (e.g. Seidenkrantz et al., 1995; Galaasen et al., 2014; Pol et al., 2014). However, the scarcity of precise age constraints within the LIG limits their interpretation and cross-comparison between different archives. The same uncertain age allocation is true for the two high LIG sea level highstands, which have been observed in some studies (e.g. Kopp et al., 2009; Thompson et al., 2011) (Fig. 3). Finally, Asian speleothem $\delta^{18}O$ records suggest so far a relatively stable Asian LIG climate (Fig. 5), with little millennial- to centennial-scale variability. In contrast with this common pattern, European speleothem $\delta^{18}O$ records exhibit higher spatial and centennial to millennial-scale variability during the LIG (Fig. 5, section 3).

9.3. The last glacial inception

We identify three successive phases of events (Table 5B).

(1) The first phase (~122–120 ka) includes early changes in (sub) polar and monsoon regions. The change towards lower growth rates recorded in Asian speleothems (Fig. 5) and the increase in Asian speleothem (Sanbao, Dongge) $\delta^{18}O$ at 122–121 ka (± 0.8 ka) indicate an early weakening of the Asian summer monsoon, probably in response to the decrease in boreal summer insolation starting at 127.5 ka. While CH_4 declines progressively directly after its maximum, a more pronounced CH_4 decrease is recorded at 120.6 ± 1.7 ka. It is essentially in phase with the more pronounced decreases in Greenland NEEM ice $\delta^{18}O$ (120.3 ± 2.3 ka) and Antarctic reconstructed temperatures (120.3 ± 1.7 ka). Those results are in line with those of Landais et al. (2006). This high-latitude cooling occurs at a time when North Atlantic subpolar waters become colder (e.g. Oppo et al., 1997; Oppo et al., 2006; Bauch and Kandiano, 2007) and boreal forest starts to retreat in northern Europe (Sánchez Goñi et al., 2005). Slight reduction in the ventilation of North Atlantic deep waters (at ~3100 m) is also recorded at 121.1 ± 2.5 ka, which may reflect early reorganisations in the North Atlantic circulation (Guihou et al., 2011).

(2) The second phase (~118–113 ka) corresponds to the intensification of the glaciation. The cooling intensifies in the subpolar North Atlantic region at 117.2 ± 2.3 ka (e.g. Oppo et al., 2006; Bauch and Kandiano, 2007). It is referred to the North Atlantic C26 cold event (Fig. 13) during which a southward shift of the Arctic front south of Iceland is also observed (Mokeddem et al., 2014). In parallel, the growth interruptions of most European speleothems highlight the degradation of climate over Europe at ~118 ± 1.5 ka (118.0 ± 1 ka in the Entrische Kirche cave (Meyer et al., 2008) and 118.5 ± 1.5 ka in the Cobre cave (Rossi et al., 2014)) (Fig. 5), likely in relation with the onset of GS-26. Antarctic Bottom Waters expand at 116.2 ± 2.0 ka in the deep Southern Ocean (at ~3400 m), in response to southern high-latitude cooling and equatorward shift of Southern Ocean surface fronts (Govin et al., 2009), while CO_2 starts decreasing at 115.5 ± 1.8 ka. The sea level decrease from 116.0 ± 0.8 ka on (Dutton and Lambeck, 2012) indicates that ice sheets already started growing in Northern America (e.g. Bonelli et al., 2009). Finally, the decrease in temperate tree pollen in Greece suggests the development of colder and drier conditions around 114.7 ± 2.4 ka, in line with the establishment of an enhanced meridional vegetation gradient over Europe (Sánchez Goñi et al., 2005) and the shift toward cooler conditions and reduced forest cover at 115.8 ± 1.6 ka in southern Italy (Brauer et al., 2007).

(3) During the third phase (~113–106 ka), glacial conditions are progressively established. CH_4 and CO_2 reach two relative minimum values at 112.7 ± 1.8 ka and 109.1 ± 1.9 ka, respectively (Landais et al., 2006; Schneider et al., 2013). The interval between 108 and 106 ka is the period when glacial conditions are fully established in most records (Table 5B). Relative minimum values are observed at 107.8 ± 2.0 ka and 107.7 ± 1.6 ka, in Antarctic reconstructed temperatures and Greenland NGRIP ice $\delta^{18}O$, respectively. It is also the time when the North Atlantic cooling reaches mid latitudes (e.g. Chapman and Shackleton, 1998; Cortijo et al., 1999; Martrat et al., 2014) and when the polar front moves south of Iceland (Mokeddem et al., 2014). Low percentages of temperate tree pollen at 110.7 ± 2.4 ka suggest the presence of cold and dry conditions in Greece, in agreement with the establishment of glacial vegetation types in Europe (e.g. Sánchez Goñi et al., 2005; Brauer et al., 2007). The first large iceberg discharge is observed at 107.3 ± 1.9 ka in the North Atlantic ODP980 core (e.g. Oppo et al., 2006; Bauch and Kandiano, 2007) and indicates the presence of well-established ice sheets. Simultaneously, deep-water ventilation decreased at ~3100 m in the North Atlantic (106.0 ± 2.5 ka), which reflects the global shoaling of North Atlantic Deep Water (e.g. McManus et al., 2002; Guihou et al., 2010).

This sequence of events highlights that CO_2 and global sea level start decreasing at about the same time (Table 5B). This feature does not imply that the onset of CO_2 decrease had sufficient radiative impact to act on ice sheet growth. Indeed, modelling results demonstrate the dominant role of changes in boreal summer insolation (Calov et al., 2005; Bonelli et al., 2009). The coincident changes in CO_2 and continental ice volume may reflect the impact of colder climatic conditions on both ice sheet growth and ocean circulation, itself driving changes in atmospheric CO_2 concentration. Moreover, the early high-latitude cooling, changes in European vegetation and in deep ocean circulation highlighted in this sequence of events points to a succession of climate feedbacks associated with vegetation and ocean circulation changes (Table 4B). Modelling results have shown the role of such feedbacks to amplify the initial high-latitude cooling induced by the summer insolation decrease and enhance ice sheet growth (e.g. Khodri et al., 2001; Wang et al., 2005). There are still uncertainties with respect to the respective contributions of vegetation and ocean feedbacks in the glacial inception, as they are model-dependent (e.g. Wang et al., 2005; Kubatzki et al., 2006; Born et al., 2010).

10. Conclusions

In this study, we highlight strengths and limitations of existing methods used to date or derive relative chronologies in climatic archives (corals, speleothems, ice cores, marine and lake/peat sediments) between 140 and 100 ka. We explicitly review the underlying climatic hypotheses, especially in the case of synchronisations or alignments of paleoclimatic records and provide quantitative estimates of the associated absolute and relative age uncertainties.

We also include recommendations on how best to define absolute and relative chronologies. Future climate alignments should provide (1) clear statement of climate hypotheses involved, (2) detailed understanding of environmental parameters controlling selected tracers and (3) careful evaluation of the synchronicity of aligned paleoclimatic records. The scarcity of age markers within the LIG stands out in general for all archives (ice cores, marine sediments, lake/peat sediments), which limits the detailed and quantitative investigation of interglacial millennial-scale variability. We emphasise the systematic need to estimate quantitatively relative and absolute age uncertainties. Examples presented here may offer guidance about how to estimate such uncertainties for the LIG. Bayesian chronology models, which have been recently developed are also helpful tools to propagate age uncertainties and

construct age models for ice cores (Bazin et al., 2013; Veres et al., 2013) and marine, lake and peat sediments (Parnell et al., 2011). Future studies should assess the coherence of the different chronologies used when comparing records and integrate these uncertainties in paleoclimatic interpretations.

Finally, for the first time, we propose a sequence of major climatic events with associated age uncertainties for the interval 140–105 ka. The variable duration of the LIG acme highlighted here from one record to another raises the recurring issue of how to define glacial and interglacial intervals. This issue is complex and needs to be further addressed by the paleoclimate community in the coming years. Model-data comparisons and transient climate simulations from Earth system models using this sequence of events as a benchmark may shed some light on climate feedbacks involved during the penultimate deglaciation and the last glacial inception. Such exercises should benefit in particular from the recent coupling of ice sheet and climate models (Herrington and Poulsen, 2011).

Acknowledgements

We are particularly thankful to the various authors cited in the text who gave us access to their data. The research leading to these results received funding from the European Union's Seventh Framework Programme (FP7/2007–2013) under grant agreement 243908, "Past4Future. Climate change–Learning from the past climate". A.G. was supported by the Deutsche Forschungsgemeinschaft (DFG) under the special Priority Program INTERDYNAMIC (EngLIG project, grant GO 2122/1-1) and the DFG Research Center/Cluster of Excellence "The Ocean in the Earth System". This study is also supported by the British Antarctic Survey Polar Science for Planet Earth Programme. We acknowledge support from CSIC-JAE-Pre028 contract (A.E.O.), CSIC-Ramón y Cajal post-doctoral program RYC-2013-14073 (B.M.), the Danish Council for Independent Research, Natural Science (12-126709/FNU; M.-S.S.), and the Belgian Federal Science Policy Office (BELSPO, MO/36/028, S.V.). We thank the Editor (H. Bauch) and two anonymous reviewers for their constructive comments, which greatly improved the manuscript.

Appendix A. Supplementary data

Supplementary data related to this article can be found at http://dx.doi.org/10.1016/j.quascirev.2015.09.018.

References

Abbott, P.M., Austin, W.E.N., Davies, S.M., Pearce, N.J.G., Hibbert, F.D., 2013. Cryptotephrochronology of the Eemian and the Last Interglacial–glacial transition in the North East Atlantic. J. Quat. Sci. 28, 501–514. http://dx.doi.org/10.1002/jqs.2641.

Allen, J.R.M., Huntley, B., 2009. Last Interglacial palaeovegetation, palaeoenvironments and chronology: a new record from Lago Grande di Monticchio, southern Italy. Quat. Sci. Rev. 28, 1521–1538. http://dx.doi.org/10.1016/j.quascirev.2009.02.013.

Andersen, M.B., Romaniello, S., Vance, D., Little, S.H., Herdman, R., Lyons, T.W., 2014. A modern framework for the interpretation of 238U/235U in studies of ancient ocean redox. Earth Planet. Sci. Lett. 400, 184–194. http://dx.doi.org/10.1016/j.epsl.2014.05.051.

Badertscher, S., Borsato, A., Frisia, S., Cheng, H., Edwards, R.L., Tüysüz, O., Fleitmann, D., 2014. Speleothems as sensitive recorders of volcanic eruptions – the Bronze Age Minoan eruption recorded in a stalagmite from Turkey. Earth Planet. Sci. Lett. 392, 58–66. http://dx.doi.org/10.1016/j.epsl.2014.01.041.

Baker, A., Genty, D., Dreybrodt, W., Barnes, W.L., Mockler, N.J., Grapes, J., 1998. Testing theoretically predicted stalagmite growth rate with recent annually laminated samples: implications for past stalagmite deposition. Geochim. Cosmochim. Acta 62, 393–404. http://dx.doi.org/10.1016/S0016-7037(97)00343-8.

Baker, A., Smart, P.L., Edwards, R.L., Richards, D.A., 1993. Annual growth banding in a cave stalagmite. Nature 364, 518–520. http://dx.doi.org/10.1038/364518a0.

Bakker, P., Renssen, H., 2014. Last Interglacial model-data mismatch of thermal maximum temperatures partially explained. Clim. Past. 10, 1633–1644. http://dx.doi.org/10.5194/cp-10-1633-2014.

Bakker, P., Stone, E.J., Charbit, S., Gröger, M., Krebs-Kanzow, U., Ritz, S.P., Varma, V., Khon, V., Lunt, D.J., Mikolajewicz, U., Prange, M., Renssen, H., Schneider, B., Schulz, M., 2013. Last Interglacial temperature evolution – a model intercomparison. Clim. Past 9, 605–619. http://dx.doi.org/10.5194/cp-9-605-2013.

Baldwin, M., Frappier, A.B., 2008. Toward Speleothem Tephrochronology: Experimental Simulation of Volcanic Ash Weathering in a Karst Setting. American Geophysical Union, Fall Meeting abstract #V11C-2075.

Bar-Matthews, M., Ayalon, A., Gilmour, M., Matthews, A., Hawkesworth, C.J., 2003. Sea-land oxygen isotopic relationships from planktonic foraminifera and speleothems in the Eastern Mediterranean region and their implication for paleorainfall during interglacial intervals. Geochim. Cosmochim. Acta 67, 3181–3199. http://dx.doi.org/10.1016/S0016-7037(02)01031-1.

Bar-Matthews, M., Ayalon, A., Kaufman, A., 1997. Late quaternary paleoclimate in the eastern mediterranean region from stable isotope analysis of speleothems at soreq cave, Israel. Quat. Res. 47, 155–168. http://dx.doi.org/10.1006/qres.1997.1883.

Barbetti, M., McElhinny, M., 1972. Evidence of a geomagnetic excursion 30,000 yr BP. Nature 239, 327–330. http://dx.doi.org/10.1038/239327a0.

Barker, S., Knorr, G., Edwards, R.L., Parrenin, F., Putnam, A.E., Skinner, L.C., Wolff, E., Ziegler, M., 2011. 800,000 Years of abrupt climate variability. Science 334, 347–351. http://dx.doi.org/10.1126/science.1203580.

Bauch, D., Bauch, H.A., 2001. Last glacial benthic foraminiferal δ18O anomalies in the polar North Atlantic: a modern analogue evaluation. J. Geophys. Res. Oceans 106, 9135–9143. http://dx.doi.org/10.1029/1999jc000164.

Bauch, H.A., Kandiano, E.S., 2007. Evidence for early warming and cooling in North Atlantic surface waters during the Last Interglacial. Paleoceanography 22. http://dx.doi.org/10.1029/2005pa001252. PA1201.

Bazin, L., Landais, A., Lemieux-Dudon, B., Toyé Mahamadou Kele, H., Veres, D., Parrenin, F., Martinerie, P., Ritz, C., Capron, E., Lipenkov, V., Loutre, M.F., Raynaud, D., Vinther, B., Svensson, A., Rasmussen, S.O., Severi, M., Blunier, T., Leuenberger, M., Fischer, H., Masson-Delmotte, V., Chappellaz, J., Wolff, E., 2013. An optimized multi-proxy, multi-site Antarctic ice and gas orbital chronology (AICC2012): 120–800 ka. Clim. Past. 9, 1715–1731. http://dx.doi.org/10.5194/cp-9-1715-2013.

Bender, M.L., 2002. Orbital tuning chronology for the Vostok climate record supported by trapped gas composition. Earth Planet. Sci. Lett. 204, 275–289. http://dx.doi.org/10.1016/S0012-821X(02)00980-9.

Bender, M.L., Malaize, B., Orchardo, J., Sowers, T., Jouzel, J., 1999. High precision correlations of Greenland and antarctic ice core records over the last 100 Kyr. In: Mechanisms of Global Climate Change at Millennial Time Scales. American Geophysical Union, pp. 149–164. http://dx.doi.org/10.1029/GM112p0149.

Bianchi, C., Gersonde, R., 2002. The Southern Ocean surface between marine isotope stages 6 and 5d: shape and timing of climate changes. Palaeogeogr. Palaeoclimatol. Palaeoecol. 187, 151–177. http://dx.doi.org/10.1016/S0031-0182(02)00516-3.

Bjorck, S., Kromer, B., Johnsen, S., Bennike, O., Hammarlund, D., Lemdahl, G., Possnert, G., Rasmussen, T.L., Wohlfarth, B., Hammer, C.U., Spurk, M., 1996. Synchronized terrestrial atmospheric deglacial records around the North Atlantic. Science 274, 1155–1160. http://dx.doi.org/10.1126/science.274.5290.1155.

Blockley, S.P.E., Lane, C.S., Hardiman, M., Rasmussen, S.O., Seierstad, I.K., Steffensen, J.P., Svensson, A., Lotter, A.F., Turney, C.S.M., Bronk Ramsey, C., 2012. Synchronisation of palaeoenvironmental records over the last 60,000 years, and an extended INTIMATE event stratigraphy to 48,000 b2k. Quat. Sci. Rev. 36, 2–10. http://dx.doi.org/10.1016/j.quascirev.2011.09.017.

Blunier, T., Spahni, R., Barnola, J.M., Chappellaz, J., Loulergue, L., Schwander, J., 2007. Synchronization of ice core records via atmospheric gases. Clim. Past. 3, 325–330. http://dx.doi.org/10.5194/cp-3-325-2007.

Boch, R., Cheng, H., Spötl, C., Edwards, R.L., Wang, X., Häuselmann, P., 2011. NALPS: a precisely dated European climate record 120-60 ka. Clim. Past. 7, 1247–1259. http://dx.doi.org/10.5194/cp-7-1247-2011.

Bond, G.C., Broecker, W., Johnsen, S., McManus, J., Labeyrie, L., Jouzel, J., Bonani, G., 1993. Correlations between climate records from the North Atlantic sediments and Greenland Ice. Nature 365, 143–147. http://dx.doi.org/10.1038/365143a0.

Bonelli, S., Charbit, S., Kageyama, M., Woillez, M.N., Ramstein, G., Dumas, C., Quiquet, A., 2009. Investigating the evolution of major Northern Hemisphere ice sheets during the last glacial-interglacial cycle. Clim. Past. 5, 329–345. http://dx.doi.org/10.5194/cp-5-329-2009.

Born, A., Nisancioglu, K., Braconnot, P., 2010. Sea ice induced changes in ocean circulation during the Eemian. Clim. Dyn. 35, 1361–1371. http://dx.doi.org/10.1007/s00382-009-0709-2, 1371.

Bourdon, B., Henderson, G.M., Lundstrom, C.C., Turner, S.P., 2003. Uranium-series Geochemistry. Mineralogical Society of America, Geochemical Society.

Brauer, A., Allen, J.R.M., Mingram, J., Dulski, P., Wulf, S., Huntley, B., 2007. Evidence for Last Interglacial chronology and environmental change from Southern Europe. Proc. Natl. Acad. Sci. 104, 450–455. http://dx.doi.org/10.1073/pnas.0603321104.

Brauer, A., Hajdas, I., Blockley, S.P.E., Bronk Ramsey, C., Christl, M., Ivy-Ochs, S., Moseley, G.E., Nowaczyk, N.N., Rasmussen, S.O., Roberts, H.M., Spötl, C., Staff, R.A., Svensson, A., 2014. The importance of independent chronology in integrating records of past climate change for the 60–8 ka INTIMATE time

interval. Quat. Sci. Rev. 106, 47–66. http://dx.doi.org/10.1016/j.quascirev.2014.07.006.
Breitenbach, S.F.M., Rehfeld, K., Goswami, B., Baldini, J.U.L., Ridley, H.E., Kennett, D.J., Prufer, K.M., Aquino, V.V., Asmerom, Y., Polyak, V.J., Cheng, H., Kurths, J., Marwan, N., 2012. COnstructing proxy records from age models (COPRA). Clim. Past. 8, 1765–1779. http://dx.doi.org/10.5194/cp-8-1765-2012.
Brendryen, J., Haflidason, H., Sejrup, H.P., 2010. Norwegian Sea tephrostratigraphy of marine isotope stages 4 and 5: prospects and problems for tephrochronology in the North Atlantic region. Quat. Sci. Rev. 29, 847–864. http://dx.doi.org/10.1016/j.quascirev.2009.12.004.
Broecker, W.S., van Donk, J., 1970. Insolation changes, ice volumes, and the O18 record in deep-sea cores. Rev. Geophys. 8, 169–198. http://dx.doi.org/10.1029/RG008i001p00169.
Buiron, D., Chappellaz, J., Stenni, B., Frezzotti, M., Baumgartner, M., Capron, E., Landais, A., Lemieux-Dudon, B., Masson-Delmotte, V., Montagnat, M., Parrenin, F., Schilt, A., 2011. TALDICE-1 age scale of the Talos Dome deep ice core, East Antarctica. Clim. Past. 7, 1–16. http://dx.doi.org/10.5194/cp-7-1-2011.
Buizert, C., Cuffey, K.M., Severinghaus, J.P., Baggenstos, D., Fudge, T.J., Steig, E.J., Markle, B.R., Winstrup, M., Rhodes, R.H., Brook, E.J., Sowers, T.A., Clow, G.D., Cheng, H., Edwards, R.L., Sigl, M., McConnell, J.R., Taylor, K.C., 2015. The WAIS divide deep ice core WD2014 chronology – part 1: methane synchronization (68–31 ka BP) and the gas age–ice age difference. Clim. Past. 11, 153–173. http://dx.doi.org/10.5194/cp-11-153-2015.
Caballero-Gill, R.P., Clemens, S., Prell, W., 2012. Antarctic isotope maxima events 24 and 25 identified in benthic marine $\delta^{18}O$. Paleoceanography 27. http://dx.doi.org/10.1029/2011pa002269. PA1101.
Calov, R., Ganopolski, A., Claussen, M., Petoukhov, V., Greve, R., 2005. Transient simulation of the last glaciation inception. Part I: glacial inception as a bifurcation in the climate system. Clim. Dyn. 24, 545–561. http://dx.doi.org/10.1007/s00382-005-0007-6.
Cande, S.C., Kent, D.V., 1995. Revised calibration of the geomagnetic polarity timescale for the Late Cretaceous and Cenozoic. J. Geophys. Res. Solid Earth 100, 6093–6095. http://dx.doi.org/10.1029/94jb03098.
Cape Last Interglacial Project members, 2006. Last Interglacial Arctic warmth confirms polar amplification of climate change. Quat. Sci. Rev. 25, 1383–1400. http://dx.doi.org/10.1016/j.quascirev.2006.01.033.
Capron, E., Landais, A., Lemieux-Dudon, B., Schilt, A., Masson-Delmotte, V., Buiron, D., Chappellaz, J., Dahl-Jensen, D., Johnsen, S., Leuenberger, M., Loulergue, L., Oerter, H., 2010. Synchronising EDML and NorthGRIP ice cores using $\delta^{18}O$ of atmospheric oxygen ($\delta^{18}O_{atm}$) and CH4 measurements over MIS5 (80-123 kyr). Quat. Sci. Rev. 29, 222–234. http://dx.doi.org/10.1016/j.quascirev.2009.07.014.
Capron, E., Govin, A., Stone, E.J., Masson-Delmotte, V., Mulitza, S., Otto-Bliesner, B., Rasmussen, T.L., Sime, L.C., Waelbroeck, C., Wolff, E.W., 2014. Temporal and spatial structure of multi-millennial temperature changes at high latitudes during the Last Interglacial. Quat. Sci. Rev. 103, 116–133. http://dx.doi.org/10.1016/j.quascirev.2014.08.018.
Capron, E., Landais, A., Chappellaz, J., Buiron, D., Fischer, H., Johnsen, S.J., Jouzel, J., Leuenberger, M., Masson-Delmotte, V., Stocker, T.F., 2012. A global picture of the first abrupt climatic event occurring during the last glacial inception. Geophys. Res. Lett. 39 http://dx.doi.org/10.1029/2012gl052656. L15703.
Carboni, S., Lecca, L., Hillaire-Marcel, C., Ghaleb, B., 2014. MIS 5e at San Giovanni di Sinis (Sardinia, Italy): stratigraphy, U/Th dating and “eustatic” inferences. Quat. Int. 328–329, 21–30. http://dx.doi.org/10.1016/j.quaint.2013.12.052.
Carcaillet, J., Bourlès, D.L., Thouveny, N., Arnold, M., 2004. A high resolution authigenic 10Be/9Be record of geomagnetic moment variations over the last 300 ka from sedimentary cores of the Portuguese margin. Earth Planet. Sci. Lett. 219, 397–412. http://dx.doi.org/10.1016/S0012-821X(03)00702-7.
Channell, J.E.T., Hodell, D.A., Curtis, J.H., 2012. ODP Site 1063 (Bermuda Rise) revisited: oxygen isotopes, excursions and paleointensity in the Brunhes Chron. Geochem. Geophys. Geosyst. 13, Q02001. http://dx.doi.org/10.1029/2011gc003897.
Channell, J.E.T., Wright, J.D., Mazaud, A., Stoner, J.S., 2014. Age through tandem correlation of quaternary relative paleointensity (RPI) and oxygen isotope data at IODP Site U1306 (Eirik Drift, SW Greenland). Quat. Sci. Rev. 88, 135–146. http://dx.doi.org/10.1016/j.quascirev.2014.01.022.
Channell, J.E.T., Xuan, C., Hodell, D.A., 2009. Stacking paleointensity and oxygen isotope data for the last 1.5 Myr (PISO-1500). Earth Planet. Sci. Lett. 283, 14–23. http://dx.doi.org/10.1016/j.epsl.2009.03.012.
Chapman, M.R., Shackleton, N.J., 1998. Millennial-scale fluctuations in North Atlantic heat flux during the last 150,000 years. Earth Planet. Sci. Lett. 159, 57–70. http://dx.doi.org/10.1016/S0012-821X(98)00068-5.
Chappellaz, J., Bluniert, T., Raynaud, D., Barnola, J.M., Schwander, J., Stauffert, B., 1993. Synchronous changes in atmospheric CH_4 and Greenland climate between 40 and 8 kyr BP. Nature 366, 443–445. http://dx.doi.org/10.1038/366443a0.
Cheng, H., Adkins, J., Edwards, R.L., Boyle, E.A., 2000. U-Th dating of deep-sea corals. Geochim. Cosmochim. Acta 64, 2401–2416. http://dx.doi.org/10.1016/S0016-7037(99)00422-6.
Cheng, H., Edwards, R.L., Broecker, W.S., Denton, G.H., Kong, X., Wang, Y., Zhang, R., Wang, X., 2009. Ice age terminations. Science 326, 248–252. http://dx.doi.org/10.1126/science.1177840.
Cheng, H., Edwards, R.L., Murrell, M.T., Benjamin, T.M., 1998. Uranium-thorium-protactinium dating systematics. Geochim. Cosmochim. Acta 62, 3437–3452. http://dx.doi.org/10.1016/S0016-7037(98)00255-5.
Chiang, J., Bitz, C., 2005. Influence of high latitude ice cover on the marine intertropical convergence zone. Clim. Dyn. 25, 477–496. http://dx.doi.org/10.1007/s00382-005-0040-5.
Chiu, T.-c., Fairbanks, R.G., Mortlock, R.A., Bloom, A.L., 2005. Extending the radiocarbon calibration beyond 26,000 years before present using fossil corals. Quat. Sci. Rev. 24, 1797–1808. http://dx.doi.org/10.1016/j.quascirev.2005.04.002.
Christl, M., Mangini, A., Holzkämper, S., Spötl, C., 2004. Evidence for a link between the flux of galactic cosmic rays and Earth's climate during the past 200,000 years. J. Atmos. Solar Terrestrial Phys. 66, 313–322. http://dx.doi.org/10.1016/j.jastp.2003.12.004.
Clausen, H.B., Hammer, C.U., Hvidberg, C.S., Dahl-Jensen, D., Steffensen, J.P., Kipfstuhl, J., Legrand, M., 1997. A comparison of the volcanic records over the past 4000 years from the Greenland ice core project and dye 3 Greenland ice cores. J. Geophys. Res. Oceans 102, 26707–26723. http://dx.doi.org/10.1029/97JC00587.
Combourieu Nebout, N., Londeix, L., Baudin, F.o., Turon, J.-L., von Grafenstein, R., Zahn, R., 1999. Quaternary marine and continental paleoenvironments in the western Mediterranean (site 976, Alboran Sea): palynological evidence. In: Zahn, R., Comas, M.C., Klaus, A. (Eds.), Proceedings of the Ocean Drilling Program, Scientific Results. Ocean Drilling Program, College Station, TX, p. 36.
Combourieu Nebout, N., Peyron, O., Dormoy, I., Desprat, S., Beaudouin, C., Kotthoff, U., Marret, F., 2009. Rapid climatic variability in the west Mediterranean during the last 25 000 years from high resolution pollen data. Clim. Past. 5, 503–521. http://dx.doi.org/10.5194/cp-5-503-2009.
Cortijo, E., Lehman, S., Keigwin, L., Chapman, M., Paillard, D., Labeyrie, L., 1999. Changes in meridional temperature and salinity gradients in the North Atlantic Ocean (30-72°N) during the Last Interglacial period. Paleoceanography 14, 23–33. http://dx.doi.org/10.1029/1998PA900004.
Couchoud, I., Genty, D., Hoffmann, D., Drysdale, R., Blamart, D., 2009. Millennial-scale climate variability during the Last Interglacial recorded in a speleothem from south-western France. Quat. Sci. Rev. 28, 3263–3274. http://dx.doi.org/10.1016/j.quascirev.2009.08.014.
Cruz, J.F.W., Burns, S.J., Karmann, I., Sharp, W.D., Vuille, M., 2006. Reconstruction of regional atmospheric circulation features during the late Pleistocene in subtropical Brazil from oxygen isotope composition of speleothems. Earth Planet. Sci. Lett. 248, 495–507. http://dx.doi.org/10.1016/j.epsl.2006.06.019.
Cvijanovic, I., Chiang, J.H., 2013. Global energy budget changes to high latitude North Atlantic cooling and the tropical ITCZ response. Clim. Dyn. 40, 1435–1452. http://dx.doi.org/10.1007/s00382-012-1482-1.
Davies, S.M., Abbott, P.M., Meara, R.H., Pearce, N.J.G., Austin, W.E.N., Chapman, M.R., Svensson, A., Bigler, M., Rasmussen, T.L., Rasmussen, S.O., Farmer, E.J., 2014. A North Atlantic tephrostratigraphical framework for 130–60 ka b2k: new tephra discoveries, marine-based correlations, and future challenges. Quat. Sci. Rev. 106, 101–121. http://dx.doi.org/10.1016/j.quascirev.2014.03.024.
de Beaulieu, J.L., Reille, M., 1992. Long Pleistocene pollen sequences from the Velay plateau (Massif Central, France). Veg. Hist. Archaeobotany 1, 233–242. http://dx.doi.org/10.1007/BF00189500.
de Vernal, A., Hillaire-Marcel, C., 2008. Natural variability of Greenland climate, vegetation, and ice volume during the past million years. Science 320, 1622–1625. http://dx.doi.org/10.1126/science.1153929.
Delmotte, M., Chappellaz, J., Brook, E., Yiou, P., Barnola, J.M., Goujon, C., Raynaud, D., Lipenkov, V.I., 2004. Atmospheric methane during the last four glacial-interglacial cycles: rapid changes and their link with Antarctic temperature. J. Geophys. Res. Atmos. 109 http://dx.doi.org/10.1029/2003jd004417. D12104.
Dokken, T., Jansen, E., 1999. Rapid changes in the mechanism of ocean convection during the last glacial period. Nature 401, 458–461. http://dx.doi.org/10.1038/46753.
Domínguez-Villar, D., Baker, A., Fairchild, I.J., Edwards, R.L., 2012. A method to anchor floating chronologies in annually laminated speleothems with U-Th dates. Quat. Geochronol. 14, 57–66. http://dx.doi.org/10.1016/j.quageo.2012.04.019.
Dorale, J., Edwards, R.L., Alexander Jr., E.C., Shen, C.-C., Richards, D., Cheng, H., 2004. Uranium-series dating of speleothems: current techniques, limits, & applications. In: Sasowsky, I., Mylroie, J. (Eds.), Studies of Cave Sediments. Springer, US, pp. 177–197. http://dx.doi.org/10.1007/978-1-4419-9118-8_10.
Dreybrodt, W., 1999. Chemical kinetics, speleothem growth and climate. Boreas 28, 347–356. http://dx.doi.org/10.1111/j.1502-3885.1999.tb00224.x.
Drysdale, R.N., Hellstrom, J.C., Zanchetta, G., Fallick, A.E., Sanchez Goni, M.F., Couchoud, I., McDonald, J., Maas, R., Lohmann, G., Isola, I., 2009. Evidence for obliquity forcing of glacial termination II. Science 325, 1527–1531. http://dx.doi.org/10.1126/science.1170371.
Drysdale, R.N., Zanchetta, G., Hellstrom, J.C., Fallick, A.E., McDonald, J., Cartwright, I., 2007. Stalagmite evidence for the precise timing of North Atlantic cold events during the early last glacial. Geology 35, 77–80. http://dx.doi.org/10.1130/g23161a.1.
Drysdale, R.N., Zanchetta, G., Hellstrom, J.C., Fallick, A.E., Zhao, J.-x, 2005. Stalagmite evidence for the onset of the Last Interglacial in southern Europe at 129 ± 1 ka. Geophys. Res. Lett. 32 http://dx.doi.org/10.1029/2005gl024658.
Drysdale, R.N., Zanchetta, G., Hellstrom, J.C., Fallick, A.E., Zhao, J.-x., Isola, I., Bruschi, G., 2004. Palaeoclimatic implications of the growth history and stable isotope (δ18O and δ13C) geochemistry of a Middle to Late Pleistocene stalagmite from central-western Italy. Earth Planet. Sci. Lett. 227, 215–229. http://dx.doi.org/10.1016/j.epsl.2004.09.010.
Dunbar, N.W., McIntosh, W.C., Esser, R.P., 2008. Physical setting and tephrochronology of the summit caldera ice record at Mount Moulton, West Antarctica. Geol. Soc. Am. Bull. 796–812. http://dx.doi.org/10.1130/B26140.1.

Duplessy, J.C., Labeyrie, L., Juillet-Leclerc, A., Maitre, F., Duprat, J., Sarnthein, M., 1991. Surface salinity reconstruction of the North Atlantic Ocean during the last glacial maximum. Oceanol. Acta 14, 311–324.
Dutton, A., Carlson, A.E., Long, A.J., Milne, G.A., Clark, P.U., DeConto, R., Horton, B.P., Rahmstorf, S., Raymo, M.E., 2015. Sea-level rise due to polar ice-sheet mass loss during past warm periods. Science 349. http://dx.doi.org/10.1126/science.aaa4019.
Dutton, A., Lambeck, K., 2012. Ice volume and sea level during the last interglacial. Science 337, 216–219. http://dx.doi.org/10.1126/science.1205749.
Edwards, R.L., Cheng, H., Murrell, M.T., Goldstein, S.J., 1997. Protactinium-231 dating of carbonates by thermal ionization mass spectrometry: implications for quaternary climate change. Science 276, 782–786. http://dx.doi.org/10.1126/science.276.5313.782.
Emiliani, C., 1955. Pleistocene temperatures. J. Geol. 63, 538–578. http://dx.doi.org/10.2307/30080906.
EPICA Community members, 2004. Eight glacial cycles from an Antarctic ice core. Nature 429, 623–628. http://dx.doi.org/10.1038/nature02599.
EPICA Community members, 2006. One-to-one coupling of glacial climate variability in Greenland and Antarctica. Nature 444, 195–198. http://dx.doi.org/10.1038/nature05301.
Fang, X.-M., Li, J.-J., Van der Voo, R., Mac Niocaill, C., Dai, X.-R., Kemp, R.A., Derbyshire, E., Cao, J.-X., Wang, J.-M., Wang, G., 1997. A record of the Blake Event during the Last Interglacial paleosol in the western Loess Plateau of China. Earth Planet. Sci. Lett. 146, 73–82. http://dx.doi.org/10.1016/S0012-821X(96)00222-1.
Fleitmann, D., Cheng, H., Badertscher, S., Edwards, R.L., Mudelsee, M., Göktürk, O.M., Fankhauser, A., Pickering, R., Raible, C.C., Matter, A., Kramers, J., Tüysüz, O., 2009. Timing and climatic impact of Greenland interstadials recorded in stalagmites from northern Turkey. Geophys. Res. Lett. 36 http://dx.doi.org/10.1029/2009gl040050. L19707.
Frisia, S., Borsato, A., Susini, J., 2008. Synchrotron radiation applications to past volcanism archived in speleothems: an overview. J. Volcanol. Geotherm. Res. 177, 96–100. http://dx.doi.org/10.1016/j.jvolgeores.2007.11.010.
Frogley, M.R., Tzedakis, P.C., Heaton, T.H.E., 1999. Climate variability in northwest Greece during the Last Interglacial. Science 285, 1886–1889. http://dx.doi.org/10.1126/science.285.5435.1886.
Fujita, S., Parrenin, F., Severi, M., Motoyama, H., Wolff, E., 2015. Volcanic synchronization of Dome Fuji and Dome C Antarctic deep ice cores over the past 216 kyr. Clim. Past. Discuss. 11, 407–445. http://dx.doi.org/10.5194/cpd-11-407-2015.
Galaasen, E.V., Ninnemann, U.S., Irvalí, N., Kleiven, H.F., Rosenthal, Y., Kissel, C., Hodell, D.A., 2014. Rapid reductions in North Atlantic deep water during the peak of the Last Interglacial Period. Science 343, 1129–1132. http://dx.doi.org/10.1126/science.1248667.
Genty, D., Baker, A., Vokal, B., 2001. Intra- and inter-annual growth rate of modern stalagmites. Chem. Geol. 176, 191–212. http://dx.doi.org/10.1016/S0009-2541(00)00399-5.
Genty, D., Blamart, D., Ouahdi, R., Gilmour, M., Baker, A., Jouzel, J., Van-Exter, S., 2003. Precise dating of Dansgaard-Oeschger climate oscillations in western Europe from stalagmite data. Nature 421, 833–837. http://dx.doi.org/10.1038/nature01391.
Genty, D., Quinif, Y., 1996. Annually laminated sequences in the internal structure of some Belgian stalagmites–importance for paleoclimatology. J. Sediment. Res. (SEPM) 66, 275–288.
Gewelt, M., Juvigné, E., 1986. Les 'Tephra de Remouchamps', un nouveau marqueur stratigraphique dans le Pleistocène supérieur daté par 230Th/234O dans des concrétions stalagmitiques. Ann. Soc. Géol. Belg. 109, 489–497.
Govin, A., Braconnot, P., Capron, E., Cortijo, E., Duplessy, J.C., Jansen, E., Labeyrie, L., Landais, A., Marti, O., Michel, E., Mosquet, E., Risebrobakken, B., Swingedouw, D., Waelbroeck, C., 2012. Persistent influence of ice sheet melting on high northern latitude climate during the early Last Interglacial. Clim. Past. 8, 483–507. http://dx.doi.org/10.5194/cp-8-483-2012.
Govin, A., Michel, E., Labeyrie, L., Waelbroeck, C., Dewilde, F., Jansen, E., 2009. Evidence for northward expansion of Antarctic Bottom Water mass in the Southern Ocean during the last glacial inception. Paleoceanography 24. http://dx.doi.org/10.1029/2008PA001603. PA1202.
Goy, J.L., Hillaire-Marcel, C., Zazo, C., Ghaleb, B., Dabrio, C.J., González, Á., Bardají, T., Civis, J., Preda, M., Yébenes, A., Forte, A.M., 2006. Further evidence for a relatively high sea level during the penultimate interglacial: open-system U-series ages from La Marina (Alicante, East Spain). Geodin. Acta 19, 409–426. http://dx.doi.org/10.3166/ga.19.409-426.
Guihou, A., Pichat, S., Govin, A., Nave, S., Michel, E., Duplessy, J.-C., Telouk, P., Labeyrie, L., 2011. Enhanced Atlantic meridional overturning circulation supports the Last Glacial inception. Quat. Sci. Rev. 30, 1576–1582. http://dx.doi.org/10.1016/j.quascirev.2011.03.017.
Guihou, A., Pichat, S., Nave, S., Govin, A., Labeyrie, L., Michel, E., Waelbroeck, C., 2010. Late slowdown of the Atlantic meridional overturning circulation during the last glacial inception: new constraints from sedimentary (^{231}Pa/^{230}Th). Earth Planet. Sci. Lett. 289, 520–529. http://dx.doi.org/10.1016/j.epsl.2009.11.045.
Gullentops, F., 1954. Contribution à la chronologie du Pleistocène et des formes du relief en Belgique. Mémoires de l'Institut de géologie de l'Université de Louvain, pp. 125–252.
Guyodo, Y., Valet, J.-P., 1999. Global changes in geomagnetic intensity during the past 800 thousand years. Nature 399, 249–252. http://dx.doi.org/10.1038/20420.
Harting, P., 1875. Le système éemien. Archives Neerl. Sci. Exactes Nat. Soc. Holl. des Sci. (Harlem) 10, 443–454.
Hedberg, H.D., 1958. Stratigraphic Classification and Terminology, American Association of Petroleum Geologists Bulletin, pp. 1881–1896.
Heijnis, H., 1992. Uranium/thorium Dating of Late Pleistocene Peat Deposits in N.W. Europe. Rijksuniversiteit te Groningen, p. 149.
Hellstrom, J., 2006. U-Th dating of speleothems with high initial 230Th using stratigraphical constraint. Quat. Geochronol. 1, 289–295. http://dx.doi.org/10.1016/j.quageo.2007.01.004.
Henderson, G.M., 2002. Seawater (234U/238U) during the last 800 thousand years. Earth Planet. Sci. Lett. 199, 97–110. http://dx.doi.org/10.1016/S0012-821X(02)00556-3.
Henderson, G.M., Anderson, R.F., 2003. The U-series toolbox for paleoceanography. Rev. Mineral. Geochem. 52, 493–531. http://dx.doi.org/10.2113/0520493.
Herrington, A.R., Poulsen, C.J., 2011. Terminating the Last Interglacial: the role of ice sheet-climate feedbacks in a GCM asynchronously coupled to an ice sheet model. J. Clim. 25, 1871–1882. http://dx.doi.org/10.1175/jcli-d-11-00218.1.
Heusser, L., Shackleton, N.J., 1979. Direct Marine-continental correlation: 150,000-year oxygen isotope-pollen record from the North Pacific. Science 204, 837–839. http://dx.doi.org/10.1126/science.204.4395.837.
Hillaire-Marcel, C., 2009. The U-series dating of (biogenic) carbonates. In: IOP Conf. Series: Earth and Environmental Science.
Hillaire-Marcel, C., Carro, O., Causse, C., Goy, J.-L., Zazo, C., 1986. Th/U dating of Strombus bubonius-bearing marine terraces in southeastern Spain. Geology 14, 613–616. http://dx.doi.org/10.1130/0091-7613(1986)14 <613:tdosbm>2.0.co;2.
Hillaire-Marcel, C., Causse, C., 1989. Chronologie Th/U des concr√©tions calcaires des varves du lac glaciaire de Deschaillons (Wisconsinien inf√©rieur). Can. J. Earth Sci. 26, 1041–1052. http://dx.doi.org/10.1139/e89-085.
Hodell, D.A., Minth, E.K., Curtis, J.H., McCave, I.N., Hall, I.R., Channell, J.E.T., Xuan, C., 2009. Surface and deep-water hydrography on Gardar Drift (Iceland Basin) during the Last Interglacial period. Earth Planet. Sci. Lett. 288, 10–19. http://dx.doi.org/10.1016/j.epsl.2009.08.040.
Hodge, E.J., Richards, D.A., Smart, P.L., Andreo, B. é, Hoffmann, D.L., Mattey, D.P., González-Ramón, A., 2008. Effective precipitation in southern Spain (~266 to 46 ka) based on a speleothem stable carbon isotope record. Quat. Res. 69, 447–457. http://dx.doi.org/10.1016/j.yqres.2008.02.013.
Hoffmann, D.L., Spötl, C., Mangini, A., 2009. Micromill and in situ laser ablation sampling techniques for high spatial resolution MC-ICPMS U-Th dating of carbonates. Chem. Geol. 259, 253–261. http://dx.doi.org/10.1016/j.chemgeo.2008.11.015.
Imbrie, J., Imbrie, J.Z., 1980. Modeling the climatic response to orbital variations. Science 207, 943–953. http://dx.doi.org/10.1126/science.207.4434.943.
Jessen, K., Milthers, V., 1928. Stratigraphical and Paleontological studies of interglacial fresh-water deposits in Jutland and northwest Germany. Danmarks Geol. Undersgelse 48, 379. Raekke II 48.
Jiménez-Amat, P., Zahn, R., 2015. Offset timing of climate oscillations during the last two glacial-interglacial transitions connected with large-scale freshwater perturbation. Paleoceanography 30, 768–788. http://dx.doi.org/10.1002/2014PA002710.
Jo, K.-n., Woo, K.S., Lim, H.S., Cheng, H., Edwards, R.L., Wang, Y., Jiang, X., Kim, R., Lee, J.I., Yoon, H.I., Yoo, K.-C., 2011. Holocene and Eemian climatic optima in the Korean Peninsula based on textural and carbon isotopic records from the stalagmite of the Daeya Cave, South Korea. Quat. Sci. Rev. 30, 1218–1231. http://dx.doi.org/10.1016/j.quascirev.2011.02.012.
Jo, K.-n., Woo, K.S., Yi, S., Yang, D.Y., Lim, H.S., Wang, Y., Cheng, H., Edwards, R.L., 2014. Mid-latitude interhemispheric hydrologic seesaw over the past 550,000 years. Nature 508, 378–382. http://dx.doi.org/10.1038/nature13076.
Johnsen, S.J., Dahl-Jensen, D., Gundestrup, N., Steffensen, J.P., Clausen, H.B., Miller, H., Masson-Delmotte, V., Sveinbjörnsdottir, A.E., White, J., 2001. Oxygen isotope and palaeotemperature records from six Greenland ice-core stations: Camp Century, Dye-3, GRIP, GISP2, Renland and NorthGRIP. J. Quat. Sci. 16, 299–307. http://dx.doi.org/10.1002/jqs.622.
Jonkers, L., van Heuven, S., Zahn, R., Peeters, F.J.C., 2013. Seasonal patterns of shell flux, δ18O and δ13C of small and large N. pachyderma (s) and G. bulloides in the subpolar North Atlantic. Paleoceanography 28, 164–174. http://dx.doi.org/10.1002/palo.20018.
Jouzel, J., Hoffmann, G., Parrenin, F., Waelbroeck, C., 2002. Atmospheric oxygen 18 and sea-level changes. Quat. Sci. Rev. 21, 307–314. http://dx.doi.org/10.1016/S0277-3791(01)00106-8.
Jouzel, J., Masson-Delmotte, V., Cattani, O., Dreyfus, G., Falourd, S., Hoffmann, G., Minster, B., Nouet, J., Barnola, J.M., Chappellaz, J., Fischer, H., Gallet, J.C., Johnsen, S., Leuenberger, M., Loulergue, L., Luethi, D., Oerter, H., Parrenin, F., Raisbeck, G., Raynaud, D., Schilt, A., Schwander, J., Selmo, E., Souchez, R., Spahni, R., Stauffer, B., Steffensen, J.P., Stenni, B., Stocker, T.F., Tison, J.L., Werner, M., Wolff, E.W., 2007. Orbital and millennial antarctic climate variability over the past 800,000 years. Science 317, 793–796. http://dx.doi.org/10.1126/science.1141038.
Juvigné, E., Gewelt, M., 1988. Téphra et dépôts des grottes. Intérêt stratigraphique réciproque. Ann. Soc. Géol. Belg. 11, 135–140.
Kawamura, K., Parrenin, F., Lisiecki, L., Uemura, R., Vimeux, F., Severinghaus, J., Hutterli, M.A., Nakazawa, T., Aoki, S., Jouzel, J., Raymo, M.E., Matsumoto, K., Nakata, H., Motoyama, H., Fujita, S., Goto-Azuma, K., Fujii, Y., Watanabe, O., 2007. Northern Hemisphere forcing of climatic cycles in Antarctica over the past 360,000 years. Nature 448, 912–916. http://dx.doi.org/10.1038/nature06015.
Kelly, M.J., Edwards, R.L., Cheng, H., Yuan, D., Cai, Y., Zhang, M., Lin, Y., An, Z., 2006.

High resolution characterization of the Asian Monsoon between 146,000 and 99,000 years B.P. from Dongge Cave, China and global correlation of events surrounding Termination II. Palaeogeogr. Palaeoclimatol. Palaeoecol. 236, 20–38. http://dx.doi.org/10.1016/j.palaeo.2005.11.042.

Khodri, M., Leclainche, Y., Ramstein, G., Braconnot, P., Marti, O., Cortijo, E., 2001. Simulating the amplification of orbital forcing by ocean feedbacks in the last glaciation. Nature 410, 570–574. http://dx.doi.org/10.1038/35069044.

Kindler, P., Guillevic, M., Baumgartner, M., Schwander, J., Landais, A., Leuenberger, M., 2014. Temperature reconstruction from 10 to 120 kyr b2k from the NGRIP ice core. Clim. Past. 10, 887–902. http://dx.doi.org/10.5194/cp-10-887-2014.

Kopp, R.E., Simons, F.J., Mitrovica, J.X., Maloof, A.C., Oppenheimer, M., 2009. Probabilistic assessment of sea level during the Last Interglacial stage. Nature 462, 863–867. http://dx.doi.org/10.1038/nature08686.

Kubatzki, C., Claussen, M., Calov, R., Ganopolski, A., 2006. Sensitivity of the last glacial inception to initial and surface conditions. Clim. Dyn. 27, 333–344. http://dx.doi.org/10.1007/s00382-006-0136-6.

Kuiper, K.F., Deino, A., Hilgen, F.J., Krijgsman, W., Renne, P.R., Wijbrans, J.R., 2008. Synchronizing Rock Clocks of earth history. Science 320, 500–504. http://dx.doi.org/10.1126/science.1154339.

Kukla, G.J., Bender, M.L., de Beaulieu, J.L., Bond, G.C., Broecker, W., Cleveringa, P., Gavin, J.E., Herbert, T.D., Imbrie, J., Jouzel, J., Keigwin, L.D., Knudsen, K.L., McManus, J.F., Merkt, J., Muhs, D.R., Müller, H., Poore, R.Z., Porter, S.C., Seret, G., Shackleton, N.J., Turner, C., Tzedakis, P.C., Winograd, I.J., 2002. Last Interglacial climates. Quat. Res. 58, 2–13. http://dx.doi.org/10.1006/qres.2001.2316.

Labonne, M., Hillaire-Marcel, C., 2000. Geochemical gradients within modern and fossil shells of Concholepas concholepas from northern Chile: an insight into U,ÄiTh systematics and diagenetic/authigenic isotopic imprints in mollusk shells. Geochim. Cosmochim. Acta 64, 1523–1534. http://dx.doi.org/10.1016/S0016-7037(99)00367-1.

Lachniet, M.S., 2009. Climatic and environmental controls on speleothem oxygen-isotope values. Quat. Sci. Rev. 28, 412–432. http://dx.doi.org/10.1016/j.quascirev.2008.10.021.

Laj, C., Channell, J.E.T., 2007. Geomagnetic excursions. In: Kono, M. (Ed.), Treatise on Geophysics. Elsevier, Amsterdam, pp. 373–416.

Laj, C., Guillou, H., Kissel, C., 2014. Dynamics of the earth magnetic field in the 10-75 kyr period comprising the Laschamp and Mono Lake excursions: new results from the French Chaîne des Puys in a global perspective. Earth Planet. Sci. Lett. 387, 184–197. http://dx.doi.org/10.1016/j.epsl.2013.11.031.

Laj, C., Kissel, C., Beer, J., Channell, J.E.T., Kent, D.V., Lowrie, W., Meert, J.G., 2004. High resolution global paleointensity stack since 75 kyr (GLOPIS-75) calibrated to absolute values. Geophys. Monogr. 145, 255–265. http://dx.doi.org/10.1029/145GM19.

Lal, D., 1988. Theoretically expected variations in the terrestrial cosmic-ray production rates of isotopes. In: Castagnoli, G.C. (Ed.), Theoretically Expected Variations in the Terrestrial Cosmic-ray Production Rates of Isotopes. North-Holland Publishing Company, Amsterdam, pp. 215–233.

Lamy, F., Kaiser, J., Ninnemann, U.S., Hebbeln, D., Arz, H.W., Stoner, J., 2004. Antarctic timing of surface water changes off Chile and Patagonian ice sheet response. Science 304, 1959–1962. http://dx.doi.org/10.1126/science.1097863.

Landais, A., Dreyfus, G., Capron, E., Jouzel, J., Masson-Delmotte, V., Roche, D.M., Prie, F., Caillon, N., Chappellaz, J., Leuenberger, M., Lourantou, A., Parrenin, F., Raynaud, D., Teste, G., 2013. Two-phase change in CO2, Antarctic temperature and global climate during Termination II. Nat. Geosci. 6, 1062–1065. http://dx.doi.org/10.1038/ngeo1985.

Landais, A., Dreyfus, G., Capron, E., Masson-Delmotte, V., Sanchez-Goni, M.F., Desprat, S., Hoffmann, G., Jouzel, J., Leuenberger, M., Johnsen, S., 2010. What drives the millennial and orbital variations of δ18Oatm? Quat. Sci. Rev. 29, 235–246. http://dx.doi.org/10.1016/j.quascirev.2009.07.005.

Landais, A., Dreyfus, G., Capron, E., Pol, K., Loutre, M.F., Raynaud, D., Lipenkov, V.Y., Arnaud, L., Masson-Delmotte, V., Paillard, D., Jouzel, J., Leuenberger, M., 2012. Towards orbital dating of the EPICA Dome C ice core using δO2/N2. Clim. Past. 8, 191–203. http://dx.doi.org/10.5194/cp-8-191-2012.

Landais, A., Masson-Delmotte, V., Jouzel, J., Raynaud, D., Johnsen, S., Huber, C., Leuenberger, M., Schwander, J., Minster, B., 2006. The glacial inception as recorded in the NorthGRIP Greenland ice core: timing, structure and associated abrupt temperature changes. Clim. Dyn. 26, 273–284. http://dx.doi.org/10.1007/s00382-005-0063-y.

Landais, A., Masson-Delmotte, V., Stenni, B., Selmo, E., Roche, D.M., Jouzel, J., Lambert, F., Guillevic, M., Bazin, L., Arzel, O., Vinther, B., Gkinis, V., Popp, T., 2015. A review of the bipolar see–saw from synchronized and high resolution ice core water stable isotope records from Greenland and East Antarctica. Quat. Sci. Rev. 114, 18–32. http://dx.doi.org/10.1016/j.quascirev.2015.01.031.

Lang, N., Wolff, E.W., 2011. Interglacial and glacial variability from the last 800 ka in marine, ice and terrestrial archives. Clim. Past. 7, 361–380. http://dx.doi.org/10.5194/cp-7-361-2011.

Lao, Y., Anderson, R.F., Broecker, W.S., Hofmann, H.J., Wolfli, W., 1993. Particulate fluxes of 230Th, 231Pa, and 10Be in the northeastern Pacific Ocean. Geochim. Cosmochim. Acta 57, 205–217. http://dx.doi.org/10.1016/0016-7037(93)90479-G.

Lascu, I., Feinberg, J.M., 2011. Speleothem magnetism. Quat. Sci. Rev. 30, 3306–3320. http://dx.doi.org/10.1016/j.quascirev.2011.08.004.

Laskar, J., Robutel, P., Joutel, F., Gastineau, M., Correia, A.C.M., Levrard, B., 2004. A long-term numerical solution for the insolation quantities of the Earth. Astron. Astrophys. 428, 261–285. http://dx.doi.org/10.1051/0004-6361:20041335.

Lauritzen, S.-E., 1995. High-resolution paleotemperature proxy record for the last interglaciation based on Norwegian speleothems. Quat. Res. 43, 133–146. http://dx.doi.org/10.1006/qres.1995.1015.

Leduc, G., Schneider, R., Kim, J.H., Lohmann, G., 2010. Holocene and Eemian sea surface temperature trends as revealed by alkenone and Mg/Ca paleothermometry. Quat. Sci. Rev. 29, 989–1004. http://dx.doi.org/10.1016/j.quascirev.2010.01.004.

Lemieux-Dudon, B., Bazin, L., Landais, A., Toyé Mahamadou Kele, H., Guillevic, M., Kindler, P., Parrenin, F., Martinerie, P., 2015. Implementation of counted layers for coherent ice core chronology. Clim. Past. 11, 959–978. http://dx.doi.org/10.5194/cp-11-959-2015.

Lemieux-Dudon, B., Blayo, E., Petit, J.-R., Waelbroeck, C., Svensson, A., Ritz, C., Barnola, J.-M., Narcisi, B.M., Parrenin, F., 2010. Consistent dating for Antarctic and Greenland ice cores. Quat. Sci. Rev. 29, 8–20. http://dx.doi.org/10.1016/j.quascirev.2009.11.010.

Leuenberger, M., 1997. Modeling the signal transfer of seawater $d^{18}O$ to the $d^{18}O$ of atmospheric oxygen using a diagnostic box model for the terrestrial and marine biosphere. J. Geophys. Res. 26841–26850. http://dx.doi.org/10.1029/97JC00160.

Li, H.-C., Ku, T.-L., You, C.-F., Cheng, H., Edwards, R.L., Ma, Z.-B., Tsai, W.-s., Li, M.-D., 2005. 87Sr/86Sr and Sr/Ca in speleothems for paleoclimate reconstruction in Central China between 70 and 280 kyr ago. Geochim. Cosmochim. Acta 69, 3933–3947. http://dx.doi.org/10.1016/j.gca.2005.01.009.

Lisiecki, L.E., Raymo, M.E., 2005. A Pliocene-Pleistocene stack of 57 globally distributed benthic δ18O records. Paleoceanography 20. http://dx.doi.org/10.1029/2004pa001071. PA1003.

Lisiecki, L.E., Raymo, M.E., 2009. Diachronous benthic δ18O responses during late Pleistocene terminations. Paleoceanography 24. http://dx.doi.org/10.1029/2009pa001732. PA3210.

Loulergue, L., Parrenin, F., Blunier, T., Barnola, J.M., Spahni, R., Schilt, A., Raisbeck, G., Chappellaz, J., 2007. New constraints on the gas age-ice age difference along the EPICA ice cores, 0–50 kyr. Clim. Past. 3, 527–540. http://dx.doi.org/10.5194/cp-3-527-2007.

Loulergue, L., Schilt, A., Spahni, R., Masson-Delmotte, V., Blunier, T., Lemieux, B., Barnola, J.M., Raynaud, D., Stocker, T.F., Chappellaz, J., 2008. Orbital and millennial-scale features of atmospheric CH_4 over the past 800,000 years. Nature 453, 383–386. http://dx.doi.org/10.1038/nature06950.

Lowe, D.J., 2011. Tephrochronology and its application: a review. Quat. Geochronol. 6, 107–153. http://dx.doi.org/10.1016/j.quageo.2010.08.003.

Lowe, J.J., Rasmussen, S.O., Bj¨rck, S., Hoek, W.Z., Steffensen, J.P., Walker, M.J.C., Yu, Z.C., 2008. Synchronisation of palaeoenvironmental events in the North Atlantic region during the Last Termination: a revised protocol recommended by the INTIMATE group. Quat. Sci. Rev. 27, 6–17. http://dx.doi.org/10.1016/j.quascirev.2007.09.016.

Ludwig, K., 2003. Mathematical–statistical treatment of data and errors for 230Th/U geochronology. In: Bourdon, B., Henderson, G.M., Lundstrom, C.C., Turner, S.P. (Eds.), Uranium-series Geochemistry. Mineralogical Society of America, Geochemical Society.

Ludwig, K.R., Paces, J.B., 2002. Uranium-series dating of pedogenic silica and carbonate, Crater Flat, Nevada. Geochim. Cosmochim. Acta 66, 487–506. http://dx.doi.org/10.1016/S0016-7037(01)00786-4.

Ludwig, K.R., Titterington, D.M., 1994. Calculation of 230ThU isochrons, ages, and errors. Geochim. Cosmochim. Acta 58, 5031–5042. http://dx.doi.org/10.1016/0016-7037(94)90229-1.

Lund, S., Stoner, J.S., Channell, J.E.T., Acton, G., 2006. A summary of Brunhes paleomagnetic field variability recorded in Ocean Drilling Program Cores. Phys. Earth Planet. Interiors 156, 194–204. http://dx.doi.org/10.1016/j.pepi.2005.10.009.

Lunt, D.J., Abe-Ouchi, A., Bakker, P., Berger, A., Braconnot, P., Charbit, S., Fischer, N., Herold, N., Jungclaus, J.H., Khon, V.C., Krebs-Kanzow, U., Langebroek, P.M., Lohmann, G., Nisancioglu, K.H., Otto-Bliesner, B.L., Park, W., Pfeiffer, M., Phipps, S.J., Prange, M., Rachmayani, R., Renssen, H., Rosenbloom, N., Schneider, B., Stone, E.J., Takahashi, K., Wei, W., Yin, Q., Zhang, Z.S., 2013. A multi-model assessment of Last Interglacial temperatures. Clim. Past. 9, 699–717. http://dx.doi.org/10.5194/cp-9-699-2013.

Lüthi, D., Le Floch, M., Bereiter, B., Blunier, T., Barnola, J.M., Siegenthaler, U., Raynaud, D., Jouzel, J., Fischer, H., Kawamura, K., Stocker, T.F., 2008. High-resolution carbon dioxide concentration record 650,000-800,000 years before present. Nature 453, 379–382. http://dx.doi.org/10.1038/nature06949.

Magri, D., Tzedakis, P.C., 2000. Orbital signatures and long-term vegetation patterns in the Mediterranean. Quat. Int. 73, 69–78. http://dx.doi.org/10.1016/S1040-6182(00)00065-3. Äì74.

Margari, V., Skinner, L.C., Hodell, D.A., Martrat, B., Toucanne, S., Grimalt, J.O., Gibbard, P.L., Lunkka, J.P., Tzedakis, P.C., 2014. Land-ocean changes on orbital and millennial time scales and the penultimate glaciation. Geology 42, 183–186. http://dx.doi.org/10.1130/g35070.1.

Martinson, D.G., Pisias, N.G., Hays, J.D., Imbrie, J., Moore Jr., T.C., Shackleton, N.J., 1987. Age dating and the orbital theory of the ice ages: development of a high-resolution 0 to 300,000-year chronostratigraphy. Quat. Res. 27, 1–29. http://dx.doi.org/10.1016/0033-5894(87)90046-9.

Martrat, B., Jimenez-Amat, P., Zahn, R., Grimalt, J.O., 2014. Similarities and dissimilarities between the last two deglaciations and interglaciations in the North Atlantic region. Quat. Sci. Rev. 99, 122–134. http://dx.doi.org/10.1016/j.quascirev.2014.06.016.

Masarik, J., Beer, J., 1999. Simulation of particle fluxes and cosmogenic nuclide

production in the Earth's atmosphere. J. Geophys. Res. Atmos. 104, 12099–12111. http://dx.doi.org/10.1029/1998jd200091.
Masson-Delmotte, V., Buiron, D., Ekaykin, A., Frezzotti, M., Gallée, H., Jouzel, J., Krinner, G., Landais, A., Motoyama, H., Oerter, H., Pol, K., Pollard, D., Ritz, C., Schlosser, E., Sime, L.C., Sodemann, H., Stenni, B., Uemura, R., Vimeux, F., 2011. A comparison of the present and Last Interglacial periods in six Antarctic ice cores. Clim. Past. 7, 397–423. http://dx.doi.org/10.5194/cp-7-397-2011.
Masson-Delmotte, V., Schulz, M., Abe-Ouchi, A., Beer, J., Ganopolski, A., González Rouco, J.F., Jansen, E., Lambeck, K., Luterbacher, J., Naish, T., Osborn, T., Otto-Bliesner, B., Quinn, T., Ramesh, R., Rojas, M., Shao, X., Timmermann, A., 2013. Information from paleoclimate archives. In: Stocker, T.F., Qin, D., Plattner, G.-K., Tignor, M., Allen, S.K., Boschung, J., Nauels, A., Xia, Y., Bex, V., Midgley, P.M. (Eds.), Climate Change 2013: the Physical Science Basis. Contribution of Working Group I to the Fifth Assessment Report of the Intergovernmental Panel on Climate Change. Cambridge University Press, Cambridge, United Kingdom and New York, NY, USA, pp. 383–464 (Chapter 5).
Masson-Delmotte, V., Stenni, B., Blunier, T., Cattani, O., Chappellaz, J., Cheng, H., Dreyfus, G., Edwards, R.L., Falourd, S., Govin, A., Kawamura, K., Johnsen, S.J., Jouzel, J., Landais, A., Lemieux-Dudon, B., Lourantou, A., Marshall, G., Minster, B., Mudelsee, M., Pol, K., Röthlisberger, R., Selmo, E., Waelbroeck, C., 2010a. Abrupt change of Antarctic moisture origin at the end of Termination II. Proc. Natl. Acad. Sci. 107, 12091–12094. http://dx.doi.org/10.1073/pnas.0914536107.
Masson-Delmotte, V., Stenni, B., Pol, K., Braconnot, P., Cattani, O., Falourd, S., Kageyama, M., Jouzel, J., Landais, A., Minster, B., Barnola, J.M., Chappellaz, J., Krinner, G., Johnsen, S., Röthlisberger, R., Hansen, J., Mikolajewicz, U., Otto-Bliesner, B., 2010b. EPICA Dome C record of glacial and interglacial intensities. Quat. Sci. Rev. 29, 113–128. http://dx.doi.org/10.1016/j.quascirev.2009.09.030.
Mazaud, A., Laj, C., Bender, M., 1994. A geomagnetic chronology for antarctic ice accumulation. Geophys. Res. Lett. 21, 337–340. http://dx.doi.org/10.1029/93gl02789.
McKay, N.P., Overpeck, J.T., Otto-Bliesner, B.L., 2011. The role of ocean thermal expansion in Last Interglacial sea level rise. Geophys. Res. Lett. 38 http://dx.doi.org/10.1029/2011GL048280. L14605.
McManus, J.F., Oppo, D.W., Keigwin, L.D., Cullen, J., Bond, G.C., 2002. Thermohaline circulation and prolonged interglacial warmth in the North Atlantic. Quat. Res. 58, 17–21. http://dx.doi.org/10.1006/qres.2002.2367.
Ménabréaz, L., Bourlès, D.L., Thouveny, N., 2012. Amplitude and timing of the Laschamp geomagnetic dipole low from the global atmospheric 10Be overproduction: contribution of authigenic 10Be/9Be ratios in west equatorial Pacific sediments. J. Geophys. Res. Solid Earth 117. http://dx.doi.org/10.1029/2012jb009256. B11101.
Ménabréaz, L., Thouveny, N., Bourlès, D.L., Vidal, L., 2014. The geomagnetic dipole moment variation between 250 and 800 ka BP reconstructed from the authigenic 10Be/9Be signature in West Equatorial Pacific sediments. Earth Planet. Sci. Lett. 385, 190–205. http://dx.doi.org/10.1016/j.epsl.2013.10.037.
Mey, J.L., 2008. The Uranium Series Diagenesis and the Morphology of Drowned Barbadian Paleo-reefs. University of New York, p. 349.
Meyer, M.C., Spötl, C., Mangini, A., 2008. The demise of the Last Interglacial recorded in isotopically dated speleothems from the Alps. Quat. Sci. Rev. 27, 476–496. http://dx.doi.org/10.1016/j.quascirev.2007.11.005.
Meyer, M.C., Spötl, C., Mangini, A., Tessadri, R., 2012. Speleothem deposition at the glaciation threshold – an attempt to constrain the age and paleoenvironmental significance of a detrital-rich flowstone sequence from Entrische Kirche Cave (Austria). Palaeogeogr. Palaeoclimatol. Palaeoecol. 319–320, 93–106. http://dx.doi.org/10.1016/j.palaeo.2012.01.010.
Mokeddem, Z., McManus, J.F., Oppo, D.W., 2014. Oceanographic dynamics and the end of the Last Interglacial in the subpolar North Atlantic. Proc. Natl. Acad. Sci. 111, 11263–11268. http://dx.doi.org/10.1073/pnas.1322103111.
Moller, L., Sowers, T., Bock, M., Spahni, R., Behrens, M., Schmitt, J., Miller, H., Fischer, H., 2013. Independent variations of CH_4 emissions and isotopic composition over the past 160,000 years. Nat. Geosci. 6, 885–890. http://dx.doi.org/10.1038/ngeo1922.
Mudelsee, M., 2000. Ramp function regression: a tool for quantifying climate transitions. Comput. Geosci. 26, 293–307. http://dx.doi.org/10.1016/S0098-3004(99)00141-7.
Müller, H., 1974. Pollenanalytische Untersuchungen und Jahresschichtenzählungen an der eem-zeitlichen Kieselgur von Bispingen/Luhe. Geologisches Jahrbuch, A21. Schweizerbart, pp. 149–169.
Müller, U.C., Kukla, G.J., 2004. North Atlantic Current and European environments during the declining stage of the Last Interglacial. Geology 32, 1009–1012. http://dx.doi.org/10.1130/g20901.1.
Muñoz García, M.B., Rossi, C., Ford, D.C., Schwarcz, H.P., Martín Chivelet, J., 2007. Chronology of Termination II and the Last Interglacial Period in North Spain based on stable isotope records of stalagmites from Cueva del Cobre (Palencia). J. Iber. Geol. 33, 17–30.
Naughton, F., Sanchez Goñi, M.F., Desprat, S., Turon, J.L., Duprat, J., Malaizé, B., Joli, C., Cortijo, E., Drago, T., Freitas, M.C., 2007. Present-day and past (last 25 000 years) marine pollen signal off western Iberia. Mar. Micropaleontol. 62, 91–114. http://dx.doi.org/10.1016/j.marmicro.2006.07.006.
NEEM community members, 2013. Eemian interglacial reconstructed from a Greenland folded ice core. Nature 493, 489–494. http://dx.doi.org/10.1038/nature11789.
North Greenland Ice Core Project members, 2004. High-resolution climate record of Northern Hemisphere climate extending into the Last Interglacial period. Nature 431, 147–151. http://dx.doi.org/10.1038/nature02805.
Ogg, J.G., 2012. 5. The geomagnetic polarity time scale. In: Gradstein, F.M., Ogg, J.G., Schmitz, M.D., Ogg, G.M. (Eds.), The Geologic Time Scale 2012, vol. 1. Elsevier, pp. 85–113.
Ólafsdóttir, S., Geirsdóttir, Á., Miller, G.H., Stoner, J.S., Channell, J.E.T., 2013. Synchronizing Holocene lacustrine and marine sediment records using paleomagnetic secular variation. Geology 41, 535–538. http://dx.doi.org/10.1130/g33946.1.
Opdyke, N.D., Channell, J.E.T., 1996. Magnetic Stratigraphy. Academic Press, San Diego.
Oppo, D.W., Horowitz, M., Lehman, S.J., 1997. Marine core evidence for reduced deep water production during Termination II followed by a relatively stable substage 5e (Eemian). Paleoceanography 12, 51–63. http://dx.doi.org/10.1029/96PA03133.
Oppo, D.W., McManus, J.F., Cullen, J., 2006. Evolution and demise of the Last Interglacial warmth in the subpolar North Atlantic. Quat. Sci. Rev. 25, 3268–3277. http://dx.doi.org/10.1016/j.quascirev.2006.07.006.
Osete, M.-L., Martén-Chivelet, J., Rossi, C., Edwards, R.L., Egli, R., Muñoz-Garcéa, M.B., Wang, X., Pavón-Carrasco, F.J., Heller, F., 2012. The Blake geomagnetic excursion recorded in a radiometrically dated speleothem. Earth Planet. Sci. Lett. 353–354, 173–181. http://dx.doi.org/10.1016/j.epsl.2012.07.041.
Otto-Bliesner, B.L., Rosenbloom, N., Stone, E.J., McKay, N.P., Lunt, D.J., Brady, E.C., Overpeck, J.T., 2013. How warm was the Last Interglacial? New model-data comparisons. Philosophical Trans. R. Soc. A Math. Phys. Eng. Sci. 371 http://dx.doi.org/10.1098/rsta.2013.0097.
Parnell, A.C., Buck, C.E., Doan, T.K., 2011. A review of statistical chronology models for high-resolution, proxy-based Holocene palaeoenvironmental reconstruction. Quat. Sci. Rev. 30, 2948–2960. http://dx.doi.org/10.1016/j.quascirev.2011.07.024.
Parrenin, F., Bazin, L., Capron, E., Landais, A., Lemieux-Dudon, B., Masson-Delmotte, V., 2015. IceChrono1: a probabilistic model to compute a common and optimal chronology for several ice cores. Geosci. Model Dev. 8 (5), 1473–1492. http://dx.doi.org/10.5194/gmd-8-1473-2015.
Parrenin, F., Barker, S., Blunier, T., Chappellaz, J., Jouzel, J., Landais, A., Masson-Delmotte, V., Schwander, J., Veres, D., 2012. On the gas-ice depth difference (Δdepth) along the EPICA Dome C ice core. Clim. Past 8, 1239–1255. http://dx.doi.org/10.5194/cp-8-1239-2012.
Parrenin, F., Barnola, J.-M., Beer, J., Blunier, T., Castellano, E., Chappellaz, J., Dreyfus, G., Fischer, H., Fujita, S., Jouzel, J., Kawamura, K., Lemieux-Dudon, B., Loulergue, L., Masson-Delmotte, V., Narcisi, B., Petit, J.-R., Raisbeck, G., Raynaud, D., Ruth, U., Schwander, J., Severi, M., Spahni, R., Steffensen, J.P., Svensson, A., Udisti, R., Waelbroeck, C., Wolff, E., 2007. The EDC3 chronology for the EPICA Dome C ice core. Clim. Past. 3, 485–497. http://dx.doi.org/10.5194/cp-3-485-2007.
Parrenin, F., Jouzel, J., Waelbroeck, C., Ritz, C., Barnola, J.-M., 2001. Dating the Vostok ice core by an inverse method. J. Geophys. Res. 106, 31837–31852. http://dx.doi.org/10.1029/2001JD900245.
Petit, J.R., Jouzel, J., Raynaud, D., Barkov, N.I., Barnola, J.M., Basile, I., Bender, M.L., Chappellaz, J., Davis, M., Delaygue, G., Delmotte, M., Kotlyakov, V.M., Legrand, M., Lipenkov, V.Y., Lorius, C., Pépin, L., Ritz, C., Saltzman, E., Stievenard, M., 1999. Climate and atmospheric history of the past 420,000 years from the Vostok ice core, Antarctica. Nature 399, 429–436. http://dx.doi.org/10.1038/20859.
Pisias, N.G., Martinson, D.G., Moore Jr., T.C., Shackleton, N.J., Prell, W., Hays, J., Boden, G., 1984. High resolution stratigraphic correlation of benthic oxygen isotopic records spanning the last 300,000 years. Mar. Geol. 56, 119–136. http://dx.doi.org/10.1016/0025-3227(84)90009-4.
Plagnes, V., Causse, C., Genty, D., Paterne, M., Blamart, D., 2002. A discontinuous climatic record from 187 to 74 ka from a speleothem of the Clamouse Cave (south of France). Earth Planet. Sci. Lett. 201, 87–103. http://dx.doi.org/10.1016/S0012-821X(02)00674-X.
Pol, K., Masson-Delmotte, V., Cattani, O., Debret, M., Falourd, S., Jouzel, J., Landais, A., Minster, B., Mudelsee, M., Schulz, M., Stenni, B., 2014. Climate variability features of the Last Interglacial in the East Antarctic EPICA Dome C ice core. Geophys. Res. Lett. 41 http://dx.doi.org/10.1002/2014gl059561, 2014GL059561.
Pons-Branchu, E., Hillaire-Marcel, C., Deschamps, P., Ghaleb, B., Sinclair, D.J., 2005. Early diagenesis impact on precise U-series dating of deep-sea corals: example of a 100-200-year old Lophelia pertusa sample from the northeast Atlantic. Geochimica Cosmochim. Acta 69, 4865–4879. http://dx.doi.org/10.1016/j.gca.2005.06.011.
Pouclet, A., Juvigné, E., Pirson, S., 2008. The Rocourt Tephra, a widespread 90-74 ka stratigraphic marker in Belgium. Quat. Res. 70, 105–120. http://dx.doi.org/10.1016/j.yqres.2008.03.010.
Railsback, L.B., Gibbard, P.L., Head, M.J., Voarintsoa, N.R.G., Toucanne, S., 2015. An optimized scheme of lettered marine isotope substages for the last 1.0 million years, and the climatostratigraphic nature of isotope stages and substages. Quat. Sci. Rev. 111, 94–106. http://dx.doi.org/10.1016/j.quascirev.2015.01.012.
Raisbeck, G.M., Yiou, F., Jouzel, J., Stocker, T.F., 2007. Direct north-south synchronization of abrupt climate change record in ice cores using Beryllium 10. Clim. Past 3, 541–547. http://dx.doi.org/10.5194/cp-3-541-2007.
Rasmussen, S.O., Bigler, M., Blockley, S.P., Blunier, T., Buchardt, S.L., Clausen, H.B., Cvijanovic, I., Dahl-Jensen, D., Johnsen, S.J., Fischer, H., Gkinis, V., Guillevic, M., Hoek, W.Z., Lowe, J.J., Pedro, J.B., Popp, T., Seierstad, I.K., Steffensen, J.P., Svensson, A.M., Vallelonga, P., Vinther, B.M., Walker, M.J.C., Wheatley, J.J., Winstrup, M., 2014. A stratigraphic framework for abrupt climatic changes during the Last Glacial period based on three synchronized Greenland ice-core

records: refining and extending the INTIMATE event stratigraphy. Quat. Sci. Rev. 106, 14–28. http://dx.doi.org/10.1016/j.quascirev.2014.09.007.
Rasmussen, T.L., Oppo, D.W., Thomsen, E., Lehman, S.J., 2003a. Deep sea records from the southeast Labrador Sea: ocean circulation changes and ice-rafting events during the last 160,000 years. Paleoceanography 18. http://dx.doi.org/10.1029/2001PA000736, 1018.
Rasmussen, T.L., Thomsen, E., Kuijpers, A., Wastegård, S., 2003b. Late warming and early cooling of the sea surface in the Nordic seas during MIS 5e (Eemian Interglacial). Quat. Sci. Rev. 22, 809–821. http://dx.doi.org/10.1016/S0277-3791(02)00254-8.
Raynaud, D., Lipenkov, V., Lemieux-Dudon, B., Duval, P., Loutre, M.-F., Lhomme, N., 2007. The local insolation signature of air content in Antarctic ice. A new step toward an absolute dating of ice records. Earth Planet. Sci. Lett. 261, 337–349. http://dx.doi.org/10.1016/j.epsl.2007.06.025.
Regattieri, E., Zanchetta, G., Drysdale, R.N., Isola, I., Hellstrom, J.C., Dallai, L., 2014a. Lateglacial to holocene trace element record (Ba, Mg, Sr) from corchia cave (Apuan Alps, central Italy): paleoenvironmental implications. J. Quat. Sci. 29, 381–392. http://dx.doi.org/10.1002/jqs.2712.
Regattieri, E., Zanchetta, G., Drysdale, R.N., Isola, I., Hellstrom, J.C., Roncioni, A., 2014b. A continuous stable isotope record from the penultimate glacial maximum to the Last Interglacial (159–121 ka) from Tana Che Urla Cave (Apuan Alps, central Italy). Quat. Res. 82, 450–461. http://dx.doi.org/10.1016/j.yqres.2014.05.005.
Risebrobakken, B., Balbon, E., Dokken, T., Jansen, E., Kissel, C., Labeyrie, L., Richter, T., Senneset, L., 2006. The penultimate deglaciation: high-resolution paleoceanographic evidence from a north-south transect along the eastern Nordic Seas. Earth Planet. Sci. Lett. 241, 505–516. http://dx.doi.org/10.1016/j.epsl.2005.11.032.
Roberts, A.P., Tauxe, L., Heslop, D., 2013. Magnetic paleointensity stratigraphy and high-resolution quaternary geochronology: successes and future challenges. Quat. Sci. Rev. 61, 1–16. http://dx.doi.org/10.1016/j.quascirev.2012.10.036.
Rosell-Melé, A., Prahl, F.G., 2013. Seasonality of temperature estimates as inferred from sediment trap data. Quat. Sci. Rev. 72, 128–136. http://dx.doi.org/10.1016/j.quascirev.2013.04.017.
Rosen, J.L., Brook, E.J., Severinghaus, J.P., Blunier, T., Mitchell, L.E., Lee, J.E., Edwards, J.S., Gkinis, V., 2014. An ice core record of near-synchronous global climate changes at the Bolling transition. Nat. Geosci. 7, 459–463. http://dx.doi.org/10.1038/ngeo2147.
Rossi, C., Mertz-Kraus, R., Osete, M.-L., 2014. Paleoclimate variability during the Blake geomagnetic excursion (MIS 5d) deduced from a speleothem record. Quat. Sci. Rev. 102, 166–180. http://dx.doi.org/10.1016/j.quascirev.2014.08.007.
Ruth, U., Barnola, J.M., Beer, J., Bigler, M., Blunier, T., Castellano, E., Fischer, H., Fundel, F., Huybrechts, P., Kaufmann, P., Kipfstuhl, S., Lambrecht, A., Morganti, A., Oerter, H., Parrenin, F., Rybak, O., Severi, M., Udisti, R., Wilhelms, F., Wolff, E., 2007. "EDML1": a chronology for the EPICA deep ice core from Dronning Maud Land, Antarctica, over the last 150 000 years. Clim. Past. 3, 475–484. http://dx.doi.org/10.5194/cp-3-475-2007.
Sagawa, T., Kuroyanagi, A., Irino, T., Kuwae, M., Kawahata, H., 2013. Seasonal variations in planktonic foraminiferal flux and oxygen isotopic composition in the western North Pacific: Implications for paleoceanographic reconstruction. Mar. Micropaleontol. 100, 11–20. http://dx.doi.org/10.1016/j.marmicro.2013.03.013.
Sánchez Goñi, M.F., Landais, A., Fletcher, W.J., Naughton, F., Desprat, S., Duprat, J., 2008. Contrasting impacts of Dansgaard-Oeschger events over a western European latitudinal transect modulated by orbital parameters. Quat. Sci. Rev. 27, 1136–1151. http://dx.doi.org/10.1016/j.quascirev.2008.03.003.
Sánchez Goñi, M.F., Loutre, M.F., Crucifix, M., Peyron, O., Santos, L., Duprat, J., Malaizé, B., Turon, J.L., Peypouquet, J.P., 2005. Increasing vegetation and climate gradient in Western Europe over the Last Glacial Inception (122-110 ka): data-model comparison. Earth Planet. Sci. Lett. 231, 111–130. http://dx.doi.org/10.1016/j.epsl.2004.12.010.
Schneider, R., Schmitt, J., Köhler, P., Joos, F., Fischer, H., 2013. A reconstruction of atmospheric carbon dioxide and its stable carbon isotopic composition from the penultimate glacial maximum to the last glacial inception. Clim. Past. 9, 2507–2523. http://dx.doi.org/10.5194/cp-9-2507-2013.
Scholz, D., Hoffmann, D.L., 2011. StalAge – an algorithm designed for construction of speleothem age models. Quat. Geochronol. 6, 369–382. http://dx.doi.org/10.1016/j.quageo.2011.02.002.
Scholz, D., Hoffmann, D.L., Hellstrom, J., Bronk Ramsey, C., 2012. A comparison of different methods for speleothem age modelling. Quat. Geochronol. 14, 94–104. http://dx.doi.org/10.1016/j.quageo.2012.03.015.
Seidenkrantz, M.-S., 1993. Benthic foraminiferal and stable isotope evidence for a "Younger Dryas-style" cold spell at the Saalian-Eemian transition, Denmark. Palaeogeogr. Palaeoclimatol. Palaeoecol. 102, 103–120. http://dx.doi.org/10.1016/0031-0182(93)90008-7.
Seidenkrantz, M.-S., Bornmalm, L., Johnsen, S.J., Knudsen, K.L., Kuijpers, A., Lauritzen, S.-E., Leroy, S.A.G., Mergeal, I., Schweger, C., Van Vliet-Lanoë, B., 1996. Two-step deglaciation at the oxygen isotope stage 6/5E transition: the Zeifen-Kattegat climate oscillation. Quat. Sci. Rev. 15, 63–75. http://dx.doi.org/10.1016/0277-3791(95)00086-0.
Seidenkrantz, M.-S., Kristensen, P., Knudsen, K.L., 1995. Marine evidence for climatic instability during the Last Interglacial in shelf records from northwest Europe. J. Quat. Sci. 10, 77–82. http://dx.doi.org/10.1002/jqs.3390100108.
Severinghaus, J.P., Sowers, T., Brook, E.J., Alley, R.B., Bender, M.L., 1998. Timing of abrupt climate change at the end of the Younger Dryas interval from thermally fractionated gases in polar ice. Nature 391, 141–146. http://dx.doi.org/10.1038/34346.
Shackleton, N., 1967. Oxygen isotope analyses and Pleistocene temperatures re-assessed. Nature 215, 15–17. http://dx.doi.org/10.1038/215015a0.
Shackleton, N.J., 1969. The Last Interglacial in the marine and terrestrial records. Proc. Roy. Soc. Lond. B 174, 135–154. http://dx.doi.org/10.1098/rspb.1969.0085.
Shackleton, N.J., Chapman, M.R., Sanchez-Goni, M.F., Pailler, D., Lancelot, Y., 2002. The classic Marine Isotope Substage 5e. Quat. Res. 58, 14–16. http://dx.doi.org/10.1006/qres.2001.2312.
Shackleton, N.J., Hall, M.A., Vincent, E., 2000. Phase relationships between millenial-scale events 64,000-24,000 years ago. Paleoceanography 15, 565–569. http://dx.doi.org/10.1029/2000PA000513.
Shackleton, N.J., Sanchez-Goni, M.F., Pailler, D., Lancelot, Y., 2003. Marine Isotope Substage 5e and the Eemian Interglacial. Glob. Planet. Change 36, 151–155. http://dx.doi.org/10.1016/S0921-8181(02)00181-9.
Shopov, Y.Y., Ford, D.C., Schwarcz, H.P., 1994. Luminescent microbanding in speleothems: high-resolution chronology and paleoclimate. Geology 22, 407–410. http://dx.doi.org/10.1130/0091-7613(1994)022<0407:lmishr>2.3.co;2.
Siani, G., Michel, E., De Pol-Holz, R., DeVries, T., Lamy, F., Carel, M., Isguder, G., Dewilde, F., Lourantou, A., 2013. Carbon isotope records reveal precise timing of enhanced Southern Ocean upwelling during the last deglaciation. Nat. Commun. 4 http://dx.doi.org/10.1038/ncomms3758.
Sicre, M.A., Labeyrie, L., Ezat, U., Duprat, J., Turon, J.L., Schmidt, S., Michel, E., Mazaud, A., 2005. Mid-latitude southern indian ocean response to northern hemisphere heinrich events. Earth Planet. Sci. Lett. 240, 724–731.
Singer, B.S., 2014. A quaternary geomagnetic instability time scale. Quat. Geochronol. 21, 29–52. http://dx.doi.org/10.1016/j.quageo.2013.10.003.
Singer, B.S., Guillou, H., Jicha, B.R., Zanella, E., Camps, P., 2014. Refining the quaternary geomagnetic instability time scale (GITS): Lava flow recordings of the blake and Post-Blake excursions. Quat. Geochronol. 21, 16–28. http://dx.doi.org/10.1016/j.quageo.2012.12.005.
Skinner, L.C., Shackleton, N.J., 2005. An Atlantic lead over Pacific deep-water change across Termination I: implications for the application of the marine isotope stage stratigraphy. Quat. Sci. Rev. 24, 571–580. http://dx.doi.org/10.1016/j.quascirev.2004.11.008.
Spötl, C., Mangini, A., 2002. Stalagmite from the Austrian Alps reveals Dansgaard-Oeschger events during isotope stage 3: implications for the absolute chronology of Greenland ice cores. Earth Planet. Sci. Lett. 203, 507–518. http://dx.doi.org/10.1016/S0012-821X(02)00837-3.
Stirling, C.H., Esat, T.M., Lambeck, K., McCulloch, M.T., 1998. Timing and duration of the Last Interglacial: evidence for a restricted interval of widespread coral reef growth. Earth Planet. Sci. Lett. 160, 745–762. http://dx.doi.org/10.1016/S0012-821X(98)00125-3.
Stoner, J., St-Onge, G., 2007. Magnetic stratigraphy in paleoceanography: reversals, excursions, paleointensity and secular variation. In: Hillaire-Marcel, C., de Vernal, A. (Eds.), Proxies in Late Cenozoic Paleoceanography. Elsevier, pp. 99–137.
Stoner, J.S., Channell, J.E.T., Hillaire-Marcel, C., 1998. A 200 ka geomagnetic chronostratigraphy for the Labrador Sea: Indirect correlation of the sediment record to SPECMAP. Earth Planet. Sci. Lett. 159, 165–181. http://dx.doi.org/10.1016/S0012-821X(98)00069-7.
Stoner, J.S., Channell, J.E.T., Hillaire-Marcel, C., Kissel, C., 2000. Geomagnetic paleointensity and environmental record from Labrador Sea core MD95-2024: global marine sediment and ice core chronostratigraphy for the last 110 kyr. Earth Planet. Sci. Lett. 183, 161–177. http://dx.doi.org/10.1016/S0012-821X(00)00272-7.
Suwa, M., Bender, M.L., 2008. Chronology of the Vostok ice core constrained by O_2/N_2 ratios of occluded air, and its implication for the Vostok climate records. Quat. Sci. Rev. 27, 1093–1106. http://dx.doi.org/10.1016/j.quascirev.2008.02.017.
Svensson, A., Andersen, K.K., Bigler, M., Clausen, H.B., Dahl-Jensen, D., Davies, S.M., Johnsen, S.J., Muscheler, R., Parrenin, F., Rasmussen, S.O., Röthlisberger, R., Seierstad, I., Steffensen, J.P., Vinther, B.M., 2008. A 60 000 year Greenland stratigraphic ice core chronology. Clim. Past. 4, 47–57. http://dx.doi.org/10.5194/cp-4-47-2008.
Svensson, A., Bigler, M., Kettner, E., Dahl-Jensen, D., Johnsen, S., Kipfstuhl, S., Nielsen, M., Steffensen, J.P., 2011. Annual layering in the NGRIP ice core during the Eemian. Clim. Past 7, 1427–1437. http://dx.doi.org/10.5194/cp-7-1427-2011.
Swart, P.K., Hubbard, J.A.E.B., 1982. Uranium in scleractinian coral skeletons. Coral Reefs 1, 13–19. http://dx.doi.org/10.1007/bf00286535.
Thomas, A.L., Henderson, G.M., Deschamps, P., Yokoyama, Y., Mason, A.J., Bard, E., Hamelin, B., Durand, N., Camoin, G., 2009. Penultimate deglacial sea-level timing from uranium/thorium dating of Tahitian corals. Science 324, 1186–1189. http://dx.doi.org/10.1126/science.1168754.
Thompson, W.G., Allen Curran, H., Wilson, M.A., White, B., 2011. Sea-level oscillations during the Last Interglacial highstand recorded by Bahamas corals. Nat. Geosci. 4, 684–687. http://dx.doi.org/10.1038/ngeo1253.
Thompson, W.G., Goldstein, S.L., 2005. Open-system coral ages reveal persistent suborbital sea-level cycles. Science 308, 401–404. http://dx.doi.org/10.1126/science.1104035.
Thouveny, N., Carcaillet, J., Moreno, E., Leduc, G., Nérini, D., 2004. Geomagnetic moment variation and paleomagnetic excursions since 400 kyr BP: a stacked record from sedimentary sequences of the Portuguese margin. Earth Planet. Sci. Lett. 219, 377–396. http://dx.doi.org/10.1016/S0012-821X(03)00701-5.
Thouveny, N., Creer, K.M., Blunk, I., 1990. Extension of the Lac du Bouchet palaeomagnetic record over the last 120,000 years. Earth Planet. Sci. Lett. 97, 140–161. http://dx.doi.org/10.1016/0012-821X(90)90105-7.
Turney, C.S.M., Jones, R.T., 2010. Does the Agulhas Current amplify global

temperatures during super-interglacials? J. Quat. Sci. 25, 839–843. http://dx.doi.org/10.1002/jqs.1423.
Turon, J.-L., 1984. Direct land/sea correlations in the Last Interglacial complex. Nature 309, 673–676. http://dx.doi.org/10.1038/309673a0.
Tzedakis, C., 2003. Timing and duration of Last Interglacial conditions in Europe: a chronicle of a changing chronology. Quat. Sci. Rev. 22, 763–768. http://dx.doi.org/10.1016/S0277-3791(03)00004-0.
Tzedakis, P.C., Frogley, M.R., Heaton, T.H.E., 2003. Last Interglacial conditions in southern Europe: evidence from Ioannina, northwest Greece. Glob. Planet. Change 36, 157–170. http://dx.doi.org/10.1016/S0921-8181(02)00182-0.
Tzedakis, P.C., Wolff, E.W., Skinner, L.C., Brovkin, V., Hodell, D.A., McManus, J.F., Raynaud, D., 2012. Can we predict the duration of an interglacial? Clim. Past. 8, 1473–1485. http://dx.doi.org/10.5194/cp-8-1473-2012.
Valet, J.-P., Meynadier, L., Guyodo, Y., 2005. Geomagnetic dipole strength and reversal rate over the past two million years. Nature 435, 802–805. http://dx.doi.org/10.1038/nature03674.
Veres, D., Bazin, L., Landais, A., Toyé Mahamadou Kele, H., Lemieux-Dudon, B., Parrenin, F., Martinerie, P., Blayo, E., Blunier, T., Capron, E., Chappellaz, J., Rasmussen, S.O., Severi, M., Svensson, A., Vinther, B., Wolff, E.W., 2013. The Antarctic ice core chronology (AICC2012): an optimized multi-parameter and multi-site dating approach for the last 120 thousand years. Clim. Past. 9, 1733–1748. http://dx.doi.org/10.5194/cp-9-1733-2013.
Verheyden, S., Baele, J., Keppens, E., Genty, D., Cattani, O., Cheng, H., Lawrence, E., Zhang, H., Van Strijdonck, M., Quinif, Y., 2006. The Proserpine stalagmite (Han-Sur-Lesse Cave, Belgium): preliminary environmental interpretation of the last 1000 years as recorded in a layered speleothem. Geol. Belg. 9, 245–256.
Waelbroeck, C., Frank, N., Jouzel, J., Parrenin, F., Masson-Delmotte, V., Genty, D., 2008. Transferring radiometric dating of the Last Interglacial sea level high stand to marine and ice core records. Earth Planet. Sci. Lett. 265, 183–194. http://dx.doi.org/10.1016/j.epsl.2007.10.006.
Waelbroeck, C., Skinner, L.C., Labeyrie, L., Duplessy, J.C., Michel, E., Vazquez Riveiros, N., Gherardi, J.M., Dewilde, F., 2011. The timing of deglacial circulation changes in the Atlantic. Paleoceanography 26. http://dx.doi.org/10.1029/2010pa002007. PA3213.
Wang, X., Auler, A.S., Edwards, R.L., Cheng, H., Ito, E., Solheid, M., 2006. Interhemispheric anti-phasing of rainfall during the last glacial period. Quat. Sci. Rev. 25, 3391–3403. http://dx.doi.org/10.1016/j.quascirev.2006.02.009.
Wang, Y., Cheng, H., Edwards, R.L., Kong, X., Shao, X., Chen, S., Wu, J., Jiang, X., Wang, X., An, Z., 2008. Millennial- and orbital-scale changes in the East Asian monsoon over the past 224,000 years. Nature 451, 1090–1093. http://dx.doi.org/10.1038/nature06692.
Wang, Y.J., Cheng, H., Edwards, R.L., An, Z.S., Wu, J.Y., Shen, C.C., Dorale, J.A., 2001. A high-resolution absolute-dated late Pleistocene monsoon record from hulu cave, China. Science 294, 2345–2348. http://dx.doi.org/10.1126/science.1064618.
Wang, Z., Cochelin, A.-S.B., Mysak, L.A., Wang, Y., 2005. Simulation of the last glacial inception with the green McGill Paleoclimate Model. Geophys. Res. Lett. 32 http://dx.doi.org/10.1029/2005gl023047. L12705.
Woillard, G.M., 1978. Grande Pile peat bog: a continuous pollen record for the last 140,000 years. Quat. Res. 9, 1–21. http://dx.doi.org/10.1016/0033-5894(78)90079-0.
Wolff, E., Basile, I., Petit, J.-R., Schwander, J., 1999. Comparison of Holocene electrical records from Dome C and Vostok, Antarctica. Ann. Glaciol. 29, 89–93. http://dx.doi.org/10.3189/172756499781820888.
Wolff, E.W., Chappellaz, J., Blunier, T., Rasmussen, S.O., Svensson, A., 2010. Millennial-scale variability during the last glacial: the ice core record. Quat. Sci. Rev. 29, 2828–2838. http://dx.doi.org/10.1016/j.quascirev.2009.10.013.
Wulf, S., Keller, J., Paterne, M., Mingram, J., Lauterbach, S., Opitz, S., Sottili, G., Giaccio, B., Albert, P.G., Satow, C., Tomlinson, E.L., Viccaro, M., Brauer, A., 2012. The 100–133 ka record of Italian explosive volcanism and revised tephrochronology of Lago Grande di Monticchio. Quat. Sci. Rev. 58, 104–123. http://dx.doi.org/10.1016/j.quascirev.2012.10.020.
Yuan, D., Cheng, H., Edwards, R.L., Dykoski, C.A., Kelly, M.J., Zhang, M., Qing, J., Lin, Y., Wang, Y., Wu, J., Dorale, J.A., An, Z., Cai, Y., 2004. Timing, duration, and transitions of the Last Interglacial Asian Monsoon. Science 304, 575–578. http://dx.doi.org/10.1126/science.1091220.
Zagwijn, W.H., 1996. An analysis of Eemian climate in Western and Central Europe. Quat. Sci. Rev. 15, 451–469. http://dx.doi.org/10.1016/0277-3791(96)00011-X.
Zazo, C., Goy, J.L., Hillaire-Marcel, C., Dabrio, C.J., Gonzalez-Delgado, J.A., Cabero, A., Bardaji, T., Ghaleb, B., Soler, V., 2010. Sea level changes during the last and present interglacials in Sal Island (Cape Verde archipelago). Glob. Planet. Change 72, 302–317. http://dx.doi.org/10.1016/j.gloplacha.2010.01.006.
Zazo, C., Goy, J.L., Hillaire-Marcel, C., Gillot, P.-Y., Soler, V., González, J.Á., Dabrio, C.J., Ghaleb, B., 2002. Raised marine sequences of Lanzarote and Fuerteventura revisited – a reappraisal of relative sea-level changes and vertical movements in the eastern Canary Islands during the Quaternary. Quat. Sci. Rev. 21, 2019–2046. http://dx.doi.org/10.1016/S0277-3791(02)00009-4.
Zhao, J.-x., Yu, K.-f., Feng, Y.-x., 2009. High-precision 238U-234U-230Th disequilibrium dating of the recent past: a review. Quat. Geochronol. 4, 423–433. http://dx.doi.org/10.1016/j.quageo.2009.01.012.
Zhu, R., Zhou, L., Laj, C., Mazaud, A., Ding, I.L., 1994. The Blake geomagnetic polarity episode recorded in Chinese loess. Geophys. Res. Lett. 21, 697–700. http://dx.doi.org/10.1029/94GL00532.